Modelling for Control of a Steckel Hot Rolling Mill

by

Ernst Scholtz

Submitted in partial fulfillment of the requirements for the degree

Master of Engineering (Electronic Engineering)

in the

Faculty of Engineering

UNIVERSITY OF PRETORIA

October 1999

Typeset using LaTeX 2ε

Abstract

Steckel hot rolling forms part of the larger steelmaking process. Steckel hot rolling is not the most common type of hot rolling mill, found in the industry. Steckel mills are normally associated with developing countries and are also very similar to cold rolling mills. The modelling aspect of this dissertation focuses on a practical investigated Steckel rolling mill, which is used in the production of stainless steel strip. Various types of rolling mills that can roll various shapes and dimensions of products are found in the industry, but only hot strip rolling is investigated in this dissertation.

In this dissertation models were identified in order to create a mill simulator that can adequately simulate Steckel rolling mill behaviour. The constructed simulator is able to simulate the thickness crown behaviour of the hot strip as well as the tension in the sheet while rolling. The simulator is not able to simulate the temperature, shape and flatness behaviour of the Steckel rolling process.

The mill simulator consists of a roll gap model, stand model, tension model as well as models accounting for the dynamics associated with the hydraulic actuators. The integration of these models in order to form the mill simulator, and the application of this simulator in an investigation of the interactions in the Steckel rolling mill process is considered a substantial contribution to the literature.

This dissertation forms the basis of a continuing research project, which aim is to apply a model based predictive control method, to regulate the centerline gauge and strip tension in the hot rolling mill. Tension control of the strip is normally associated with multistand hot rolling mills and little literature exists concerned with the tension and gauge interactions associated with the Steckel hot rolling mill process. This dissertation addresses this issue and the dynamic interaction is identified.

The nonlinear mill simulator was used to identify a linear model for control system design. The linear model was identified around a certain operating point associated with a certain pass of a multiple pass rolling schedule. Step tests were applied to the manipulated variables of the nonlinear mill simulator, and by doing system identification a linear time invariant multivariable transfer function model was derived.

Open loop simulation results were compared with time responses found in the literature and practical logged data as far as possible, in order to asses the performance of the mill simulator.

This dissertation ends with an initial control problem formulation and a discussion of how to implement the linear model in a Model Predictive Control (MPC) structure.

Keywords

steelmaking, hot rolling, Steckel rolling mill, dynamic modelling, system identification, control problem formulation, nonlinear, mill simulator, centerline gauge, tension, strip crown

Opsomming

Die Steckel warm walsingproses vorm 'n integrale deel in staal-vervaardiging. Dié wals is egter nie die mees algemene warmwals nie en word hoofsaaklik gebruik in ontwikkelende lande. Die wals is baie soortgelyk aan kouewalse. Die modellering in hierdie verhandeling is gebaseer op 'n praktiese Steckel warmbandwals wat gebruik word om vlekvrye staal band te produseer. Verskeie tipes walse wat verskillende vorme en groottes produkte kan rol bestaan; maar slegs warm band walsing word in hierdie verhandeling ondersoek.

Verskeie modelle is ondersoek om 'n wals-simulator op te stel wat die Steckel wals gedrag akkuraat naboots. Die simulator kan die dikte kroon gedrag en die spanning in die band voorspel. Temperatuur variasies, vorm en platheid word nie deur die simulator in ag geneem nie.

Die wals simulator bestaan uit walsgaping-, walsraamwerk-, en spanning modelle, sowel as modelle vir die hidrouliese aktueerders. Die koppeling en verband ondersoek, tussen die voorafgenoemde modelle word beskou as 'n groot bydrae to die literatuur.

Die verhandeling is deel van 'n navorsings projek wat ten einde sal poog om model gebaseerde voorspellings beheer te gebruik om middel dikte en band spanning in die warm wals te reguleer. Spannings beheer word gewoonlik geassosieer met veelvoudige stand warm walse en min literatuur bestaan oor die interaksie tussen spanning en dikte in die Steckel. Hierdie verhandeling beskou die dinamiese interaksie.

Die nie-lineêre simulator is gebruik om 'n lineêre model af te lei wat geskik sou wees om 'n beheerder vir die proses te ontwerp. Die lineêre model was afgelei om 'n werkspunt wat verkty is vanaf 'n tipiese verloop van die veelvoudige verloop wals skedule. Stap toetse is op die gemanipuleerde veranderlikes van die nie-lineêre wals simulator gedoen, en die resultate gebruik om deur middel van stelsel identifikasie 'n linieêre tyd invariante model te verkry. Ope lus tyd simulasie resultate is met die literatuur en praktiese data vergelyk om die doeltreffendheid van die simulator te ondersoek.

Die verhandeling eindig met 'n aanvanklike beheer probleem uiteensetting en bespreek die kwessies omtrent die gebruik van die lineêre model vir die toepassing van model gebaseerde voorspellings beheer.

Sleutelwoorde

staalproses, warmband walsing, Steckel wals, dinamiese modellering, beheerstelsel probleem formulering, nie-lineêre, wals simuleerder, middel plaat uitset dikte, aangelegde plaat spanning, plaat kroon

Acknowledgements

The author wishes to thank the following persons and institutions for their contribution to this dissertation.

Prof. Ian K. Craig, the promoter, for the dedication, leadership and advice undertaken during this dissertation. Furthermore for the motivation and inspiration provided to the author to pursue a Ph.D.

Prof. P. Chris Pistorius for advice regarding the process aspects of this dissertation.

Prof. F. W. Leuschner for making the undertaking of this dissertation a possibility, as well as the opportunity provided to the author to pursue a Ph.D.

Liaan Lewis of Columbus Stainless Steel for organizing of plant visits and personal conversations regarding the Steckel Mill at Columbus Stainless Steel at Middelburg, South Africa. Petrus Bothma, previously of Highveld Steel and Vanadium, for an initial explanation of the Steckel hot rolling mill process. Cobus Potgieter of Columbus Stainless Steel for the excellent effort regarding the completion of the comprehensive questionnaire compiled by the author, and Arno Ferreira of Columbus Stainless Steel with help provided with the logged data of the Steckel mill under consideration.

Gerald Hearns of the University of Strathclyde for providing some crucial literature for this dissertation.

Rudolph Bester of the University of Pretoria for his time and the numerous discussions concerned with the mechanical modelling aspects featured in this dissertation.

Academic staff at the University of Pretoria for advice regarding various aspects of the dissertation, especially Prof. X. Xia and Prof. Y. Yavin; and colleagues: Fernando Camisani, Hans Bekker, Niel Kemp, Martin Smit, Kobus Oosthuizen, Leon Staphorst, Stefan Swanepoel, Bennie Waldeck and Jacques van Wyk.

The Foundation for Research Development for financial assistance during the course of the dissertation. The University of Pretoria that provided funding in order for the author to attend an international training course concerned with hot rolling mill control and technology at the University of Strathclyde, Glasgow.

My parents for creating opportunities for me and their guidance. My brother, sister-in-law, and grandparents for their loving support. I would like to praise the Lord for making everything possible.

This thesis is dedicated to my late mother and grandfather.

Contents

Chapter 1

Introduction

This dissertation deals with the modelling for control of a Steckel hot rolling mill process. Hot rolling is the process of shaping metal by passing it between rolls revolving at the same peripheral speed and in opposite directions, while the the strip metal is at temperatures of about $1000°C$. Conservation of mass (massflow) holds as the metal deforms predominantly plastically across the roll gap. The roll gap is set at a gap setting calculated in order to achieve a desired reduction in strip thickness. A reheated slab is transferred from a reheating furnace on a transfer table to a roughing mill, where the initial thickness reduction is done, and then to the hot rolling finishing mill that shapes the metal into a finished or semi-finished product.

Different kinds of flat rolling mills exists, e.g. Sendzimer, Cluster, Steckel, 4-high, 5-high, 6-high, Z-high and Planetary mills [1, 2, 3]. In this dissertation the modelling of the hot rolling mill process is based on a Steckel Hot Rolling Mill. In the Appendix a short definition of common rolling terms are given.

1.1 Background

Modern Steckel Mills (manufactured after 1980 [4]) can be divided into two main categories regarding production. The first type of the new generation of Steckel Mills has been installed in industrial countries producing mainly Stainless Steels. The production capacity of these mills lies between 150,000 and 450,000 t/yr [4]. For these steel grades the Steckel Mills are suitable due to their high flexibility and low investment costs. The second category of modern Steckel Mills is characterized by a very large product mix regarding materials and strip sizes that can be economically produced. Beside carbon, stainless and silicon steels, non-ferrous metals and alloys such as titanium, copper, brass are also rolled [4].

Most of the new Steckel mills are equipped with two stands, capable of producing 500,000 t/yr., but in

some cases single stand Steckel mills, capable of 10,000-100,000 t/yr., are installed [4]. Single stand Steckel Mills are usually installed for low production capacities or for products without very high requirements regarding surface quality [4]. The capital expenditure associated with the installation of a Steckel mill is less in comparison to the capital investment associated with the installation of a multi-stand (5-7 stands) hot rolling mill.

Over capacity of steel production has introduced much more competition and the quality of the produced strip, i.e. dimensional accuracy, surface finish, flatness, and physical properties [4, 5, 3], is used to distinguish strip manufacturers from each other. Rolling mill companies are installing advanced control systems to improve the overall quality of their products.

The conventional hot rolling operation has developed significantly during the past thirty years [3]. The main driving forces behind this development are the need to increase the throughput and improve the strip's quality, with the emphasis on the dimensional accuracy, surface finish, flatness and the strip's physical properties. Automation projects of modern hot rolling mill focusses on [4]:

1. Material tracking;
2. Automatic slab and coil storage control;
3. Reheating furnace control;
4. Automatic control of the rolling process focussing on mill sequence control, mill-setup and correction, pass schedule calculation and optimization [6], automatic crop shear control, automatic gauge/thickness control (AGC) [7, 8], automatic crown and shape control [9, 10], finishing/coiling temperature control as well as control of the mechanical properties of the strip [5, 11];
5. Data logging.

The bulk of the current research projects concerned with hot rolling of metals addresses issues reported in point 4 as can be seen in [12, 13, 14]. In this dissertation the focus falls on some of these subjects (in particular thickness profile control and tension control).

The drive for automation of the rolling process is part of larger projects, valued at millions of dollars, the aim to automate the process of steel manufacturing. These automation specialists conduct research on these processes and develop propriety models, that ensure their survival in a competitive market.

The largest part of this dissertation deals with model derivation and integration in order to create a nonlinear plant simulator. Nonlinear modelling is necessary, due to the unavailability of suitable models, simulators and data. The lack of models and data is attributed to the competitive rolling mill environment. The development of nonlinear models can be time consuming and control system experts estimate that modelling can make up 90% of the time taken to establish an industrial control system [15].

1.2 Dissertation Motivation

The control of strip thickness has largely been solved and the application of advanced control methods are being investigated for application on industrial mills. Most of the literature concerned with thickness and tension control in the hot rolling mill environment are done for multiple stand rolling mills [13, 16] with loopers that control the interstand tension. The Steckel mill layout is similar to that of a single stand cold rolling mill and strip tension plays a larger role for a Steckel mill process than it would for a multiple stand mill. In [3] it is reported that a Steckel mill relies on a drawing process rather than a rolling process to achieve the desired reduction. Further it is suggested that the coiler motors supply the energy necessary to draw the strip through the roll gap. For a hot rolling Steckel mill, however the tension aids the rolling process and the bulk of the reduction is done with a rolling process, where the work rolls are driven. In the literature only a few articles dealing with Steckel Mills are found. This can be attributed to the scarcity of Steckel mills as was reported in [4].

In hot rolling emphasis is increasingly being placed on the control of strip crown and shape [17], and hence the this dissertation will investigate the strip crown behaviour. The simulation of the shape forming of the strip falls outside the scope of this dissertation.

Industrial Steckel automation projects[1] focuses on:

- Dual gaugemeter system, featuring mean and differential gaugemeter loops
- X-Ray thickness feedback and feedforward control
- Speed compensation
- Tail end compensation
- Roll thermal compensation
- Backup roll eccentricity control

In this dissertation selective items of the above items are modelled, and the distinction can be summarized as follows:

Dissertation emphasis

- The dual gaugemeter principle, arising from the difference of mill stiffness on either side of the mill.
- The difference in entrance speed and exit speed of the roll gap.

[1]Document compiled by Dr. Tony Bilkhu of Cegelec Projects Ltd. Rugby England, concerned with Cegelec Steckel Mill AGC.

Outside the scope of this dissertation

- The modelling of the eccentricity of the backup rolls.
- The modelling of roll thermal expansion and roller wear.
- In depth temperature modelling of the rolling process is not the emphasis of this work. Many compensation techniques exists for head and tail end compensation consists, of which compensation for the increase in the rolling force, attributed to the thermal rundown of the strip temperature is one.

One of the aims of this dissertation is to initiate an investigation into the potential benefits that can be gained if a modern advanced control method such as MPC is applied in the rolling mill environment on a supervisory level. The application of advanced MIMO control to rolling mills is increasingly being investigated [13].

The regulation of the mill outputs at threading speed have exhaustively been investigated [18] and the current trend is to improve the control on the head and tail end of the strip, in order to reduce the amount of off-specification product [19]. The Steckel hot rolling mill process investigated in this dissertation can be seen as a batch process with process start ups and process shut downs. The process start ups and stops are reflected through the speed up and down of the mill drive speed respectively. In this dissertation an investigation is initiated into the feasibility of thickness and tension control on such a process start up.

In the literature there is at least one reference of the application of Generalized Predictive Control (GPC) to a multiple stand rolling mill [18], showing that the investigation undertaken in this dissertation is not an isolated case. This application of GPC is on a supervisory level, which utilizes cascaded control schemes for its local control of the mill drive speed, hydraulic actuator strokes etc. The traditional Smith predictor feedback control scheme for the thickness control loop can be replaced by a model based predictive control method [20]. The controlled variables in this dissertation, namely:

- centerline exit gauge,
- thickness crown,
- strip tension,

are similar as is discussed in [18].

1.3 Aims and Contributions

One of the aims of this dissertation is to develop the basis for a continuing research program that will ultimately investigate the feasibility of applying MPC or other advanced control methods to a Steckel

Hot Rolling Mill process. The main contributions of this work towards this aim can be broken down into the following tasks and intermediate aims:

- A nonlinear plant simulator is developed, with which investigations into the nonlinear behaviour and interactions between the;
  - hydraulic actuators,
  - mill dynamics,
  - and the material properties of the strip being rolled can be conducted.

  One of the leading rolling mill researchers, R-M Guo [8], states that in order to evaluate a comprehensive total gauge control loop it might be necessary to model all of the above components as well as the dynamics of the drives and the motors. In [8] this involved modelling was not done, and only the hydraulic actuators were modelled in detail. In this dissertation the modelling and the identification of the interactions between the key components itemized above is done. Such an investigation, concerned with dynamic hot rolling mill modelling, incorporates the following:

- The nonlinear plant simulator should reflect adequate practical process behaviour;
- The nonlinear simulator should be able to simulate the thickness profile (and in particular the centerline exit thickness) and tension behaviour of a hot rolled strip while rolling;
- The simulator should be constructed in a modular fashion such that it can be extended easily;
- The simulator should be made operable at any part of the process speed curve, in order to derive different linear models at any chosen operating point;
- An initial linear model should be identified on the process start up, in order to test certain control ideas;
- An initial control problem should be formulated, so that the performance of a proposed control method can be evaluated, by utilising the simulator as the process that has to be controlled.

With this dissertation a research program is launched that will ultimately help with the industrial research of rolling mills in South Africa.

1.4 Organization

This dissertation is organized as shown in table 1.1. In chapter 2 a general steel manufacturing process description is given, and it is accentuated where the hot rolling mill fits into the larger manufacturing process. The layout and practical operation of the hot rolling mill are then given. Finally the mechanics of the Steckel hot rolling mill process are described.

In chapter 3 models are identified that will be connected to each other in order to create the mill simulator. These model derivations are shown and their incorporation into the mill simulator is discussed. In chapter 4 the solution methodology for each model is discussed and the necessary physical constants are calculated or identified from the literature.

In chapter 5 simulation results are shown for the separate models. These results are discussed and their accuracy assessed compared to results stated in the literature. The design of steps that are applied to the manipulated variables of the mill simulator during the identification of the linear model are discussed, and some time simulation results from these tests are shown. The derivation of the linear model by using system identification is shown in this chapter. It is shown that the linear model can be used for controller design, although this dissertation does not focus on the design of controllers.

In chapter 6 general control problems in the rolling mill environment are discussed and an initial control problem formulation is stated. The proposed control method, Model Predictive Control (MPC), is discussed and controller specifications for this method are identified.

In chapter 7 conclusions are drawn and contributions discussed. Some recommendations for future research projects regarding rolling mill modelling and rolling mill control are identified and briefly discussed.

Table 1.1: Organization of this dissertation.

Chapter	Description
1	**Introduction:** A general introduction of the rolling mill environment is given.
	A motivation for this dissertation and the control problem formulation is given.
2	**Process description:** A general description of the practical operation of a Stec-
	kel rolling mill is given. The hot rolling process is described, focussing on: material
	behaviour in the roll gap; tension in the sheet whilst rolling; the mill stand's
	elastic stretching; the elastic bending of the rollers.
3	**Model derivation:** The models identified to simulate the thickness profile behaviour
	and the strip tension behaviour while rolling are discussed and derived.
	The roll gap model, stand model, hydraulic actuator model and tension
	models are derived and discussed in more detail.
4	**Nonlinear plant simulator:** The solution methodologies and steps followed to
	solve the models identified in chapter 3 and to incorporate them into the simulator
	are discussed. The practical input data for the simulator are identified and
	analyzed. Model coefficients are calculated and motivated.
5	**Simulation results:** Simulation results of model components are given.
	The strategy followed to identify the linear plant model is described, and
	the resulting LTI MIMO transfer function model is derived.
6	**Control problem formulation:** An initial control problem formulation is given. Constraints
	are defined on the manipulated variables and the output variables. These constraints
	result in a constrained optimization problem of a performance index associated
	with Model Predictive Control.
7	**Conclusions and recommendations:** A summary of the work and its contributions are given.
	Suggestions for future research projects are also given.

Chapter 2

Process Description

2.1 Introduction

In this chapter a general process description of the steel manufacturing process is presented. This is done in order to show where the hot rolling mill fits into the steel manufacturing process. In this dissertation the focus falls on a Steckel Hot Rolling Mill process, and the practical operation of a hot rolling mill process is described according to how a Steckel Rolling Process is operated. The mechanics of the rolling process is also discussed, and the reader is referred to the appendix for the definitions of some rolling terms that are used in this chapter and throughout this dissertation.

2.2 General Production Route

The production of steel can be characterized into three areas where processing takes place namely, Iron Manufacturing, Steelmaking and Rolled products [21].

Iron making or manufacturing can be defined as the extraction of metallic iron from iron ore via a reductant such as coal or natural gas. Application of this principle gives rise to a number of possible processing routes, of which only a few are implemented in industry. In the Blast Furnace Route, coke is manufactured from coal via the coking plant, and sinter (partially reduced iron ore) is produced by a sinter plant using fine ore and dolomite in a reducing atmosphere. These, along with pulverized coal, dolomite and iron ore are the raw materials used by the blast furnace to produce pig iron. The pig iron is produced in a molten state and still contains many impurities. The next processing step of the pig iron is conducted at the steel plant.

The Direct Reduction Route has two common types of direct reduction furnaces and the product of the direct reduction process is referred to as DRI (direct reduced iron). Firstly a vertical shaft furnace where pelletized ore is fed to the top of the furnace, whilst a reducing gas, such as reformed natural

gas, is fed in a countercurrent fashion from the bottom. Reduction of the particles takes place during retention inside the furnace and the reduced iron particles with high metallic iron content are extracted at the bottom.

The second type of direct reduction process is a rotary kiln process. Coal, iron ore and a desulphurising agent such as dolomite are fed countercurrent, combusting the carbon monoxide product above the solids bed to provide heat. The degree of metallization is also determined by the retention time in the kiln. After the product is cooled, it is separated into metallic and non-metallic fractions.

Steelmaking can be defined as the purification of the products of ironmaking to yield desired steel grades. Two routes for steelmaking exists in the industry namely the the Basic Oxygen Furnace (BOF) Route and the Electric Arc Furnace (EAF) Route.

In the BOF Route, Pig-Iron is transferred from the blast furnace to the BOF. DRI and scrap metal are introduced along with various fluxes and oxygen as required. The main reaction in the process is oxidation of excess carbon. From the BOF, the molten steel is tapped into a ladle and taken to the Secondary Steelmaking process/plant.

In the Electric Arc Furnace (EAF) Route, DRI and scrap metal are used as raw material inputs for this process. The material inputs (charge) are melted by transmitting huge quantities of electrical energy through electrodes into the charge. Oxygen is also blown into the charge to assist with the release of carbon and other impurities. The molten steel is tapped into a ladle and taken to the Secondary Steelmaking process. For more information on the working of the EAF process the reader is referred to [22].

During the Secondary Steelmaking process argon is injected as a means of stirring the molten steel. Alloys are added, degassing performed and sometimes powder reagents are injected as required. From this stage of processing the molten steel, with the desired steel grade and temperature, is taken to the continuous caster.

During the continuous casting process molten steel is poured into a tundish, that acts as a reservoir, at the top of the machine. It is fed through a water cooled mould and sprayed with water to produce a continuous slab, billet or bloom depending on the mould size and its shape. The slabs, billets or blooms are transported to the hot rolling mill for further processing. For more information on continuous casting the reader is referred to [23].

Steel products can be classified according to shape, such as flat products and long/structural products. Slabs are used to roll flat products such as steel plate or strip, while blooms and billets are used to roll long products such as beams.

Semi-finished products are first reheated in a reheating furnace to about 1200°C. These products are then fed to the applicable roughing mill where the initial reduction is performed until the shape and dimension approaches values that can be handled by the finishing mill. Plate mills and strip mills

handle slabs. Blooms and billets are handled by long product mills.

The processing of plates in a plate mill consists of turning the plate 90° after some passes and effectively rolling the plate in the length and the width. Plate is perhaps 10 to 20mm thick and up to 3 meters wide.

Strip, produced from slab, is further processed by a finishing mill until the desired reduction and dimension are achieved for the strip. The long strip is cooled on a run-out table with water curtain sprays installed in order to ensure that the right coiling temperature is achieved, which will guarantee the required mechanical properties. The cooled down strip is then coiled or cut up in sheets.

An alternative finishing strategy is the so-called Steckel mill (see figure 2.2), which is the focus of this investigation and will be described in more detail in the following sections.

If necessary, the coiled product can be treated further by means of cold rolling to improve surface quality and of course to produce a thinner product.

A roughing mill also handles the initial stage of processing of blooms and billets. After the roughing stand, the piece of steel passes through a succession of finishing stands that change its size and shape. In a universal mill, all sides of the product are rolled at the same time, whilst in other mills only two sides are rolled at a time, and the product has to be turned over to allow rolling on the other sides.

Long products are produced in a vast number of shapes and sizes. They can have cross-sections shaped like a H, I, U, T, squares, rectangles, circles, hexagons, angles and rails.

Forms of further processing that hot rolled products may undergo before they are finally used to make an end product include the following:

- Fabricating: Steel sections are cut, welded and otherwise prepared to form the steel frame of a building.
- Coating: Corrosion preventative coatings are applied to the steel surface.
- Cold rolling and drawing: Changes thickness and surface quality.
- Profiling: Sheet pressed into the correct shape for specific applications.

2.3 Hot Rolling Process Flow

A typical reversing hot rolling process with a Steckel mill as the finishing mill consists of the following units, as can be seen in figure 2.1 [21, 4, 1]:

- Slab reheat furnace: After the continuous casting of the slabs they are stored until the hot rolling mill process is ready for further working of the slab. These slabs are reheated to a

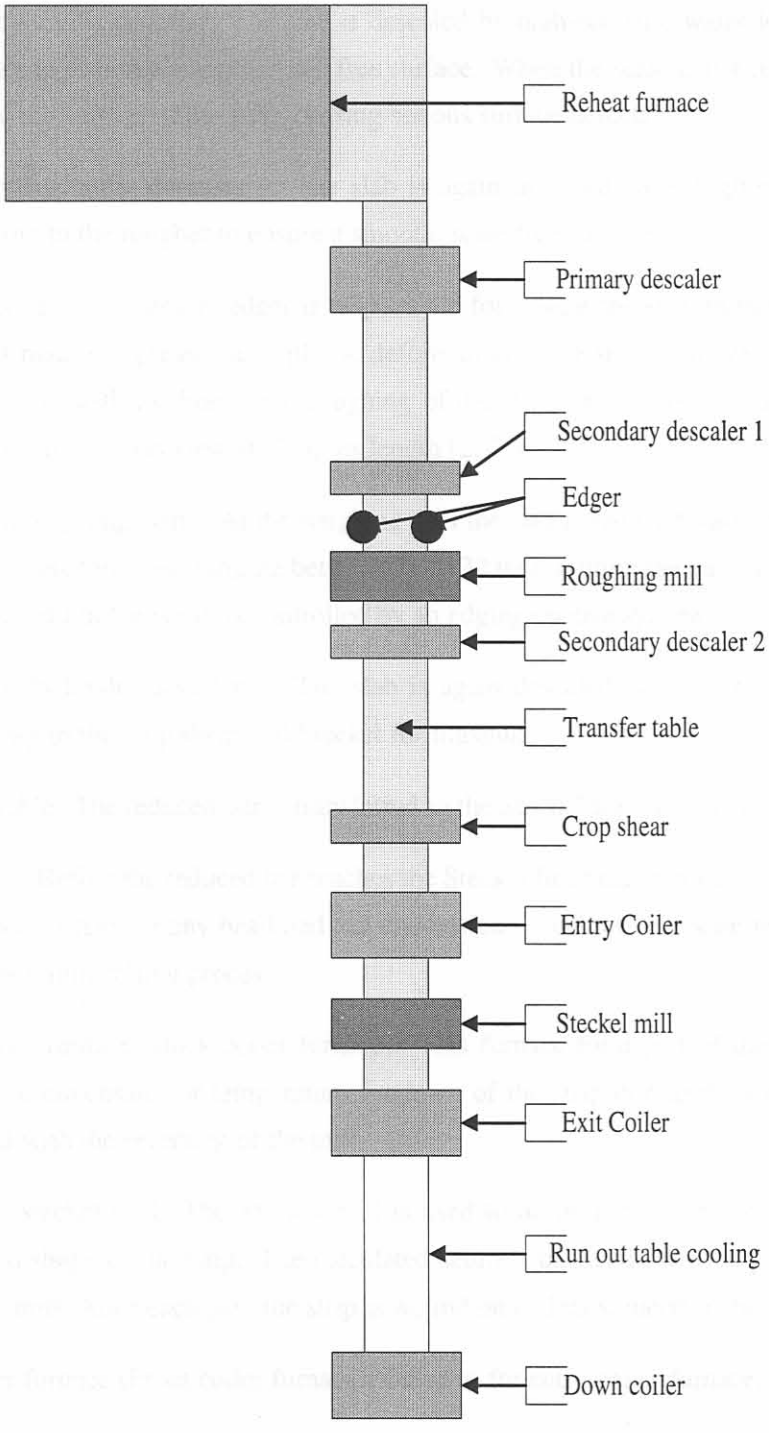

Figure 2.1: Hot rolling process flow.

temperature in excess of 1200°C. The slab is discharged from the reheat furnace at a pre-set discharge temperature, as calculated by the setup program. The temperature is measured and a recalculation of the Rougher setpoints is performed to ensure that the material can be rolled.

- Primary hydraulic descaler: The slab is descaled by high-pressure water jets before going to the rougher to ensure a smooth, scale free surface. When the scale is not removed the scale is rolled into the surface of the strip, causing serious surface defects.
- Secondary hydraulic descaler 1: The slab is again descaled, with high-pressure water jets, before going to the rougher to ensure a smooth, scale free surface.
- Vertical edger: The vertical edger is responsible for rolling the strip in the width to limit the amount of material spread due to plastic deformation of the strip. This vertical edging is done in conjunction with the horizontal roughing of the strip. The resulting strip has a dog-bone shape, when the strip is viewed along its length [2, 24].
- Horizontal roughing stand: At the roughing mill the slab is reduced through a set of passes to an intermediate thickness ranging between 22 to 32 mm. During the passes at the Rougher, the material spread in the width is controlled by an edging control system.
- Secondary hydraulic descaler 2: The slab is again descaled, with high-pressure water jets, before going to the crop shear and Steckel for finishing.
- Transfer table: The reduced bar is transferred to the Steckel finishing stand on this table.
- Crop shear: Before the reduced bar reaches the Steckel finishing stand the head- and tail pieces are cropped to remove any head and tail end- defects, such as crocodile teeth[1] [2], caused by the roughing mill rolling process.
- Entry coiler furnace (Back coiler furnace): This furnace form part of the finishing mill and is used to compensate for temperature rundown of the strip due to the longer process times associated with the reversing of the mill.
- Finishing Steckel mill: The Steckel mill is used to accurately control the centerline gauge, profile and shape of the strip. The calculated setup is changed for each pass before the strip enters the mill. After each pass the strip is wound on coilers situated in the coiler furnaces.
- Exit coiler furnace (Front coiler furnace): Same as for entry coiler furnace.
- Run-out table cooling: When the strip completes its passes on the Steckel mill and is on final gauge, the strip is cooled by water curtains on the run-out to table fix the microstructure of the metal and thus its mechanical properties [25, 5].
- Down coiler: After the completion of the previous steps, the strip is coiled on the downcoiler for packaging or to be cut up into plates at the dividing shear.

Before a slab can be rolled, certain critical control setpoints are calculated. The setpoint calculation determines rolling parameters such as [21]:

- Reheat furnace discharge temperature;
- Number of odd passes to be completed by the roughing mill;
- Number of odd passes to be completed by the Steckel mill;
- The reduction taken at each pass for both the roughing and Steckel mill;
- The magnitude of edging for each pass on the roughing mill;
- Shape control settings for each pass on the finishing Steckel mill;
- Descaling practice for each pass on the Steckel mill;
- Run-out table cooling settings, e.g. run-out table speed and water cooling spray patterns;
- Downcoiling temperature of the strip.

The setup and control strategy selection falls into Level 2[2] of the automation control system architecture [1]. There are two main approaches that exist for setpoint calculation [21, 6, 26]:

- The first is based on experimental data gathered from rolling test slabs from which fixed setpoints for each material type, width-group and aimed gauge are calculated. These rolling schedules are stored in tables and referenced when the mill is setup for a slab. This approach does not allow for process variations and does not yield very good quality steel. This type of scheduling is not used much in modern times.
- The second approach is based on mathematical models that simulate the interaction between the material and the mill [1]. Using an optimization search criteria, the optimal solution, the rolling setup, is found by solving a static optimization problem. The employed models used in this optimization problem are adapted on a long time scale and after each pass the setup schedule is updated during the completion of the rolling schedule as soon as plant measurements become available. The long term adaption of the process models is termed bar-to-bar adaption and the updating of the rolling schedule is termed in-bar adaption.

[1]This is encountered when the head or tail end splits open like a gaping mouth of a crocodile.

[2]In [1] the control system architecture is explained for the rolling mill environment. Level 1 is the dynamic control level accounting for dynamic control. Level 2 is termed as the supervisory control level. Level 3 is termed as the plant wide control level. Level 2 is responsible for mill setup, slab routing, fault diagnosis, maintenance management, direct tracking and analysis, alarm management, statistical process control and data analysis. Level 3 is responsible for dynamic scheduling, order book management and batch tracking.

The Steckel mill pass schedule calculation is an iterative steady state optimization problem that finds an optimal or suboptimal solution for the various criteria [1, 21]:

- The minimum number of odd passes;
- The correct shape at final gauge;
- Rolling forces and rolling torque that are within the mill designed specification;
- The correct profile at 9 mm thickness[3];
- Work roll bending requirements that are within the control range;
- Run out table cooling and mill speeds that will ensure the correct downcoiling temperature for the required mechanical properties of the material.

Before each pass a recalculation of the Steckel mill setpoints are done and the setpoints are updated (in-bar adaption). The procedure normally followed is:

- Setting the roll gap using the Automatic Gauge Control (AGC) System;
- Shifting the work rolls laterally for a predefined distance to minimize work roll wear (20 mm each time);
- Apply pre-bending to the work rolls for profile and shape control;
- Squaring the strip to the center line of the mill using side guides;
- For each pass the strip is passed through the roll gap and wound in the opposite coiler furnace, where the strip is annealed while the pass is completed;
- During rolling the bending of the work rolls is dynamically controlled to ensure the correct shape and profile of the strip. Whilst the strip is thicker than 9 mm, profile control is performed, and below this gauge shape control is done. The profile of the strip is typically measured using a scanning X-Ray thickness measurement device. The movement of the strip and the fixed position of the scanning X-Ray give a zig-zag reading of the strip crown. The shape and flatness is measured after the completion of the rolling passes by a surface inspection system that can for example use neural network technology and intelligent image processing algorithms to identify shape/flatness defects such as quarter buckle [1].
- The Automatic Gauge Controller (AGC) controls the roll gap to ensure a constant centerline thickness along the length of the strip;

[3]It is generally regarded that below 9mm of thickness, little control can be exerted in order to control the strip profile. The strip shape and flatness are controlled during the later passes when the strip thickness is less than 9mm.

- The BISRA-Davy gauge-meter compensator predicts the stretch in the mill housing [27, 1] due to the rolling forces and adds a trim to the setpoint of the roll gap setting. In order to compensate for the stretch the roll gap setting is manipulated in order to achieve the required draft. This compensator employs a positive force feedback strategy in order to regulate the output gauge.

Because the strip thickness is measured some distance from the mill bite, a normal closed loop control strategy will either be too slow or unstable due to transport time (t_d). To combat this phenomenon a Smith predictor is normally employed in the feedback loop to compensate for the transport delay [20].

2.4 Steckel Finishing Mill

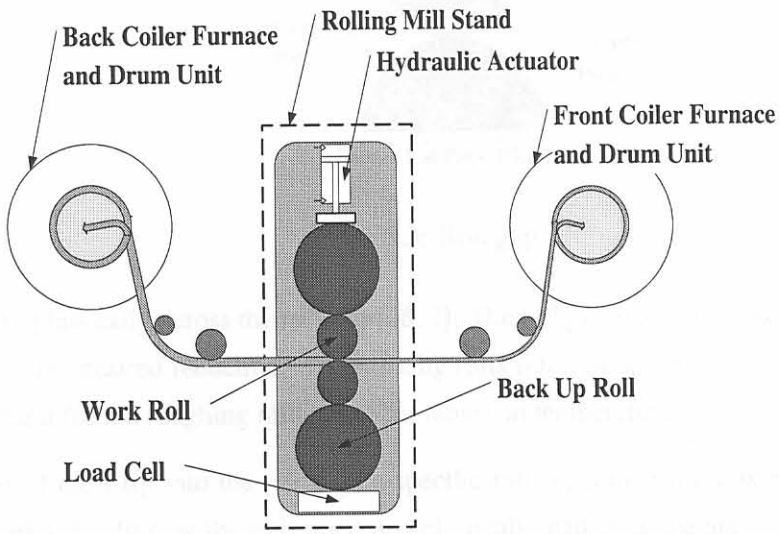

Figure 2.2: Steckel Hot Rolling Mill.

Rolling is the process of shaping metal by passing it between rolls revolving at the same peripheral speed and in opposite directions. The Steckel mill (see figure 2.2) is usually a single stand, four high, reversing mill consisting of two work rolls and two back up rolls. The mill employs multiple passes to achieve the desired final thickness reduction of the strip. The reversing of the strip during the multiple passes results in a temperature rundown of the strip. This temperature reduction makes it more difficult to to work the strip as the rolling forces increase. The temperature rundown is compensated for by winding the strip on coiler drums situated in coiler furnaces regulated at a temperature of $970°C$.

Massflow holds across the roll gap [2, 28] (see figure 2.3), and with negligible metal spreading in the width of the strip, it is found that:

$$v_1 h_1 = v_2 h_2 \tag{2.1}$$

v_1: strip's entrance velocity into the roll gap

h_1: strip's entrance thickness into the roll gap

v_2: strip's exit velocity from the roll gap

h_2: strip's exit thickness from the roll gap

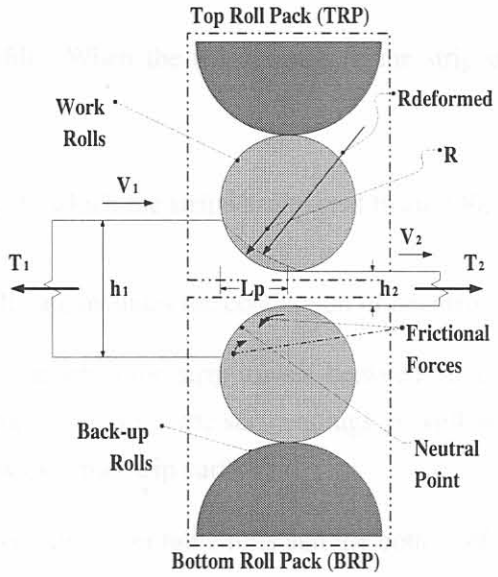

Figure 2.3: Roll gap.

The metal flows plastically across the roll gap [28, 2]. The roll gap is set at a gap setting calculated in order to achieve the desired reduction. The working rolls rotate at a speed, v_{roll}, and the strip enters the finishing stand from a roughing mill, on roller tables, at temperatures in excess of $1000°C$.

Upon entrance of the strip into the roll gap, a specific roll separating force is exerted by the metal strip on the work rolls, forcing the rolls apart and elastically flattening the arc of contact. The rolling mill frame has a finite stiffness and stretches due to this forcing phenomenon. This stretch affects h_2 adversely. The working rolls furthermore bend elastically over the width of the strip [7, 10]. This elastic deformation is due to the separating force that pushes the working rolls further apart. The uncontrolled elastic bending of the rolls is greater in the mill center. The plastic behavior of the metal in the roll gap assures that the metal fills the whole gap, thus due to the bending of the rolls the strip is thicker at its center. This thickness deviation of the strip over the width is defined as crown.

Factors that influence the strip crown and shape are [29]:

- Initial roll camber: The rollers can have a natural positive or negative camber (crown). In this dissertation it is assumed that the natural camber is zero.
- Roll thermal camber: The temperature build-up on the rollers creates thermal expansions of the roller diameters (especially the work rolls).
- Roll deflection: The elastic bending of the rollers falls into this category.

- Roll wear: The rolling campaign determines how much the rolls deteriorate with time due to wear. Rolls are typically changed after the rolling of 16000 km strip.
- Material structure: If the material is hard the roller wear is greater and the roller deflection is also significant.
- Strip temperature profile: When the temperature of the strip declines it becomes harder to deform the strip.

The elements of heat transfer to which the strip is subjected to are [30, 25]:

- Heat transfer in the roll gap, includes the conduction of heat from the strip to the working rolls.
- Radiation and convection when the strip travels between the coiler furnaces account for the heat that is radiated from the strip to the surroundings as well as the convection cooling of the strip due to the air flow over the strip surfaces.
- Heat conduction between the roller table rolls and the bottom of the strip.
- The descaling sprays situated between the coiler furnaces and the finishing rolling stand cool down the strip, by spraying the strip with water at a temperature of typically 35°C.
- The sheet is reheated in the coiler furnaces to compensate for heat loss during the completion of the pass.

Temperature of the strip as a function of time and position in the mill is of great importance because the temperature of the strip influences the material yield stress and in effect the rolling loads. The thermal crown on the working rolls increases with strip temperature and the amount of plastic working in the roll gap [10], and influences the output thickness crown of the strip. Heat transfer during rolling is investigated in [30] and only an introduction to the heat transfer problem is given in this dissertation, as modelling of heat transfer phenomena falls outside the scope of this work.

Slipping occurs between the work rolls and the strip along the arc of contact, and thus the strip speed is only equal to the work roll speed at the neutral point (see figure 3.2). The velocities, v_1 and v_2, are respectively slower and faster than the roll speed. This results in friction forces acting along the arc of contact that pull the strip into the roll gap. At the exit of the roll gap the friction forces are reversed and oppose the delivery of the strip from the roll gap [2]. The net effect of these friction forces is the creation of a friction hill [28, 2, 24].

The position of the neutral point can be shifted by applying tension to the strip between the down coiler and the roll gap (back tension, T_2) as well as between the up coiler and the roll gap (front tension, T_1). If back tension is applied the neutral point moves towards the entrance of the roll gap and with the application of front tension the neutral point is shifted towards the exit of the roll gap.

The application of tension to the strip reduces the rolling load by means of reducing the friction force components. The application of back tension is more effective in reducing the friction force component of the rolling load than the application of front tension [2].

The working rolls also deform elastically along their axis and over the width of the sheet [2]. This elastic deformation is due to the separating force that pushes the working rolls further apart. The elastic deformation of the rolls is greater in the center of the sheet, due to the fixed end positions of the roll neck of the rolls. This elastic deformation of the work rolls has the effect to make the sheet thicker in the center than at the edges, thus giving the sheet a positive crown[4].

2.5 Conclusion

In this chapter a brief discussion was given on where the hot rolling process fits into the steelmaking process. The practical operation of a hot rolling process was described and discussed, and the elements of the hot rolling process were identified and described. The Steckel finishing hot rolling mill is the focuses of this dissertation, and in this chapter this finishing mill was defined and discussed. Lastly the general process behaviour of the Steckel rolling mill was discussed.

In the following chapter the nonlinear models necessary to simulate the centerline thickness and tension in the sheet whilst rolling are identified. These models are developed mathematically and further process behaviour is discussed during the model derivations.

[4] In the Appendix rolling definitions are given.

Chapter 3

Simulator model derivation

3.1 Introduction

This section deals with the identification of models that are deemed necessary to adequately simulate the thickness profile behaviour of the strip as well as the tension in the sheet whilst rolling. Nonlinear and linear model derivations are shown and some modelling choices are motivated for these models. In this chapter use will be made of general rolling terms. Some of these terms are defined in Appendix A.

3.2 Nonlinear models

The hot rolling mill process is a very complex process to model. The complexity is dependent on the desired capability and accuracy of the mill simulator. Most of the process variables are implicit functions of other process variables, requiring iterative numerical solution methods. The main protagonist of the rolling process is temperature [31], and temperatures of the strip and the rollers influence rolling variables such as the rolling force, rolling torque, crown, and mechanical properties of the product to name a few. The heat transfer problem associated with the Steckel hot rolling mill is very complex [32, 33], and some aspects of this problem will be discussed later in this chapter.

The models identified in this dissertation and their relative dependencies are shown in figure 3.1. The models and their function as part of the simulator can be described as:

1. **Roll gap model:** The roll gap model predicts the specific rolling load across the width of the strip. This model forms the connecting block between all the possible models of the simulator.

2. **Stand model:** This model describes the elastic stretch of the mill stand due to the rolling of the strip as well as the work roll and back-up roll interface flattening. The result is a deviation

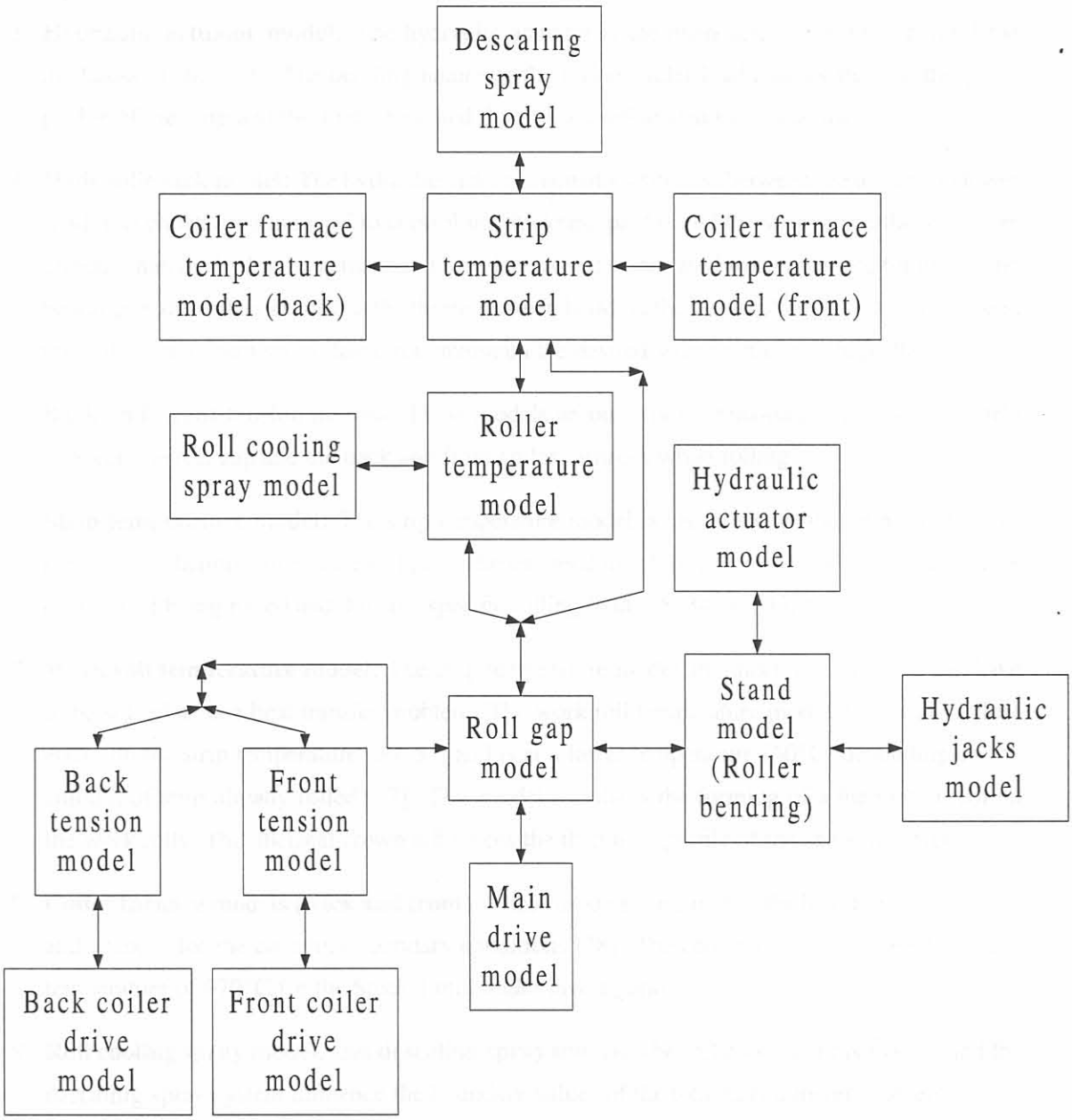

Figure 3.1: Models identified in order to constitute a comprehensive nonlinear mill simulator.

in the draft from the setup reduction draft. The roll bending phenomena of the rollers are incorporated in the stand model. The modelling of the bending phenomena adds the capability of strip thickness profile simulation to the mill simulator. This model can be 3-dimensional or 2-dimensional as shown in [10]. The 2-dimensional model's coordinates are perpendicular and form a yz plane to the rolling direction (x) with the origin chosen at the center of the roll gap.

3. **Hydraulic actuator model:** The hydraulic actuator is the main actuator used to control the thickness of the strip. The bending nature of the rollers under load assures that the thickness profile of the strip and the strip shape and flatness are influenced by this actuator.

4. **Hydraulic jack model:** The hydraulic jacks are actuators situated between the upper and lower work roll chocks and are used to control the thickness profile and the strip shape/flatness more directly than the hydraulic actuators. These jack actuators are used to compensate for the elastic bending of the rollers as well as the thermal crown build on the work rollers, by striving to bend the rollers in a counterwise fashion to maintain the desired strip profile and shape/flatness.

5. **Back and Front tension models:** These models account for the tension behaviour in the strip between the roll gap and the back and front coiler furnaces while rolling.

6. **Strip temperature model:** The strip temperature model is necessary to find an accurate temperature prediction value in the roll gap. The temperature of the sheet influences the yield stress of the steel being rolled and thus the specific rolling load [28, 34, 35, 36, 11].

7. **Work roll temperature model:** The strip temperature model and this model interact and have to be solved as one heat transfer problem. The work roll temperature model has a roll chilling effect on the strip temperature [30, 32] and is at a lower temperature (60°C) depending on the amount of strip already rolled [37]. This model simulates the forming of a thermal crown on the work rolls. This thermal crown influences the thickness profile of the sheet adversely.

8. **Coiler furnace models (back and front):** These models form part of the heat transfer problem and account for the changing boundary conditions [38]. The coiler furnaces are regulated at a temperature of 970°C for the Steckel mill under investigation.

9. **Roll cooling spray model, and descaling spray model:** The roll cooling spray system and the descaling spray system influence the boundary values of the total heat transfer problem.

10. **Mill drive and motor model:** The main drive model incorporates the motor dynamics into the problem. With this model a controller can be designed using the current of the motor in order to control the roll speed and the rolling torque. This model can also be used to investigate the rotational vibration of the connecting spindles on the plastic deformation process in the roll gap [39]. In [40], this mill chattering effect is noted as one of the causes of the asymmetrical vertical displacement for a 2-dimensional stand model.

11. **Back coiler and front coiler drive and motor models:** Two similar motors are used for each coiler and these models will be essentially the same. These two models will also be similar to the main mill drive motor model. These models also relate the speed of the coilers to the motor dynamics and drive dynamics. The limitation of the drive motor can place a limit on the amount of tension control that can be applied.

Not all of these identified models will be modelled in this dissertation. The following models will not be modelled, and the influence on the simulator this lack of modelling will have as well as possible means for compensating for these deficiencies are as follows:

- **Temperature models:** Although temperature was identified as an important parameter, the modelling of the heat transfer problem is too complex for the proposed investigation. The necessary temperature inputs for the simulator are obtained by conditioning practical plant data of the Steckel hot rolling mill under investigation.
- **Main Mill Drive:** The main mill drive speed is not considered as a manipulated variable in this dissertation. Little insight other than the effect of torsional vibrations of the spindles on the roll gap deformation process could be gained by modelling the main mill drive and its connecting work roll shafts in detail.
- **Coiler Motor Drives:** The dynamics of the coiler motors and their loads, which they drive have large inertias that limit the severity of the control action that can be taken for tension control, e.g. speed up/down of the coiler drums. The modelling might be deemed necessary in order to identify possible velocity actuator limits.
- **Hydraulic Jack models:** The simulator developed in this dissertation is not aimed at investigating profile and shape control methods, although some fundamental theory is addressed and some initial modelling is done concerning strip profile and shape issues. In this dissertation these actuators are modelled as discrete spring elements forming part of the stand model.

In the rest of this chapter, nonlinear and linear models for the roll gap, rolling mill stand and strip tension will be derived and an introduction to the heat transfer problem will be discussed.

3.3 Roll gap model

3.3.1 Introduction

Roll gap models can be divided into two groups, namely analytical rolling theory models and numerical Finite Element models. Usually the analytical models is static used for predicting the rolling force

and torque. The Finite Element models either predicts the rolling force and torque or the material behaviour.

Many roll gap models of varying degree of complexity exist in the literature, and the roll gap model is constantly refined and the current trend is to use Finite Element Methods (FEM) to solve the stress-strain partial differential equation model of the roll gap in order to model the plastic metal flow through the roll gap and the microstructure evaluation of the material [36, 41, 42, 43].

The pioneering work on analytical rolling theory models was done by Siebel and Kármán in 1924 and 1925 [28, 44]. Orowan (1943) extended this work and based his analysis on a simplifying assumption that the deformation in the roll gap resembles the compression between rough inclined plates [44]. A similar problem was solved partially by Nadai in 1931. Sims (1954) simplified Orowan's differential equation model by solving the differential equation for certain rolling conditions, for example rolling where sticking friction is assumed [44]. Current research on analytical rolling theory models focuses on special investigations on the roll gap geometry and the angle at which the strip enters the roll gap. One such example of roll gap geometry investigation is discussed in the article by Fleck et al. [45] dealing with cold rolling modelling.

It must be stressed that the Orowan roll gap model is used as a benchmark to validate the performance of other analytical models, such as Sims's model [44] and the Ford and Alexander model [46], as well as FEM models [36]. The theory of plasticity [47] can be used to model the plastic flow through the roll gap and these models are then solved using FEM [41, 42, 43]. These static models accurately describe the stress, the strain and the strain rate which the metal is subjected to by solving the partial differential equations such as the strain rate tensor. For the mechanics of engineering metals (yield criteria, structural analysis, plasticity) the interested reader is referred to [47, 48].

The thermal analysis combined with the roll gap analysis was done by Samarasekera et al. [33] using a FEM model. This article, which forms part of a larger research program is concerned with a static study focussing on the thermo-mechanical system found in the roll gap. This program is aimed at predicting more accurate rolling forces and torques for a hot rolling process [35, 36] as well as the mechanical properties of the strip, by modelling the microstructural evolution of the material by computing the austenite grain size of the strip during hot rolling [11]. The modelling of the microstructural evolution in the roll gap is not the main focus of this dissertation, where the only requirement is to predict the rolling force. Orowan's model has been tried and tested and adhere to the stated requirement, and is thus adequate for use in this dissertation.

The rolling load is a function of the material yield stress (k), rolling geometry and the applied tensions to the strip. The material yield stress is a function of the type of material being rolled, its temperature, the thickness reduction (draft) and the rolling speed. These variables are defined in the sections that follow together with the derivation and adaption of Orowan's model for use in the simulator. Next Orowan's roll gap model will be derived and discussed.

3.3.2 Orowan's differential equation derivation

Table 3.1: Definition of variables for the Orowan model.

Symbol	Definition
$\mu =$	friction coefficient (no dimension)
$s =$	normal roll pressure along the arc of contact (Pa)
$f =$	horizontal force in the roll gap (N)
$p =$	vertical pressure in the roll gap (Pa)
$h_1 =$	sheet centerline thickness at the entrance of the roll gap (m)
$h_2 =$	sheet centerline thickness at the exit of the roll gap (m)
$k(\epsilon, \dot{\epsilon}, \theta) =$	yield stress of the material being rolled (Pa)
$\epsilon =$	strain ($\frac{m}{m}$)
$\dot{\epsilon} =$	strain rate (s^{-1})
$v_{roll} =$	rolling velocity ($m.s^{-1}$)
$R =$	roll radius (m)
$R' =$	deformed roll radius (m)
$\sigma_1 =$	tension stress in the strip at the entrance of the roll gap (Pa)
$\sigma_2 =$	tension stress in the strip at the exit of the roll gap (Pa)
$x_{rg} =$	x coordinate, with the origin at the exit of the roll gap (+ direction against rolling direction) (m)
$\phi_m =$	bite angle (rad)
$\phi =$	angle of arc of contact, measured from the exit of the roll gap (rad)
$\overline{\sigma}(\epsilon, \dot{\epsilon}, \theta) =$	mean flow stress in the roll gap (Pa)
$\theta =$	temperature (°C)
$P' =$	specific rolling force, taking the deformed roll radius into account ($\frac{N}{m}$)
$L_p =$	length of the arc of contact (m)
$S_{arc} =$	arc length of the arc of contact (m)
$\delta = h_1 - h_2$	draft, thickness reduction across the roll gap (m)

Orowan's theory for the calculation of the specific rolling force is implemented [28, 49] in this dissertation. The static model prediction of the specific rolling force is influenced by the strip temperature, roll radius and the deformed roll radius, rolling speed, the material being rolled and the applied tensions.

Orowan's differential equations for the vertical roll pressure and the horizontal roll force in the roll gap will be derived referring to figure 3.2 and table 3.1, where all the necessary variables are defined. The first step in the derivation of the model is to equate the horizontal force balance on the roll gap

element. This force balance is as follows:

$$f(x_{rg}) - f(x_{rg} + dx_{rg}) + 2s(x_{rg})sin\phi\frac{dx}{cos\phi} \pm 2\mu s(x_{rg})cos\phi\frac{dx_{rg}}{cos\phi} = 0, \tag{3.1}$$

note that the top and bottom signs of the double signs ($\pm$ and $\mp$), in Eq. 3.1 and the rest of this derivation, is applicable to the entrance and the exit of the roll gap respectively. The first two terms on the left hand side of Eq. 3.1 can be expressed as,

$$f(x_{rg}) - f(x_{rg} + dx_{rg}) = \frac{-df(x_{rg})}{dx_{rg}}dx_{rg}. \tag{3.2}$$

Substituting the latter into Eq. 3.1 it follows that,

$$\frac{df(x_{rg})}{dx_{rg}} = 2s(x_{rg})\left[tan\phi \pm \mu\right]. \tag{3.3}$$

The horizontal coordinate can be approximated as follows,

$$x_{rg} \approx R'sin\phi. \tag{3.4}$$

Differentiating Eq. 3.4 gives,

$$dx_{rg} = R'cos\phi d\phi. \tag{3.5}$$

If Eq. 3.5 is substituted into Eq. 3.3 the derivative of the horizontal force along the arc of contact can be found,

$$\frac{df(\phi)}{d\phi} = 2R's(\phi)\left[sin\phi \pm \mu cos\phi\right]. \tag{3.6}$$

Equating a vertical force balance on the element of length dx delivers,

$$p(\phi)dx_{rg} = s(x)cos\phi\frac{dx_{rg}}{cos\phi} \mp \mu s(\phi)sin\phi\frac{dx_{rg}}{cos\phi}. \tag{3.7}$$

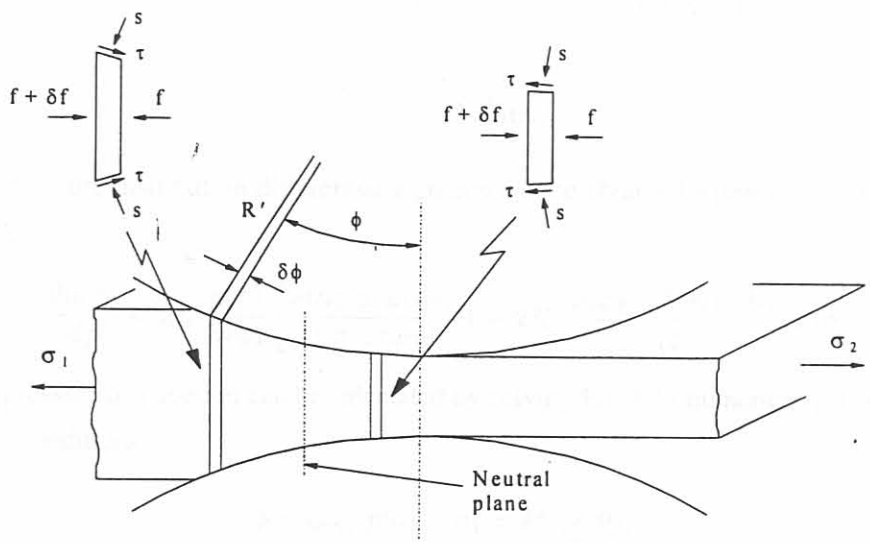

Figure 3.2: Forces acting upon the roll gap element (figure adapted from [1]).

Simplifying Eq. 3.7, the vertical roll pressure as a function of the arc of contact can be obtained,

$$p(\phi) = s(\phi)\left[1 \mp \mu tan\phi\right]. \tag{3.8}$$

Orowan [28] implemented the Huber-Mises yield criterion [24] to account for the plastic deformation in the roll gap. The resulting relation between the vertical roll pressure, horizontal force and yield stress is,

$$p(\phi) - \frac{f(\phi)}{h(\phi)} = k(\epsilon, \dot{\epsilon}, \theta). \tag{3.9}$$

If Eq. 3.8 and Eq. 3.9 are substituted into Eq. 3.6, Orowan's differential equation is obtained,

$$\frac{df(\phi)}{d\phi} = 2R'\left[\frac{f(\phi)}{h(\phi)} + k(\epsilon, \dot{\epsilon}, \theta)\right]\left[\frac{sin\phi \pm \mu cos\phi}{1 \mp \mu tan\phi}\right]. \tag{3.10}$$

The horizontal rolling force, $f(\phi)$, can be used to calculate the specific rolling force (P'), which is a function of the vertical roll pressure. Eq. 3.10 can be manipulated to express the derivative of the vertical roll pressure along the arc of contact.

Defining the spatial coordinate origin at the exit of the roll gap (ϕ and x increases against the rolling direction). The thickness of the sheet at any point in the roll gap can be expressed as:

$$h(\phi) = h_2 + 2R'(1 - cos\phi). \tag{3.11}$$

The Huber-Mises yield criterion (Eq. 3.9) can also be written as,

$$f(\phi) = h(\phi)\left[p(\phi) - k(\epsilon, \dot{\epsilon}, \theta)\right]. \tag{3.12}$$

Differentiating Eq. 3.12 and Eq. 3.11 it follows that,

$$\frac{dh(\phi)}{d\phi}\left[p(\phi) - k\right] + h(\phi)\frac{dp(\phi)}{d\phi} = 2R'p(\phi)\frac{(sin\phi \pm \mu cos\phi)}{(1 \mp \mu tan\phi)}, \tag{3.13}$$

$$\frac{dh(\phi)}{d\phi} = 2R'sin\phi. \tag{3.14}$$

The vertical pressure distribution differential equation can be obtained when Eq. 3.14 is substituted into Eq. 3.13,

$$\frac{dp(\phi)}{d\phi} = 2R'\frac{p(\phi)}{h(\phi)}\left[\frac{sin\phi \pm \mu cos\phi}{1 \mp \mu tan\phi}\right] - 2R'\frac{(p(\phi) - k(\epsilon, \dot{\epsilon}, \theta))}{h(\phi)}sin\phi. \tag{3.15}$$

The vertical pressure distribution can be calculated by solving Eq. 3.15 numerically using the following boundary conditions:

$$\phi = \phi_m,\ p(0) + \sigma_1 = k(\epsilon, \dot{\epsilon}, \theta); \tag{3.16}$$

$$\phi = 0,\ p(\phi_m) + \sigma_2 = k(\epsilon, \dot{\epsilon}, \theta). \tag{3.17}$$

When the vertical pressure distribution is integrated over the arc of contact, the specific rolling force per unit width can be calculated as follows:

$$P' = R' \int_0^{\phi_m} p(\phi) d\phi. \tag{3.18}$$

Assuming that ϕ is small, $1 - cos\phi$ can be substituted with its approximation ($\frac{\phi^2}{2}$) [2, 24], and Eq. 3.11 can be rewritten as,

$$h(\phi) = h_2 + R'\phi^2. \tag{3.19}$$

The arc of contact can then be calculated as,

$$\phi_m = \sqrt{\frac{h(\phi_m) - h_2}{R'}} = \sqrt{\frac{\delta}{R'}}, \tag{3.20}$$

and the horizontal length of the arc of contact is approximated as the arc length,

$$L_p = S_{arc} = R'\phi_m = \sqrt{\delta R'}. \tag{3.21}$$

3.3.3 Roll gap variables

In the previous section and table 3.1 the roll gap variables are listed without a proper description of their characteristics and their influences on the solution methodology of the differential equation model. These variables are mainly functions of temperature, material properties and the draft taken.

3.3.3.1 Deformed roll radius

The vertical rolling pressure causes the work roll to flatten along the arc of contact. For hot rolling processes this flattened arc can be modelled as a larger circular radius with a shifted center [44, 46, 3]. This assumption however might not hold for cold thin strip rolling, temper rolling and foil rolling where the modelling of the roll gap can consist of an alternating combination of five elastic and plastic deformation regions [45, 49].

The specific rolling force, P', is however dependent on the deformed roll radius, R', and the deformed roll radius is again dependent on the specific rolling force associated with the deformed roll radius. This implicit relationship necessitates an iterative solution process in order to solve for the specific rolling force and the deformed roll radius.

The flattened arc radius is calculated using Hitchcock's formula [44, 28]:

$$R' = R\left[1 + \frac{16(1-\nu^2)P'}{\pi E \delta}\right], \tag{3.22}$$

where ν is Poisson's ratio for steel (0.3) [2] and E is Young's modulus of the work rolls.

Elastic recovery of the strip [28, 3] changes the roll gap behaviour. At the entrance and exit of the roll gap there are regions where the strip does not deform plastically but rather elastically, due to higher values of yield stress at these points. The effect of this strip elastic recovery is that the exit thickness of the roll gap is not the final strip thickness and the strip recovers over some small distance to its final thickness. The final sheet thickness is greater than the compressed exit thickness from the roll gap. At the entrance of the roll gap the entrance thickness is elastically compressed before plastic deformation occurs.

Modifying Orowan's differential equation model (Eq. 3.15) by substituting an elastic relationship, instead of the Huber-Mises plastic yielding relationship (Eq. 3.9), into Eq. 3.10 the same differential equation model can be used to solve for the elastic recovery regions of the roll gap. For hot rolling, these elastic recovery effects are negligible and can be omitted from the simulator without loss of generality [3].

3.3.3.2 Friction Coefficient

In the case of hot rolling the friction coefficients at the work rolls and strip interfaces generally fall in the following range: $0.25 \leq \mu \leq 0.45$. A lubricated roll gap exhibits smaller friction coefficients ($0.25 \leq \mu \leq 0.31$) whilst in unlubricated cases the coefficients are between 0.31 and 0.45 [45, 34, 36, 49]. In this work the friction coefficient was taken as a linear function of the roll gap temperature, θ, as follows [50]:

$$\mu(\theta) = 4.86 \times 10^{-4}\theta - 0.0714. \tag{3.23}$$

The friction coefficients of the mill simulator over the temperature range under investigation are,

$$0.342|_{\theta=850^\circ C} \leq \mu(\theta) \leq 0.405|_{\theta=980^\circ C}, \tag{3.24}$$

which correspond to the unlubricated cases.

3.3.3.3 Yield stress model

The material characteristics of the strip are taken into account in this model. Different relationships can be used to describe the flow stress of the metal in the roll gap. Yield stress criterions, such as the Tresca, von-Mises and the Huber-Mises, relate the flow stress to the yield stress [47, 48, 24]. One such flow stress relationship is the Zener-Holoman equation, which describes the relationship between the mean flow stress ($\overline{\sigma}$), mean strain ($\overline{\epsilon}$) and the mean strain rate ($\dot{\overline{\epsilon}}$) which the material is subjected to in the roll gap [2]. This relationship (based on Arrhenius's law) takes the work hardening of the strip and the strain rate sensitivity of the material [34, 2, 24] into account as follows,

$$\overline{\sigma} = A\overline{\epsilon}^{n}\dot{\overline{\epsilon}}^{m} exp(\frac{Q}{R_{ideal}\theta}), \tag{3.25}$$

with,

Q: the activation energy for onset of plastic deformation;

m: the strain rate sensitivity exponent;

n: the work hardening exponent;

R_{ideal}: the ideal gas constant.

The mean strain rate can be calculated by taking the mean strain and dividing it by the time it takes for the material to travel through the roll gap,

$$\dot{\overline{\epsilon}} = \frac{\overline{\epsilon} v_{roll}}{L_p} = \frac{ln\left(\frac{h_1}{h_2}\right) v_{roll}}{\sqrt{R'\delta}}. \tag{3.26}$$

If an appropriate yield criterion is used the yield stress of the material can be calculated from the flow stress across the roll gap [24, 2]. The von-Mises yield criterion defines the mean flow stress as,

$$\overline{\sigma}(\epsilon, \dot{\epsilon}, \theta) = \frac{\sqrt{3}k(\epsilon, \dot{\epsilon}, \theta)}{2}. \tag{3.27}$$

Another approach is to use an equation that relates the yield stress to the roll gap geometry and the temperature in the roll gap as follows:

$$k(\epsilon, \dot{\epsilon}, \theta) = k_{fo} exp^{-k_f \theta} \left(\frac{v}{\sqrt{R'h_1}} \sqrt{\frac{h_1 - h_2}{h_1}} ln\left(\frac{h_1}{h_2}\right) \right)^{k_{fspeed}}, \tag{3.28}$$

where k_{fo}, k_f and k_{fspeed} are model coefficients. This equation was found to yield satisfactory results compared to real plant data[1]. If Eq. 3.28 is investigated there are a few differences from the Zener-Holoman relationship but the similarities outnumber the former. The term $ln\left(\frac{h_1}{h_2}\right)$ represents the mean material strain and $\frac{v}{\sqrt{R'h_1}}$ has a time rate unit representing the mean strain rate. The biggest difference is the different expressions used to calculate the power of the exponential in Eq. 3.25 and Eq. 3.28. In Eq. 3.28 the power expression reflects a linearization, of the hyperbole function in Eq. 3.25, over the temperature range under investigation.

3.4 Tension Model

3.4.1 Introduction

The pieces of strip between the coiler furnaces and the roll gap are continuous distributed parameter mass elements and the theory of continuous dynamics can be employed to model the tensions in the

[1]Eq. 3.28 is used by a large stainless steel manufacturer in South Africa for their setup calculations. The values of the model coefficients are given in chapter 4.

strip. The reason for modelling the tension is to get accurate values of the tension at the entrance and exit of the roll gap. Tension-stresses, $\sigma_1(t), \sigma_2(t)$, decrease the rolling load as can be seen in Eqs. 3.16 and 3.17. In this dissertation it is proposed that tension modelling can be done by approximating the pieces of strip between the coiler furnaces and the roll gap as longitudinal bars that are subjected to longitudinal vibrations [51, 52, 53, 54].

The pieces of strip are however also subjected to transverse vibration. The lateral and longitudinal vibrations of the strip can be viewed separately and their results superimposed on each other, or it can be viewed as a continuous system where the two PDE's have to be solved simultaneously.

There are two possible ways of modelling the transverse vibration of the strip:

1. **Transverse Vibration Strip Model 1:** The strip can be modelled as a bar or beam exhibiting lateral vibration with an axial force applied to the bar or beam [51]. The axial force will typically be the horizontal force ($f(x)$ see figure 3.2) found from the roll gap analysis. The theory used for this model is usually applied to the study of vibration of cables and guy wires [51].

2. **Transverse Vibration Strip Model 2:** The strip can be modelled as a string exhibiting free transverse vibration [54].

A distributed parameter system that vibrates transversely has two sources that act as restoring forces to bring the system to its equilibrium point. These two sources are the axial tension and the bending stiffness [54]. The bending stiffness of the system is the dominant restoring force for the Transverse Vibration Strip Model 1. It can be argued that this model can be reduced to a beam model without the applied axial force; the result being a normal transverse vibration model of a beam, where the solution of this model will give the transverse translation of the system. The strip is however in a temperature range were plastic deformation can easily take place, and it can be argued that the strip will not exhibit meaningful bending stiffness. The strip can thus not be modelled as a bar or beam subjected to transverse vibration.

For Transverse Vibration Strip Model 2 the axial tension is the dominant restoring force. It is debatable whether the second model will give a more accurate reflection of the transverse vibration of the sheet outside the roll gap. With the second model the lateral and transverse vibration problems can be combined and the mutual influences on each other, for the rolling mill application, can be accounted for as follows:

- The longitudinal vibration of the strip, for both sides of the roll gap, can be modelled as a uniform bar, for which the longitudinal vibration is given as follows,

$$E_{ss}A\frac{\partial^2 u}{\partial x^2}(x,t) \pm f(x,t) = \rho A\frac{\partial^2 u}{\partial t^2}(x,t). \tag{3.29}$$

- The tension force in the strip, when modelled as a bar, can be expressed as,

$$T(x) = E_{ss}A\frac{\partial u}{\partial x}(x,t). \tag{3.30}$$

- Eq. 3.30 can then be substituted into the PDE describing the transverse vibration of a string,

$$\frac{\partial}{\partial x}\left[T(x)\frac{\partial y}{\partial x}(x,t)\right] = \rho A\frac{\partial^2 y(x,t)}{\partial t^2}, \tag{3.31}$$

where,

E_{ss}: Young's modulus of the strip;

A: Cross sectional area perpendicular to the rolling direction;

ρ: Density of the strip metal;

x: Rolling direction;

$u(x,t)$: Lateral displacement of the strip metal;

$y(x,t)$: Transverse displacement of the strip metal;

$T(x)$: Tension in the sheet as a function of the rolling direction expressed as a force;

$f(x,t)$: Horizontal force per unit width found from the roll gap analysis[2].

It should be stressed that the transverse vibration will not be symmetrical for the physical system due to the roller table that will limit downward transverse displacement.

Since only the tension into the roll gap and tension just outside the roll gap need to be known for solving Orowan's static differential equations, in depth modelling of the tension of the sheet is not necessary for this investigation. However, if the simulator's capability is to be increased to account for shape formation and the residual stress build-up in the sheet, it will be necessary to account for the non-uniform elongation of the strip along the length and across the width of the strip. The suggested modelling approach might be worthwhile investigating to create a simulator that can account for the stress and strain of the strip at different points on the strip.

For the purpose of this dissertation it is sufficient to model the tension behaviour of the strip (in the mill simulator) as discrete springs in tension [55, 56], as will be described in the following section.

3.4.2 Tension Model

In practice, a certain tension is required in the strip in order to reap the benefit of a reduced rolling load. This required tension is determined by a setup program that calculates all the mill parameters

[2] $+f(x,t)$: Strip piece from back coiler to the entrance of the roll gap.

$-f(x,t)$: Strip piece from the roll gap exit to the front coiler.

before rolling commences, as is discussed in section 2.3. The tension in the strip is perturbed around this required tension because of factors such as roll gap thickness adjustments[3]. If the rolling load can be reduced, the draft taken off the strip can be increased without violating the physical constraint on the total rolling force (40 MN) for the Steckel Mill under consideration. Thus, the main control aim is to regulate the tension in the sheet around the setup tension value.

It is assumed that the base tension is established before the mill drive is accelerated towards the threading speed for the particular pass. At threading speed the coiler motors' speeds are controlled in such a manner that the tangential speed of the strip at the front/back coiler drum remains approximately the same as the exit/entrance speed of the roll gap respectively. The radiuses of the front and back coils are increasing and decreasing respectively with time. In order to keep the tangential strip speeds constant, the angular velocities of the coiler motors have to be controlled according to the relationship, $\omega_{coiler\ drive} = \frac{v_{tangential}}{R_{coil}}$.

If a mismatch in coiler speeds and roll gap speeds should occur, the strip tension increases or decreases depending on the change in speeds and on which side of the roll gap this change occurs. The strip reflects these changes by stretching more or less respectively. It is not desirable that the strip should break due to necking[4] or vibrate transversely (perpendicular to the rolling direction) due to the relaxation of tension[5]. In order to model this phenomena it was decided to model the strip pieces from the roll gap to the coilers as discrete springs already under tension. The setup values for the applied tensions are calculated using the following[6],

$$T_i = 47wh_i^{0.27}, \forall i \in [1,2], \tag{3.32}$$

where T_i is expressed in Newtons and w, h_i are both expressed in millimeter.

The tension model can be expressed as follows [55, 56]:

$$T_1 = \frac{E_{ss}(h_1 w_{strip})}{L_{cf\leftrightarrow rg}} \int_0^t (v_1(\tau) - v_{bc}(\tau))\, d\tau \tag{3.33}$$

$$T_2 = \frac{E_{ss}(h_2 w_{strip})}{L_{cf\leftrightarrow rg}} \int_0^t (v_{fc}(\tau) - v_2(\tau))\, d\tau \tag{3.34}$$

with,

[3]When the roll gap distance is changed, the draft of the strip varies, changing the entrance and exit speed of the roll gap. These speed changes cause the tension to vary according to Eqs. 3.33 and 3.34.

[4]Necking occurs when the strip deforms plastically (the tension stress in the strip is larger than the strip's yield stress) outside the roll gap, resulting in an observable thickness reduction and a less observable width reduction.

[5]In this instance tension can be seen as negative and the effect of applied tension to the roll gap model should be zero.

[6]This setup equation for the tension is used by a large stainless steel manufacturing company in South Africa for their tension setup calculations.

T_1: Tension in the strip piece from the back coiler to the roll gap (expressed in N);

T_2: Tension in the strip piece from the roll gap to the front coiler (expressed in N);

E_{ss}: Young's modulus for Stainless Steel Grade 304 (Pa);

w_{strip}: Strip width (m);

v_{fc}: Tangential velocity of the strip taken up on the front coiler (m/s);

v_{bc}: Tangential velocity of the strip paid off by the back coiler (m/s);

$L_{cf\leftrightarrow rg}$: The length from the coiler furnaces to the roll gap (ignoring the length of the arc of contact[7], m).

3.5 Stand Model

3.5.1 Introduction

The stand model derived in this section is unique and more comprehensive than stand models found in the literature [7, 40]. There are some similarities between the stand model derived in this section and the models depicted in [7, 40]. The distinctions and similarities of the stand model and the models in [7, 40] will be highlighted during the following discussion and model derivation.

The model is divided into a continuous mass system (4 rolls) interacting with discrete elements (lumped masses and springs) as depicted in figure 3.3. The lumped masses are formed by lumping the roll chock and bearing combinations together, resulting in eight discrete masses. Although it can be argued that the system exhibits symmetry properties, it was however decided not to make symmetry approximations, setting this model apart from models in [7, 40].

This modelling choice can be motivated by referring to the practical behaviour of the rolling stand [40, 27, 7]. Shearing forces at the end points of the rollers interact with the discrete modelled masses and springs, representing the roll chocks and bearings, as well as with hydraulic actuators and jacks. The top back-up roll chocks are connected to hydraulic actuators keeping the top back-up roll at the desired setting. The hydraulic actuator is mounted in the mill frame. The rolling force is transmitted to the mill frame from the roller end points to the hydraulic actuator and then to the mill frame. The rolling mill stand does not exhibit infinite stiffness and the large rolling forces, necessary to achieve the plastic deformation of the strip, cause the rolling mill frame to stretch. This stretch is asymmetrical and in an upwards direction, when the base of the rolling mill frame is chosen as the reference point. This stretch is also asymmetrical around the mill's width centerline, due to different mill springs for

[7]The length of the arc of contact is 50 mm and $L_{cf\leftrightarrow rg}$ is approximately 6.4m. The first value was obtained from simulation of the roll gap model as discussed in chapter 4 and 5. The second value was calculated from data obtained from a questionnaire about the Steckel mill under investigation.

the **D**rive and **O**perator **S**ides (DS and OS) of the rolling mill.

The action and reaction forces in the roll gap push the working rolls apart while at the same time also bending them. The width of the mill stand is larger than the width of the strip. If mill stretch is neglected the setup of the roll gap position is kept constant at the end points of the top back-up roll. The relative displacements of the rollers at their end points deviate slightly, but the objective is to keep them fixed by controlling the hydraulic stroke. The rollers deform elastically by bending along their axes in order to cope with the large rolling forces on the strip/work roll interfaces.

The rollers are designed to be very rigid and limit the amount of bending of the rolls along their axis. The stiffness of a roller decreases as the diameter of the roll decreases and the roller is bended more easily. Back up rollers are normally used to limit the amount of bending of the thinner work rolls. In order to roll thinner gauges smaller diameter work rolls are used [57]. From the preceding discussion it is evident that these small diameter rolls will easily bend and the need for other larger diameter rollers, to decrease the amount of bending of the working rolls, arise. There is thus a tradeoff between the diameter of the work rolls and the amount of allowed bending. The Z-high mill and the Sendzimer cold rolling mills serve as examples, where the rolling of thinner gauges, with small diameter work rolls and a number of supporting rolls.

3.5.2 Literature review

Different methods have been developed to predict the strip thickness profile and shape. These can be divided into the following groups [10, 17, 58]:

- Elastic Foundation Method
- Influence Coefficient Method
- Slit Beam Models
- Finite Element Method (FEM)
- Spring and Beam Method
- Transport matrix Method

The modelling approach decided upon was the elastic foundation method although in [10, 17, 58] it is suggested that this type of modelling is inferior to some of the other models. These limitations to simple beam models are given in the literature as follows:

- **Remark 1:** Usually static bending models [10] are obtained from this method and are not suitable for mill setup and on-line control due to their limited application and are used for

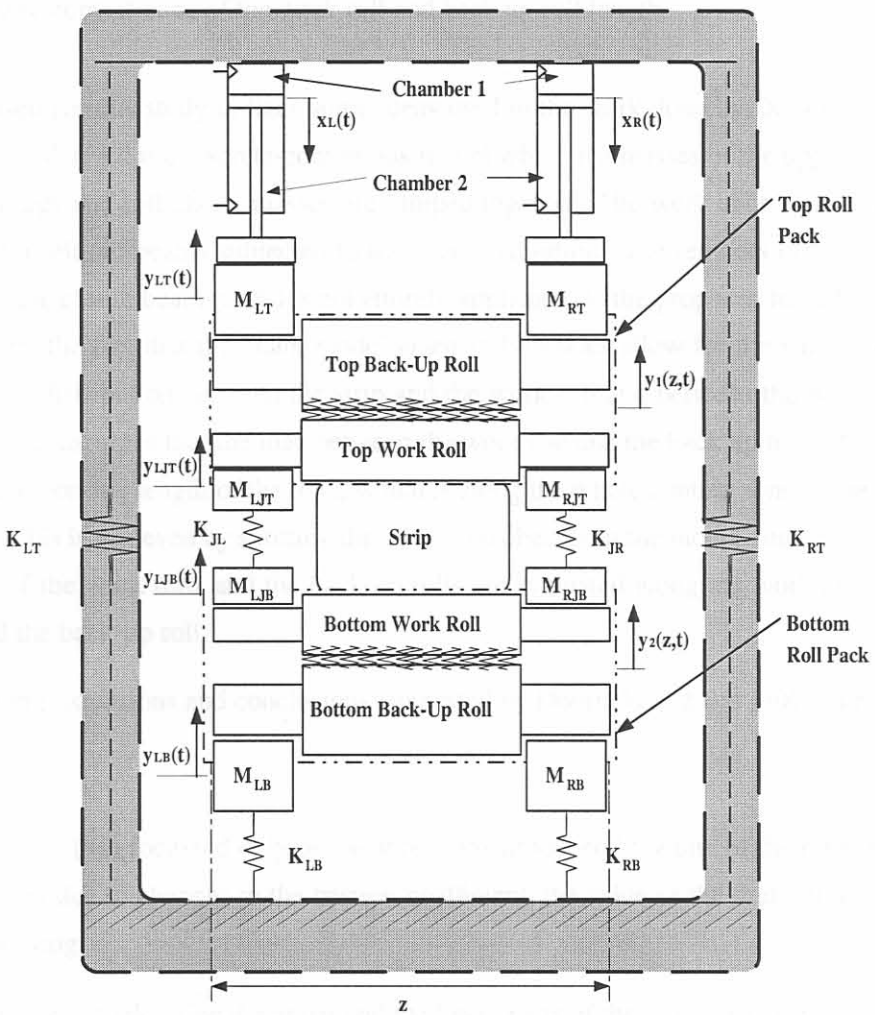

Figure 3.3: Cross sectional view of the mill stand and the hydraulic cylinders.

approximate estimations of control devices during the mill design stage [17, 58]. However, in [59] this type of modelling approach was successfully used for the design of an observer and a MIMO controller.

- **Remark 2:** The simple beam models given in [10] do not allow for the simulation of uneven transverse load distributions between the strip and the work roll and between the work roll and back-up roll. Furthermore it is assumed that the load between the work roll and the back up roll is transmitted only along the strip width, which contradicts the actual loading, which is along the whole contact zone of the work roll and back up roll length.

The model used for this study utilizes some ideas used in the work done by Dobrucki and Bar [40]. The model they derived is a discrete-continuous model where the masses of the upper part of the mill housing, bearings and roll chock masses are lumped together. The work rolls and the back-up rolls are modelled as elastic beams subjected to transverse vibration. The remarks of various authors on the quality of the elastic beam model is not entirely applicable to the proposed model. This statement is motivated by the fact that the beam model given in [40] does allow for the simulation of uneven transverse load distribution between the strip and the work roll and between the work roll and back up roll. It further assumes that the load between the work roll and the back up roll is transmitted only along the axial working length of the rolls, which is along the whole contact zone of the work roll and back up roll. This is achieved by splitting the continuous beams of the model, into five smaller beams. The loading of the work rolls and the back-up rolls are evaluated along the working axial length of the work and the back-up roll.

Some modelling extensions and conclusions suggested by Dobrucki and Bar [40] can be described as follows:

- Their study [40] focussed only on the vibrations produced by a bite of the rolls, neglecting the vibrations due to changes in the friction coefficient, the value of the draft, and the phenomena of chattering.
- They propose to describe the upper and the lower parts of the stand in an asymmetrical fashion.
- They found that there was a discrepancy between their model and the real plant data used to test their model. It was found that the periods and the amplitudes of the vibrations of the rolls, on the mill drive side, is greater than on the operator side. Thus the model has to be asymmetric, with respect to the mass of the spindles. This phenomenon can be attributed to the chattering (torsional vibration of the mill drive spindles) of the mill, as well as the difference in the mill spring of the mill frame on both sides of the mill.

In this dissertation some of the modelling extensions proposed by Dobrucki and Bar are taken into account.

- Firstly, the vibration effect due to changing draft and the variation of the friction coefficient with temperature are taken into account in the simulator roll gap model. The specific rolling force interacts on its part with the dynamic stand model and the forced vibration results in a draft deviation, which again influences the calculation of the specific rolling force at the next time step. Thus the vibration due to the varying draft is incorporated in the mill simulator.
- Secondly the upper and lower part of the rolling mill are investigated in an asymmetrical fashion.
- Thirdly in order to account for the asymmetrical behaviour between the DS and OS vertical roller displacements, different mill stretch curves for either side of the mill frame are modelled. The effect of chattering of the mill drive spindles is not taken into account in this dissertation.

3.5.3 Modelling Assumptions

It is assumed that the bending and deflection of the work and back-up rolls can be modelled as beams that interact with each other and with the discrete components. An example on how to construct the PDE model to account for the interaction between discrete model components and a continuous mass beam is shown in [51]. The beam-beam interaction can be modelled as a beam on an elastic foundation [54, 60]. In the following section a more elaborate description of the modelling choices will be given.

In this work a few simplifying assumptions are made that is in accordance with assumptions made in [40, 59, 61]):

- The second moment of area is taken as a constant and the bending of the beam does not influence the second moment of area appreciably along the length of the roll, z;
- Time varying effects that increase/decrease the radiuses of the rollers, such as thermal crown build-up and deformed roll radiuses on the strip/roll and roll/roll interfaces are assumed negligible. Thus the cross-sectional area of the rolls do not change along the length of the rolls (z) due to these varying effects and only changes due to the different radiuses for the working interface of the roll and the roll necks;
- Poisson deformation of the rollers along the width of the rollers is negligible.

3.5.4 Partial Differential Equation (PDE) Model

The basic PDE for an unforced elastic beam is given as [51, 54, 60],

$$\rho A(z)\frac{\partial^2}{\partial t^2}y(z,t) + \frac{\partial^2}{\partial z^2}\left[EI(z)\frac{\partial^2}{\partial z^2}y(z,t)\right] = 0. \tag{3.35}$$

The beam's second moment of area (taking the simplifying assumptions into consideration) can be expressed as follows:

$$I_i(z) = \begin{cases} I_{i1} = \frac{\pi(2r_{neck_{is}})^4}{64}, \forall -\frac{l_i}{2} \leq z < -\frac{w}{2}, \in z_1 \\ I_{i2} = \frac{\pi(2r_{work_i})^4}{64}, \forall -\frac{w}{2} \leq z \leq \frac{w}{2}, \in z_2 \\ I_{i3} = \frac{\pi(2r_{neck_{is}})^4}{64}, \forall \frac{w}{2} < z \leq \frac{l_i}{2}, \in z_3 \end{cases}, \tag{3.36}$$

where $i \in [1,2,3,4]$ is the index of the rollers, $s \in [L,R]$ is the index reflecting the side of the mill under consideration, l_i is the length of the roller and w is the width of the strip. The domains z_1, z_2 and z_3 can be described as follows (Assuming an uneven pass is executed):

z_1: Length of the roller from its left end (OS) point to the working roll surface;

z_2: Length of the roller's working surface;

z_3: Length of the roller from the end of the working surface, right of the mill centerline (DS), to the end of the roller.

Similarly the cross sectional areas of the rollers are expressed as:

$$A_i(z) = \begin{cases} A_{i1} = \pi r^2_{neck_{is}}, \forall z \in z_1 \\ A_{i2} = \pi r^2_{work_i}, \forall z \in z_2 \\ A_{i3} = \pi r^2_{neck_{is}}, \forall z \in z_3 \end{cases}. \tag{3.37}$$

From Eq. 3.36 it is evident that although $I_i(z)$ is an implicit function of z and the second derivative, $\left(\frac{\partial^2}{\partial z^2} EI(z)\right) \cdot \frac{\partial^2}{\partial z^2} y(z,t) = 0$, and Eq. 3.35 can be simplified to yield,

$$\rho A(z) \frac{\partial^2}{\partial t^2} y(z,t) + EI(z) \frac{\partial^4}{\partial z^4} y(z,t) = 0. \tag{3.38}$$

The work rolls and the back-up rolls interact with each other. On the interfaces between the back-up rolls and work rolls, the rolls can be compressed if the relative movement of the rolls are such that:

- The vertical displacement of the top back-up roll is less than the vertical displacement of the top work roll.
- The vertical displacement of the bottom work roll is less that the vertical displacement of the bottom back up roll.

When the rolls are compressed at the roll interfaces the equation for the value of the spring coefficient is given by Stone in [62]. The decrease in compressive distance between the centers of the two contacting rolls is given as:

$$\triangle = \frac{P'}{E} \frac{2(1-\nu^2)}{\pi} \left[\frac{2}{3} + ln\frac{2D_1}{b} + ln\frac{2D_2}{b}\right], \tag{3.39}$$

where:

P': Specific rolling force;

υ: Poisson's ratio for steel;

E: Young's modulus of the rollers (steel) ;

D_1, D_2: diameters of the rolls under compression;

$\triangle$: Compressive distance between the back-up and work roll interface.

The width of the flattened contact area of the roller interface along the axial length of the rollers is given as,

$$b = \sqrt{\frac{16(1-\nu^2)}{\pi}\frac{P'}{E}\frac{D_1 D_2}{D_1 + D_2}}. \tag{3.40}$$

With $\triangle$ known the distributed spring constant (units: $\frac{N/m}{m}$) can be calculated as,

$$k_{interface}(P') = \frac{P'}{\triangle}. \tag{3.41}$$

Due to the bending of the rolls over the width of the mill, different draft values are obtained over the width of the strip, resulting in varying specific rolling force along the width of the rolls. The varying specific rolling force results in a varying interface loading spring constant along the width of the compressed rolls.

Taking the above and the relative movement conditions into consideration, the compression of the rolls can be modelled as a nonlinear distributed spring system expressed as,

$$k_{c_j}(P'(z,t),z) = \begin{cases} k_{interface}(P'),\ y_i(z,t) \leq y_{i+1}(z,t) \\ 0,\ for\ y_i(z,t) > y_{i+1}(z,t) \end{cases}, \tag{3.42}$$

where $i \in [1,3]$ and $j \in [1 \leftrightarrow 2, 3 \leftrightarrow 4]$. In figure 3.3 the directions of the vertical displacements are shown.

3.5.5 Four-High Stand

3.5.5.1 Top Back Up Roll (TBU)

The top back-up roll's adjacent model elements are the discrete lumped masses at each of the TBU ends as well as the top work roll (TWR).

The top back up roll's adjacent model elements are the discrete lumped mass at each of its ends as well as the top work roll.

$$\rho A_1(z)\frac{\partial^2}{\partial t^2}y_1(z,t) + EI_1(z)\frac{\partial^4}{\partial z^4}y_1(z,t) = -k_{c_{1\leftrightarrow 2}}(P'(z,t),z)(y_1(z,t) - y_2(z,t)) \tag{3.43}$$

The Boundary Values of the model are:

$$\frac{\partial}{\partial z}y_1(z,t)\Big|_{z=\frac{-l_1}{2}} = 0 \tag{3.44}$$

$$\frac{\partial}{\partial z}y_1(z,t)\Big|_{z=\frac{l_1}{2}} = 0 \tag{3.45}$$

$$EI_1(z)\frac{\partial^3}{\partial z^3}y_1(z,t)\Big|_{z=\frac{-l_1}{2}} = M_{LT}\ddot{y}_{LT}(t) + F_{HAL} \tag{3.46}$$

$$-EI_1(z)\frac{\partial^3}{\partial z^3}y_1(z,t)\Big|_{z=\frac{l_1}{2}} = M_{RT}\ddot{y}_{RT}(t) + F_{HAR} \tag{3.47}$$

These boundary values are in accordance with the modelling work of Pederson [7, 59]. The boundary values for all four rollers have the same structure and their physical meaning can be described as follows:

- $\frac{\partial}{\partial z}y_i(z,t)\Big|_{z=\frac{-l_i}{2},\frac{l_i}{2}}$, $\forall i \in [1,2,3,4]$: The rollers are encapsulated in the roll neck and bearing capsule. The rolls are not able to bend in such a way that the slope of the rollers at the end of the rollers are non zero.
- $\frac{\partial^3}{\partial z^3}y_i(z,t)\Big|_{z=\frac{-l_i}{2},\frac{l_i}{2}}$, $\forall i \in [1,2,3,4]$: The shearing forces of the rolls are non-zero and interact with the discrete parts of the model.

The modelling work of Dobrucki and Bar [40] further differ from the approach given in this dissertation, than already highlighted. Dobrucki and Bar did not take the boundary condition into account that arises due to the encapsulation of the roller. They also divided each roller into five distinct beams, as was earlier remarked. Three beams were used to account for the rollers working interface and the remaining beams were used to account for the roll necks. The three beam elements that model the working interface of a roller are in contact with the adjacent roller's three beam elements. The middle beam of the work roll is the only beam that is in contact with the strip. In this dissertation it was decided to look at a roller as one beam with different radiuses for the roll necks and the working surface.

3.5.5.2 Top Work Roll (TWR)

The top work roll's adjacent model elements are the TBU, the strip and discrete elements, i.e. the bearings, roll chocks and the hydraulic jack actuator.

$$\rho A_2(z)\frac{\partial^2}{\partial t^2}y_2(z,t) + EI_2(z)\frac{\partial^4}{\partial z^4}y_2(z,t) = P'(z,t) + k_{c_{1\leftrightarrow 2}}(P'(z,t),z)(y_1(z,t) - y_2(z,t)) - k_{strip}(y_2(z,t) - y_3(z,t)) - \beta_{strip}(\dot{y}_2(z,t) - \dot{y}_3(z,t)) \quad (3.48)$$

Boundary Values:

$$\frac{\partial}{\partial z}y_2(z,t)\Big|_{z=\frac{-l_2}{2}} = 0 \quad (3.49)$$

$$\frac{\partial}{\partial z}y_2(z,t)\Big|_{z=\frac{l_2}{2}} = 0 \quad (3.50)$$

$$EI_2(z)\frac{\partial^3}{\partial z^3}y_2(z,t)\Big|_{z=\frac{-l_2}{2}} = K_J(y_2(z,t) - y_3(z,t))\Big|_{z=\frac{-l_2}{2}} - J(t) \quad (3.51)$$

$$EI_2(z)\frac{\partial^3}{\partial z^3}y_2(z,t)\Big|_{z=\frac{l_2}{2}} = -K_J(y_2(z,t) - y_3(z,t))\Big|_{z=\frac{l_2}{2}} + J(t) \quad (3.52)$$

3.5.5.3 Bottom Work Roll (BWR)

The bottom work roll's adjacent elements are the BBU, the strip and the discrete components of the hydraulic jacks and the roll chock and bearing combination.

$$\rho A_3(z)\frac{\partial^2}{\partial t^2}y_3(z,t) + EI_3(z)\frac{\partial^4}{\partial z^4}y_3(z,t) = -P'(z,t) - k_{c_{3\leftrightarrow 4}}(P'(z,t),z)(y_3(z,t) - y_4(z,t)) + k_{strip}(y_2(z,t) - y_3(z,t)) + \beta_{strip}(\dot{y}_2(z,t) - \dot{y}_3(z,t)) \quad (3.53)$$

Boundary Values:

$$\frac{\partial}{\partial z}y_3(z,t)\Big|_{z=\frac{-l_3}{2}} = 0 \quad (3.54)$$

$$\frac{\partial}{\partial z} y_3(z,t)\Big|_{z=\frac{l_3}{2}} = 0 \tag{3.55}$$

$$EI_3(z)\frac{\partial^3}{\partial z^3} y_3(z,t)\Big|_{z=\frac{-l_3}{2}} = -K_J(y_2(z,t) - y_3(z,t))\Big|_{z=\frac{-l_3}{2}} + J(t) \tag{3.56}$$

$$EI_3(z)\frac{\partial^3}{\partial z^3} y_3(z,t)\Big|_{z=\frac{l_3}{2}} = +K_J(y_2(z,t) - y_3(z,t))\Big|_{z=\frac{l_3}{2}} - J(t) \tag{3.57}$$

3.5.5.4 Bottom Back-Up Roll (BBU)

The bottom back-up roll's adjacent model components are the BWR and discrete elements, i.e. the load cells and the roll chock and bearing combinations.

$$\rho A_4(z)\frac{\partial^2}{\partial t^2} y_4(z,t) + EI_4(z)\frac{\partial^4}{\partial z^4} y_4(z,t) = -k_{c_{3\leftrightarrow 4}}(P'(z,t),z)(y_4(z,t) - y_3(z,t)) \tag{3.58}$$

Boundary Values:

$$\frac{\partial}{\partial z} y_4(z,t)\Big|_{z=\frac{-l_4}{2}} = 0 \tag{3.59}$$

$$\frac{\partial}{\partial z} y_4(z,t)\Big|_{z=\frac{l_4}{2}} = 0 \tag{3.60}$$

$$EI_4(z)\frac{\partial^3}{\partial z^3} y_4(z,t)\Big|_{z=\frac{-l_4}{2}} = m_{LB}\ddot{y}_{LB}(t) + K_{LB}y_{LB}(t) \tag{3.61}$$

$$EI_4(z)\frac{\partial^3}{\partial z^3} y_4(z,t)\Big|_{z=\frac{l_4}{2}} = -m_{RB}\ddot{y}_{RB}(t) - K_{RB}y_{RB}(t) \tag{3.62}$$

3.5.6 Two-High stand

The four high stand model can be simplified to yield a two-high stand model. It is obtained by grouping the top work roll and top back-up roll and similarly the bottom work roll and back-up

rolls together to form upper (**TRP**-Top Roll Pack) and lower (**BRP**-Bottom Roll Pack) roll packs. This simplification is in accordance with [59] and similar simplifications are suggested in [10, 40]. Dobrucki and Bar [40] stated that the modes of the vibrations of the back-up and work rolls are close to identical and they proposed that the adjacent work roll and the back-up roll be modelled as a one beam unit, supporting the modelling choice in [59] and this dissertation. In this dissertation the derived four beam model is simplified to yield a two beam model that is implemented in the mill simulator. Reasons for this simplification can be summarized as:

- The number of rolls and their interactions increase the complexity of the model and make it infeasible to simulate with the available computing power. Four p states are associated with each roller, where p is the number of accurate natural spatial vibration modes. The solution methodology followed in order to calculate these natural modes of vibration will be discussed in chapter 4.

- The interface loading between the back-up and work rollers makes the stand model time variant[8] due to the nonlinear spring associated with the interface loading, Eq. 3.42. This time dependency requires the solution of an Eigenvalue problem in an iterative solution scheme at each time step and this considerably complicates the mill simulator. The proposed solution for this model is briefly discussed in chapter 4.

- The simulator developed in this dissertation does not model the roller wear and thermal expansion of the working rolls. These two variables have a direct influence on the strip crown and shape and this influence is larger than the indirect influence of the work/back-up roll interface compression on the strip crown and shape. Following the same reasoning the accuracy of the simulator will not be influenced significantly, by the omission of the interface loading from the simulator modelling. In order to illustrate the comparison between the effects of roller wear and thermal crown on strip crown and shape the reader is referred to figure 5 in [63]. From this it can be concluded that work roll wear plays a larger part in crown evolution when compared to the thermal crown build-up on the rollers. Roller wear is a function of many factors, such as the rolling regime and natural roller crown. In figure 5, [63] the absolute value of the crown amplitude associated with roller wear was twice the amplitude of the thermal crown build-up on the rollers.

- Remark 2 in section 3.5.2 was that a problem associated with the use of the elastic beam method is that the differences in the widths of the strip/work roll interface and the work roll/back-up roll interface are not accounted for and are generally taken to be the same. For the two roll pack model, considered further in this dissertation, the difference between the roll pack width and the strip/roll pack interface width is accounted for.

[8] In state-space format it is expressed as $\dot{\mathbf{x}}(t) = \mathbf{A}(t)\mathbf{x}(t) + \mathbf{B}\mathbf{u}(t)$.

3.5.6.1 Top Roll Pack

The area of the roll pack is the summation of the areas of work roll and back roll. The second moment of area, I, of the roll pack is found by taking the second moment of area of the corresponding work roll [59, 50]. Taking this simplifications into account the 4-high model can be modified to yield the following 2-high model[9]:

$$\rho A_{12}\frac{\partial^2}{\partial t^2}y_{12} + EI_{12}\frac{\partial^4}{\partial z^4}y_{12} = P' - k_{strip}(y_{12} - y_{34}) - \beta_{strip}(\dot{y}_{12} - \dot{y}_{34}), \tag{3.63}$$

where,

y_{12}: Is the vertical displacement of the top roll pack;

y_{34}: Is the vertical displacement of the bottom roll pack;

A_{12} : is the area of the top roll pack. This area is taken as the sum of the areas of the work roll and the back-up roll ($A_{12} = A_1 + A_2$);

I_{12}: is the second moment of area of the top roll pack. Note that the second moment of area of the roll pack is taken as only the second moment of area of the work roll [59] ($I_{12} = I_2$). The definition of all the other variables are left unchanged.

The Boundary Values of the model are:

$$\frac{\partial}{\partial z}y_{12}(z,t)\Big|_{z=\frac{-l_{12}}{2}} = 0\ ; \tag{3.64}$$

$$\frac{\partial}{\partial z}y_{12}(z,t)\Big|_{z=\frac{l_{12}}{2}} = 0\ ; \tag{3.65}$$

$$EI_2\frac{\partial^3}{\partial z^3}y_{12}\Big|_{z=\frac{-l_{12}}{2}} = m_{LT}\ddot{y}_{LT} + K_J(y_{12} - y_{34})\Big|_{z=\frac{-l_{12}}{2}} - J + F_{HAL}; \tag{3.66}$$

$$EI_2\frac{\partial^3}{\partial z^3}y_{12}\Big|_{z=\frac{l_{12}}{2}} = -m_{RT}\ddot{y}_{RT} - K_J(y_{12} - y_{34})\Big|_{z=\frac{l_{12}}{2}} + J - F_{HAR}. \tag{3.67}$$

3.5.6.2 Bottom Roll Pack

$$\rho A_{34}\frac{\partial^2}{\partial t^2}y_{34} + EI_{34}\frac{\partial^4}{\partial z^4}y_{34} = -P' + k_{strip}(y_{12} - y_{34}) + \beta_{strip}(\dot{y}_{12} - \dot{y}_{34}), \tag{3.68}$$

[9]The dependency notation of the variables, A_i, y_i, I_i, P', on z and t are omitted in the following section for the sake of brevity.

where,

A_{34}: Is the area of the top roll pack ($A_{34} = A_3 + A_4$);

I_{34}: is the second moment of area of the top roll pack ($I_{34} = I_3$).

The following boundary conditions apply,

$$\frac{\partial}{\partial z} y_{34}(z,t)\Big|_{z=\frac{-l_{34}}{2}} = 0\ ; \tag{3.69}$$

$$\frac{\partial}{\partial z} y_{34}(z,t)\Big|_{z=\frac{l_{34}}{2}} = 0\ ; \tag{3.70}$$

$$EI_3 \frac{\partial^3}{\partial z^3} y_{34}\Big|_{z=\frac{-l_{34}}{2}} = -K_J(y_{12} - y_{34})\Big|_{z=\frac{-l_{34}}{2}} + J + m_{LB}\ddot{y}_{LB} + K_{LB}y_{LB} \tag{3.71}$$

$$EI_3 \frac{\partial^3}{\partial z^3} y_{34}\Big|_{z=\frac{l_{34}}{2}} = +K_J(y_{12} - y_{34})\Big|_{z=\frac{l_{34}}{2}} - J - m_{RB}\ddot{y}_{RB} - K_{RB}y_{RB} \tag{3.72}$$

The solution methodology used to solve the PDE model for the two roll pack model in order to create the mill simulator will be described in chapter 4.

3.5.7 Gaugemeter Compensation

The mill frame does not exhibit infinite stiffness and stretches significantly due to the rolling forces associated with normal operation. The classical and most employed control scheme used to compensate for the mill stretch is the BISRA-Davy gaugemeter compensator [1, 27]. This compensator uses positive force feedback to control the thickness deviation. There are a few deficiencies of this controller that make it necessary to include an X-Ray feedback or feedforward thickness control loop.

The BISRA-Davy gaugemeter compensator equation is given as [27],

$$\delta h_2 = \delta x + \frac{\delta F}{M}, \tag{3.73}$$

With the variables defined as:

M: Mill modulus;

δx: Deviation in stroke of hydraulic actuator;

δF: Deviation in rolling force;

δh_2: Deviation in strip output thickness from the roll gap.

The basic principle of the BISRA-Davy gaugemeter compensator is to regulate the rolling force and effectively combating the stretch by changing the hydraulic stroke in accordance. If the rolling force

is constant, $\delta F = 0$, the desired reduction can be achieved, $\delta h_2 = 0$, according to the BISRA-Davy gaugemeter compensator equation, Eq. 3.73.

From figure 3.4[10] it can be seen that the mill frame stretches about 5mm on either side of the mill when a total force of 30MN (15MN per side) is measured. Thus the mill stretch can be immense and if uncompensated for, no reduction will take place. The mill stretch is an essential component of the mill dynamics and has to be modelled. From simulations it became apparent that the need for the inclusion of a BISRA-Davy gaugemeter compensator need only be included for initial compensation. The dynamic gaugemeter compensator only adds a trim to the setpoint fed to the hydraulic actuators. The BISRA-Davy gaugemeter compensator were modelled as part of the plant to aid with the maintenance of steady state conditions, before step tests were applied to the plant in order to identify a linear plant using system identification. These trim values will not contribute significantly to the dynamics of the identified model as is discussed in chapter 5. A differential gaugemeter compensator was not implemented and only a mean gaugemeter compensator was modelled.

The mill stretch can be modelled as a two piece function consisting of a nonlinear power function and a linear function. The power, χ, and gain, k_a, of the non linear function can be calculated as,

$$\chi_s = \frac{F_{roll_{test_s}}}{K_{sT} M S_{test_s}}, \tag{3.74}$$

$$k_{a_s} = y_{stretch_{test_s}} F_{roll_{test_s}}^{-\chi_s}, \tag{3.75}$$

respectively, where s is an index indicating which side of the mill is under investigation and $F_{roll_{test_s}}$ is the initial force measured by the load cells with no strip in the roll gap. $y_{stretch_{test_s}}$ is the initial mill stretch that is measured under this initial load and K_{sT} is the extended linear mill spring calculated from data logged when the rolls, in the absence of a strip, are pressed against each other with increasing force steps until a measured force of 15MN per side is registered. Practical values for these parameters will be given in chapter 4. The mill stretch model as a function of the applied force for both sides of the mill frame can be expressed as:

$$y_{stretch_s}(F_{roll_s}) = \begin{cases} k_{a_s} F_{roll_s}^{\chi_s}, \forall 0 \leq F_{roll_s} \leq F_{roll_{test}} \\ \frac{1}{K_{sT}}(F_{roll_s} - F_{roll_{test_s}}) + y_{stretch_{test_s}}, \forall F_{roll_{test_s}} < F_{roll_s} \leq \frac{30MN}{2} \end{cases}, \tag{3.76}$$

where $s \in [L, R]$, F_{roll_s} is the applied force and $y_{stretch_s}$.

From figure 3.4 the mill stretch curves seem to be nearly linear over the operation range. Figure 3.5 emphasizes the asymmetry of the rolling mill frame. The calculated linear mill spring coefficients for both sides of the mill will be given in chapter 4.

[10]Figures 3.4 and 3.5 were constructed from the logged data of the Steckel Mill under consideration.

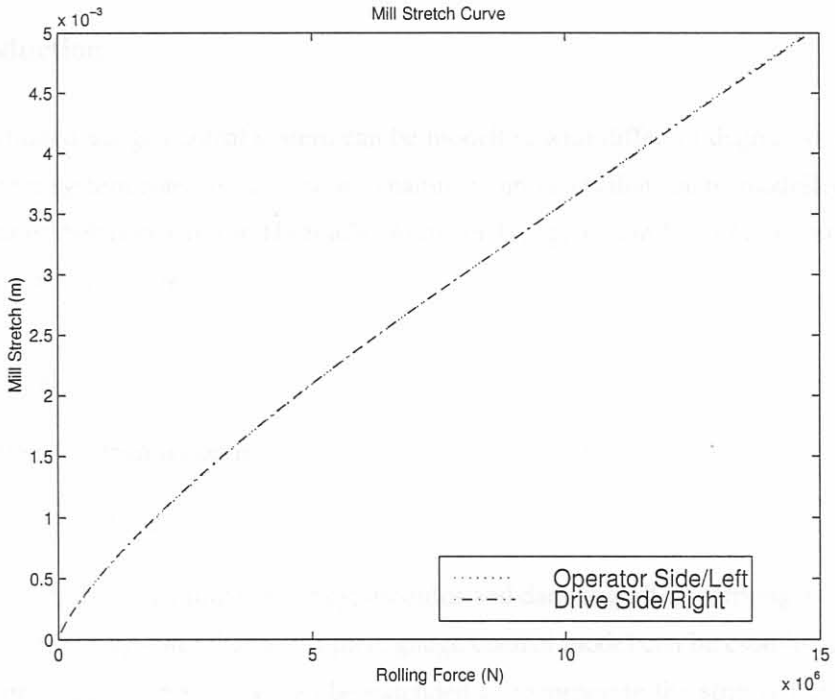

Figure 3.4: Mill stretch curves.

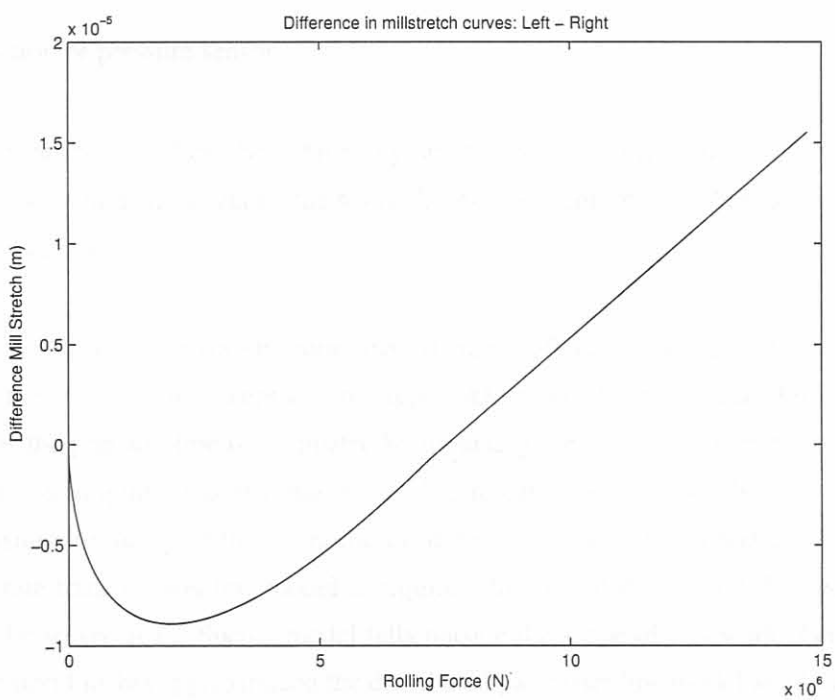

Figure 3.5: Difference in mill stretch curves.

3.6 The Hydraulic Actuator

3.6.1 Introduction

A hydraulic actuated gauge control system can be modelled with different degrees of detail [8]. The hydraulic actuator system consists of 6 major dynamic components that can be modelled to capture the nonlinear dynamic behaviour of the **H**ydraulic **A**ctuator **G**auge **C**ontrol (HAGC) system [8, 64, 65]. The components are as follows:

1. The servovalve.
2. The hydraulic transmission line.
3. The hydraulic cylinder.
4. The mill (dynamics, natural frequency, modulus and damping effect forming a compliant structure [66]). Guo [8] states that a complete gauge control model can be established if the rolling force terms, used in his study, can be extended to incorporate the strip deformation process, tension control loop and the drive control system. All the models that are mentioned by Guo, i.e. Roll Gap Model and the Tension Model, are modelled in this work, except for the drive control system.
5. The return line.
6. The position or pressure sensor.

The complexity of the model can be reduced by omitting some of the dynamic components, as was done by other researchers investigating the hydraulic AGC system [59, 64]. In this work the following components are omitted:

1. Transmission Line: The transmission line's dynamic effect can be omitted, because in modern designs the pressure line is kept as short as possible, typically shorter than 3 m (10 ft.). In some instances the pressure line is eliminated by mounting the servovalve directly onto the cylinder [8]. This assumption was also made by other researchers [59, 64]. Bhowal [64] stated that the transmission delay of the hydraulic oil in the pipe line is small and can be neglected. If an accurate transmission line model is required, the partial differential flow equations would have to be solved [67]. Such a model falls outside the scope of this work. Guo modelled the transmission line but approximated the distributed parameter line model as a lumped parameter line model [8]. The conclusion reached was that the transmission line provides extra damping in the hydraulic circuit, similar to a hydraulic accumulator.

2. Return Line: The return line was also neglected using the same train of thought followed for the transmission line modelling.

3. Sensor: The sensor can be modelled as a first order measuring system [8], but for this work the dynamics of the sensor were omitted and the sensor was modelled as a gain.

3.6.2 Modelling of the dynamic components

3.6.2.1 Operation

The servovalve assembly consists of a torque motor, hydraulic amplifier and a valve spool (figure 3.6). In [66] the working of the widely used two stage electro-hydraulic Moog Servovalve is described[11]. The input control current signal is converted to a mechanical signal, by causing a rotation of the armature to which a flapper arm is rigidly connected. The armature and flapper are supported by a thin-wall flexure sleeve. When the armature and flapper rotate about the flexure sleeve support, the spool is moved. The flapper closes off one nozzle and diverts the flow through that end of the spool. The spool moves and opens P_{high} to one control port and the other is opened to the other control port P_{low}. The spool pushes the ball end of the feedback spring creating a restoring torque on the armature-flapper connection. As the feedback torque becomes equal to the torque of the magnetic forces on the armature, the armature-flapper moves back to the centered position. The spool stops at a position where the feedback spring torque equals the torque due to the control input current. Therefore, the spool position is proportional to the input current.

The control ports are connected to either hydraulic transmission lines or directly to the hydraulic cylinder chamber entrances. By channeling flow in and out of the chambers the pressure in the chamber can be increased or decreased. The limits of the hydraulic circuit are P_{high} and P_{low}. Losses are encountered over transmission lines but in this dissertation such losses are not modelled. The interested reader is referred to [67, 66] which are references dealing with the field of hydraulic servosystems. Similar actuators were modelled for the left and the right side of the mill. The two actuators interact with the stand model as can be seen in figure 3.3.

3.6.2.2 Servovalve

The servovalve was modelled as a second order system and it is reported by Guo that this type of modelling agrees with test results obtained [8]. It is, however, reported elsewhere that it is difficult to model the servovalve with a simplified transfer function model due to the high-order non linear nature of its response [65]. The response of servovalves are functions of both the servovalve current and the pressure drop across the valve. It is suggested [65] that the frequency response curve of the

[11] A description of the working of such a servovalve can also be found on Moog's URL (http:/www.moog.com)

servovalve under investigation be obtained from its manufacturer, such as Moog and Bosch, when a suitable transfer function needs to be derived for the valve.

The chosen model can be written as,

$$\ddot{x}_{v_s} + 2\zeta_{v_s}\omega_{v_s}\dot{x}_{v_s} + \omega_{v_s}^2 x_{v_s} = \frac{\omega_{v_s}^2 x_{v_{smax}}}{I_{o_s}} I_{c_s}, \tag{3.77}$$

where the index $s \in [L, R]$ and,

x_{v_s}: Servovalve opening (spool movement);

$x_{v_{smax}}$: The maximum spool movement;

ω_{v_s}: Servovalve natural frequency (51Hz);

ζ_{v_s}: Servovalve damping ratio;

I_{c_s}: Controlled input current;

I_{o_s}: Rated servovalve current.

The controlled input current is calculated by assuming a cascaded proportional integral controller structure,

$$I_{c_s} = K_{c_s}\left((x_{sp_s} - x_s) + \frac{1}{\tau_{i_s}}\int_0^t ((x_{sp_s} - x_s)d\tau\right), \tag{3.78}$$

where K_{c_s} and τ_{i_s} is the gains of the controller and will be given chapter 4.

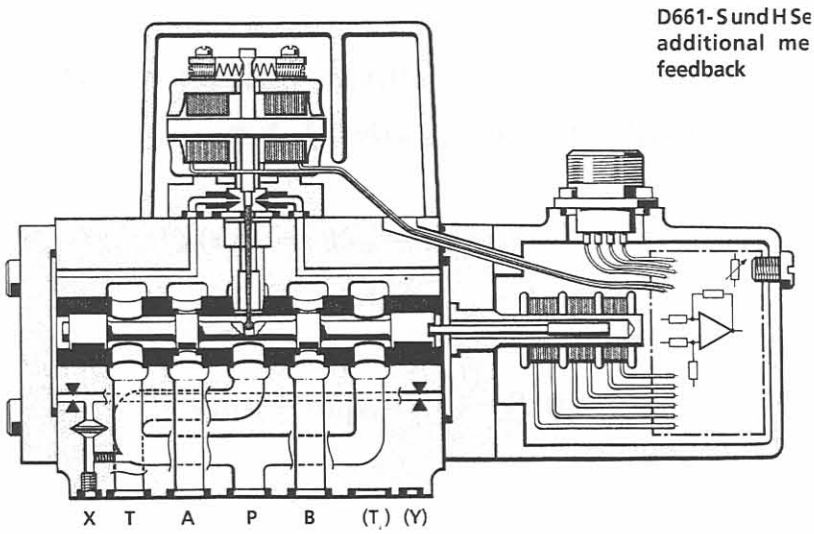

Figure 3.6: Hydraulic cylinder servovalve system (figure adapted from [68]). The top element is the torque motor, the horizontal bar channelling the flow is the servovalve spool and the vertical sleeve that moves the spool is the flexure sleeve.

3.6.2.3 Hydraulic cylinder

The hydraulic actuator being modelled is assumed to be double acting. This means that the stroke of the cylinder can be extended and contracted using the hydraulic fluid, while the mechanical stand system also influences the stroke. For a single acting hydraulic cylinder the stroke can only be extended and the stroke has to be decreased manually, for example by pushing the upper roll chocks upwards.

The cylinder pressure on either side of the cylinder are determined by four flow rates [8, 69]:

1. Cylinder flows ($Q_i \propto x_v\sqrt{\Delta P}, \forall i \in [1,2]$)
2. Leaking flow ($Q_l \propto (P_1 - P_2)$)
3. Volume change rate due to compressed oil ($Q_c = \frac{V}{\beta}\dot{P}$)
4. Flow rates due to the piston velocity ($Q_v = A\dot{x}$)

For the construction of the continuity equations the direction of positive cylinder flow is defined as flow into both chambers and the leakage flow from chamber 1 to chamber 2 (see Fig. 3.3). Constructing the continuity equations for the servo system yield [67, 69] the following:

$$Q_{s1}(t) = Q_{sl}(t) + \frac{V_{s1}(x_s)}{\beta_o}\dot{P}_{s1}(t) + A_{s1}\dot{x}_s(t); \tag{3.79}$$

$$-Q_{s2}(t) = -Q_{sl}(t) + \frac{V_{s2}(x_s)}{\beta_o}\dot{P}_{s2}(t) - A_{s2}\dot{x}_s(t); \tag{3.80}$$

$$\begin{aligned} V_{s1}(x_s) &= V_{01s} + A_{s1}x_s(t) \\ &= A_{s1}(stroke_{max_s} - h_{2_{setup}}) + A_{s1}x_s(t); \end{aligned} \tag{3.81}$$

$$\begin{aligned} V_{s2}(x_s) &= V_{02s} - A_{s2}x_s(t) \\ &= A_{s2}h_{2_{setup}} - A_{s2}x_s(t); \end{aligned} \tag{3.82}$$

$$Q_{ls}(t) = K_{leak_s}(P_{s1}(t) - P_{s2}(t)), \tag{3.83}$$

where,

Q_{s1}: Cylinder flow into the piston side chamber of the cylinder;

Q_{s2}: Cylinder flow into the rod side piston side chamber of the cylinder;

Q_{sl}: The leak flow from the piston side to the rod side of the cylinder;

P_{s1}: Cylinder pressure at the piston side of the cylinder;

P_{s2}: Cylinder pressure at the rod side of the cylinder;

x_s: The hydraulic stroke movement;

K_{leak_s}: Leakage flow coefficient;

β_o: Oil bulk modulus.

3.6.2.4 Operation and interaction with stand model

There are two cases to investigate, namely when the servovalve is charging ($x_{v_s} \geq 0$) and when the servovalve is dumping ($x_{v_s} < 0$). When $x_{v_s} \geq 0$ the cylinder flows are expressed as,

$$Q_{s1}(t) = K_{v_s} x_{v_s}(t) \sqrt{\frac{2}{\rho_o}(P_{high} - P_{s1}(t))}, \tag{3.84}$$

$$Q_{s2}(t) = K_{v_s} x_{v_s}(t) \sqrt{\frac{2}{\rho_o}(P_{s2}(t) - P_{low})}, \tag{3.85}$$

where,

P_{high}: The supply pressure of the hydraulic circuit at the high pressure side;

P_{low}: The tank pressure at the low pressure side of the hydraulic circuit;

ρ_o: Density of the hydraulic oil.

When $x_{v_s} < 0$, the leakage flow equation is kept unchanged and the flow leakage is predicted to be from the piston side to the rod side of the cylinder. The directions of the cylinder flows Q_{s1}, Q_{s2} are reversed. The cylinder flows when $x_{v_s} < 0$ are,

$$Q_{s1}(t) = K_{v_s} x_{v_s}(t) \sqrt{\frac{2}{\rho_o}(P_{s1}(t) - P_{low})}, \tag{3.86}$$

$$Q_{s2}(t) = K_{v_s} x_{v_s}(t) \sqrt{\frac{2}{\rho_o}(P_{high} - P_{s2}(t))}, \tag{3.87}$$

and x_s decreases.

The hydraulic actuator interacts with the stand model and the rolling mill frame. The thrust force of the hydraulic cylinder on either side of the mill is,

$$P_{s1}(t)A_{s1} - P_{s2}(t)A_{s2} = F_{HAs}(t). \tag{3.88}$$

Under steady state this force has to balance the transmitted rolling force on either side of the mill. The hydraulic actuator is top mounted for the configuration under investigation. This type of mounting results in a floating actuator base and the amount of floating is determined by the mill stretch.

The hydraulic stroke is increased to combat the amount of stretch and to maintain thickness control. The following relationship exists between the movement of the upper roll pack, hydraulic stroke and mill stretch,

$$x_s(t) = y_{stretch_s}(t) - y_1(z,t), \tag{3.89}$$

where $y_1(z,t) = y_{sT}(t)$ is such that, when $s = L \Rightarrow z = -\frac{l_1}{2}$ and $s = R \Rightarrow z = \frac{l_1}{2}$ (see figure 3.1). The stretch of the mill is a nonlinear function of the rolling force and strip width [59, 27, 3, 1] but with a predominant linear region. The stretch in the linear range of the mill stretch curve can be calculated as,

$$y_{stretch_s}(t) = \frac{(P_{s1}(t)A_{s1} - P_{s2}(t)A_{s2}) - F_{roll_{test_s}}}{K_{sT}} + y_{stretch_{test_s}}. \tag{3.90}$$

From figure 3.4 the mill stretch is seen to be predominantly a linear function of the applied force and Eq. 3.90 can be modified as follows,

$$y_{stretch_s}(t) \approx \frac{(P_{s1}(t)A_{s1} - P_{s2}(t)A_{s2})}{K_{sT}}. \tag{3.91}$$

Taking the derivative of the hydraulic stroke relationship (Eq. 3.89) and substituting the derivative of Eq. 3.90 into it, yields the velocity of the hydraulic stroke,

$$\dot{x}_s(t) = \frac{\dot{P}_{s1}(t)A_{s1} - \dot{P}_{s2}(t)A_{s2}}{K_{sT}} - \dot{y}_1(z,t). \tag{3.92}$$

The hydraulic cylinder rod velocity, $\dot{x}_s$, contains two pressure derivatives, Eq. 3.92. Substituting Eq. 3.92 into equations 3.79 and 3.80 yields,

$$Q_{s1}(t) = Q_{sl}(t) + \frac{V_{s1}(x_S)}{\beta_o}\dot{P}_{s1}(t) + A_{s1}\left(\frac{\dot{P}_{s1}(t)A_{s1} - \dot{P}_{s2}(t)A_{s2}}{K_{sT}} - \dot{y}_{s1}(z,t)\right), \tag{3.93}$$

$$-Q_{s2}(t) = -Q_{sl}(t) + \frac{V_{s2}}{\beta_o}\dot{P}_{s2} - A_{s2}\left(\frac{\dot{P}_{s1}(t)A_{s1} - \dot{P}_{s2}(t)A_{s2}}{K_{sT}} - \dot{y}_{s1}(z,t)\right). \tag{3.94}$$

Rearranging Eq. 3.94 making $\dot{P}_{s2}(t)$ the subject gives,

$$\dot{P}_{s2}(t) = \frac{-Q_{s2}(t) + Q_{sl}(t) - A_{s2}\dot{y}_{s1}(z,t) + \frac{\dot{P}_{s1}(t)A_{s1}A_{s2}}{K_{sT}}}{\left(\frac{V_{s2}(x_s)}{\beta_o} + \frac{A_{s2}^2}{K_{sT}}\right)}. \tag{3.95}$$

Defining, $\Delta = \frac{V_{s2}(x_s)}{\beta_o} + \frac{A_{s2}^2}{K_{sT}}$, and substituting Eq. 3.95 into Eq.3.93 yields,

$$\dot{P}_{s1}(t) = \frac{Q_{s1}(t) - Q_{sl}(t) + A_{s1}\dot{y}_{s1}(z,t) - \frac{A_{s1}A_{s2}}{K_{sT}\Delta}\left(Q_{s2} - Q_{sl} + A_{s2}\dot{y}_{s1}(z,t)\right)}{\frac{V_{s1}(x_s)}{\beta_o} + \frac{A_{s1}^2}{K_{sT}} - \frac{(A_{s1}A_{s2})^2}{K_{sT}^2\Delta}}. \tag{3.96}$$

The interactions between the linear stand model, the rolling mill frame and the hydraulic actuator have been adequately derived for the purpose of the mill simulator. These models will be expressed as a total nonlinear interacting state space model shown in chapter 4.

3.7 Temperature modelling

3.7.1 Introduction

In section 3.2 it is motivated why the heat transfer problem of the hot rolling process will not be solved. Measures taken in this dissertation to compensate for this lack of modelling are also discussed in section 3.2, and this entails using practical measured data of the Steckel mill process, and conditioning this data to form inputs to the mill simulator. In this section, however a brief introduction to temperature modelling of the hot rolling process will be given as an initiation of future modelling projects.

The Steckel mill is divided into five distinct temperature zones. These zones can be described as follows:

1. The pay-off coiler furnace
2. The radiation and convection zone of the strip before entrance into the roll gap
3. The roll gap
4. The radiation and convection zone of the strip after exit from the roll gap[12]
5. The take-up coiler furnace

The main aim of the temperature model is to calculate a more accurate temperature prediction of the temperature in the roll gap. The temperature in the roll gap influences the flow stress as well as the yield stress of the rolled material in the roll gap as can be seen in Eq. 3.25.

The modelling of the thermal behaviour of the rolling environment can be very involved as can be seen from numerous publications [30, 32, 33, 70]. The following assumptions can be made during the modelling stage in order to decrease the computation time needed to solve the implicit finite difference heat problem:

1. Disturbance variations of the input gauge does not influence the grid.
2. The deviations of the setup draft due to mill stretch etc. does not influence the grid
3. It is assumed that the temperature distribution over the width of the sheet remains constant. This can be motivated from the fact that the width of the sheet is much greater than the thickness and that the heat conduction in the transverse direction can be ignored [70].

[12]The modelling of these zones is straight forward and a static heat conduction PDE is solved with a transformation, $x = vt$ with x is the rolling direction, in order to find the dynamic model [30].

3.7.2 Roll gap temperature modelling

Yuen [32] studied the heat transfer problem found in the roll gap while rolling, by modelling a moving three layer composite strip, compressed between two rotating cylinders. The three layers that were investigated were the rotating rolls, the scale layer and the strip. For this model the scale layer was ignored, because the main aim was to keep the temperature model simple and only compute a more accurate temperature prediction in the roll gap as an input to the roll gap model.

Assuming the coordinate system is fixed in space and the material properties are constant in the temperature range under consideration, then the following heat transfer equation can be constructed for the two body system (strip and rollers).

$$\rho_i c_i \overline{v_i} \bullet \nabla T_i = k_i \nabla^2 T_i + Q_i \tag{3.97}$$

Where the index $i \subset [r, s]$, where r is used to indicate the rollers and s to indicate the strip.

When Eq.3.97 is developed, the following two heat conduction equations are found [32].

$$v_{sx}\frac{\partial T_s}{\partial x} + v_{sy}\frac{\partial T_s}{\partial y} = \alpha_s\left[\frac{\partial^2 T_s}{\partial x^2} + \frac{\partial^2 T_s}{\partial y^2}\right] + \frac{Q_s}{\rho_s c_s} \tag{3.98}$$

$$v_{rr}\frac{\partial T_r}{\partial r} + v_{r\theta}\frac{\partial T_r}{\partial \theta} = \alpha_r\left[\frac{\partial^2 T_r}{\partial r^2} + \frac{1}{r}\frac{\partial T_r}{\partial r} + \frac{1}{r^2}\frac{\partial^2 T_r}{\partial \theta^2}\right] + \frac{Q_r}{\rho_r c_r} \tag{3.99}$$

The boundary value problem, can be solved numerically with the aid of finite element methods or finite differences methods.

3.7.3 Coiler furnace models

The modelling of the coiler furnace is necessary if the temperature history of the sheet is of importance at any given time. The Steckel Mill employs multiple passes to achieve the desired reduction. Thus, the sheet is coiled on either side of the rolling mill twice or thrice before the strip's final thickness is reached. If the final aim of the research is the operation of a control system for all the passes, then these models might be necessary.

The strip is subjected to cooling during the pass and after it is wound on a coiler inside a furnace. Here the strip's temperature loss is to be minimized. A complicating factor is the conduction between adjacent sheet wraps that changes the boundary conditions of the heat transfer problem [38].

3.7.4 Thermal crown modelling

The thermal crown build-up on the rollers is not modelled in this dissertation. In [37] a basic two dimensional model is given that can be used to model the thermal crown build-up. The temperature of the rolls is between 15 - 60 °C and the average value of the crown is from 0.01-0.5 mm. The evolution of the thermal crown on the rollers is a slower process than the stand, actuator and tension model dynamics derived in this section. It is assumed that these slow dynamics will not be identifiable on the time scale under investigation.

3.8 Conclusion

In this section the mathematical theory of the nonlinear and linear models embodied in the mill simulator was derived. The models which the simulator consists of are the roll gap model, stand model, hydraulic actuator models and the tension models. The roll gap model is seen as the connecting model of the simulator. The identified inputs of the stand model are the thrust forces of the hydraulic actuators and the rollforce, which is an output of the roll gap model. The roll gap entry and exit speeds are also outputs of the roll gap model and these speeds serve as inputs to the tension models. In the following chapter the solution methodology associated with each of these models will be discussed, as well as the final model incorporation of the nonlinear plant simulator.

Chapter 4

Nonlinear plant simulator

4.1 Introduction

Figure 3.1 in chapter 3 shows the dependency between the nonlinear models which constitute the mill simulator. In this chapter these dependencies will be studied in earnest with the aim of connecting the models together. Furthermore, the tuning and choice of model constants will be discussed in order to yield realistic simulated behaviour. Plant data obtained from an actual logged Steckel Hot Rolling Mill Process are used as simulator inputs[1].

4.2 Simulator inputs

4.2.1 Introduction

The nonlinear plant simulator is to be used for identifying linear plant models around certain identified operating points. These linear models are highly dependent on the precalculated operating points associated with the generated rolling schedule [18, 59]. The generation of an optimal setup schedule falls outside the scope of this work and a practical schedule was taken as a given input for the simulator. Practical setup schedules were identified from the plant data for the Steckel Hot Rolling Mill process.

In the simulator, only the identified models of chapter 3 are solved and the modelling of the other

[1]It needs to be stressed that the measured plant data has an average time resolution of 0.423 seconds with the mill under closed loop control. This data is helpful, but not completely suited for the tuning of the open loop plant investigated in this study. The open loop data can possibly be extracted from the closed loop results with some added effort, but the impact of this procedure is questionable due to the data's under-sampled nature. It is stated that the hydraulic gauge loop has a bandwidth of 15 Hz [1, 8] which is equivalent to a first order transfer function with a time constant of 10ms, roughly 23 times smaller than the current time resolution of the data.

identified rolling parameters (see figure 3.1) falls outside the scope of this dissertation. Unmodelled parameters (discussed and motivated in section 3.2) that are critical for the functioning of the simulator are:

- The temperature in the roll gap;
- The rolling mill speed;
- Input thickness;
- Rolling schedules.

These modelling deficiencies are compensated for by conditioning real logged plant data for the above variables to be suitable as inputs for the mill simulator.

Operating points were identified from the logged plant data for two similar stainless steel strips of grade 304, which is the most common rolled product of a large stainless steel manufacturer in South Africa[2]. The data show that the strip is usually rolled in a 5-9 pass schedule and that the strip entrance thickness, as obtained from the roughing mill, is about 25mm. In table 4.1 a typical 9 pass rolling schedule is given reflecting entrance and exit thicknesses for each pass. Also shown are the pyrometer measured maximum roll gap entrance and exit temperatures, $\theta_{1_{max}}$ and $\theta_{2_{max}}$ respectively, as well as the measured starting velocity (v_{start}) , threading velocity (v_{thread}) and final velocity (v_{stop}) of the main mill drive.

Table 4.1: Typical Steckel Rolling Mill schedule for the investigated similar strips.

Pass number	$h_1(mm)$	$h_2(mm)$	$\theta^{\circ}_{1_{max}}C$	$\theta^{\circ}_{2_{max}}C$	$v_{start}m.s^{-1}$	$v_{thread}m.s^{-1}$	$v_{stop}m.s^{-1}$
1	25	18.2	980	960	2.1	6	1.8
2	18.2	13.3	967	955	2.1	3.5	1.8
3	13.3	9.7	965	950	2.1	4.8	1.8
4	9.7	7.5	962	948	2.1	6.1	1.8
5	7.5	6.1	957	942	2.1	8	1.8
6	6.1	5.1	955	940	2.1	9.2	1.8
7	5.1	4.3	950	937	2.1	10	1.8
8	4.3	3.7	948	935	2.1	10	1.8
9	3.7	3.3	945	933	2.1	8.5	3.6

The implemented simulator does not have the capability to simulate flatness behaviour of the strip and is only limited to thickness profile simulation. From practical experience[3] [3] the desired thickness profile is rolled during the early passes and during the later passes the flatness (shape) can be controlled. When the strip thickness is greater than 12mm the strip profile is controlled and zero to very

[2]This information was provided by M. Lewis during a personal meeting.

[3]Information supplied by M. Lewis during a personal discussion.

little action can be exerted to control the strip shape/flatness. When the strip thickness falls below 6mm the shape/flatness is controlled and the profile is left unchanged.

4.2.2 Motivation for the choice of simulation operating point

Two rolling schedules and the associated measured data of two similar Stainless Steel grade 304 strips were identified and this data was adapted to form the simulator inputs. It was decided to focus on data of pass 1 and pass 3 in a 5 pass schedule, as possible inputs for the simulator. Some advantages and disadvantages associated with the choice of either of these two passes can be summarized as:

Pass 1:

- If data for pass 1 are used as simulator inputs, the rolling variables might tend to be open loop data and can be used for simulator tuning.
- The possibility exists to perform step tests on the Steckel rolling mill, on which this simulator is based. If this should materialize, defects and disturbances caused by these tests can be corrected for in later passes.
- When pass 1 is chosen as the operating pass, the simulation time interval of the tension model is small and leads to longer computation times.

Pass 3:

- Logged data of pass 3 incorporates effects of control actions taken in previous passes. It might prove difficult to extract open loop data from the available closed loop data. The closed loop logged data can be used to evaluate the performance of the proposed controller against the industrial controller.
- The exit thickness of pass 3 falls on the borderline, where the controllability of profile declines and the controllability of the sheet's shape/flatness increases[4].

Of all of the above points, the computation time was considered to be the most important and weighed heavily in the final choice to make the simulator operable for pass 3.

4.2.3 Rolling variables

The rolling data associated with pass 3 for one of the two identified similar strips were manipulated to serve as input for the mill simulator. In figure 4.1 a measured process speed curve of the main mill drive speed is shown. This batch process exhibits a speed up ramp after tension in the sheet has

[4]Information supplied by M. Lewis during a personal discussion.

been established up to a threading speed. In figure 4.2 the X-ray measured strip input and output thicknesses to and from the roll gap are shown. In figure 4.3 the measured temperatures outside on either side of the roll gap are shown. These temperatures are interpolated linearly in order to obtain a temperature estimate in the roll gap.

The operation point of the simulator was chosen on the mill speed up ramp at a speed of 3.5m/s. This operating point was used, because control is not well addressed on the speed up of the curve [19]. The converse is the norm for the regulation of the rolling process at threading speed [4, 3]. The possible material saving that can result from the elimination of off specification products during the process start and stops can be significant [19].

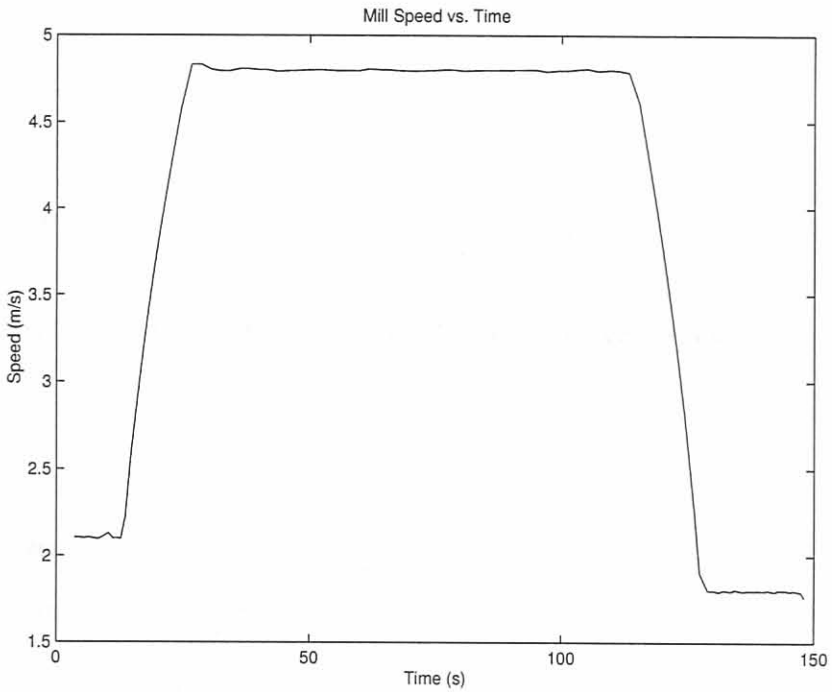

Figure 4.1: Typical speed vs. measured time for pass 3.

4.3 Roll gap model

4.3.1 Solution methodology

The solution of the roll gap model entails the solution of the differential equation model, Eq. 3.15, together with its associated boundary values. Unfortunately the ODE model consists of two independent differential equations on either side of the neutral plane. This phenomenon is due to the frictional forces that work towards the neutral point (see figure 3.2). The general method for solving this model is by numerically integrating the two independent differential equations from either end of the arc of contact while working towards the neutral point of the roll gap.

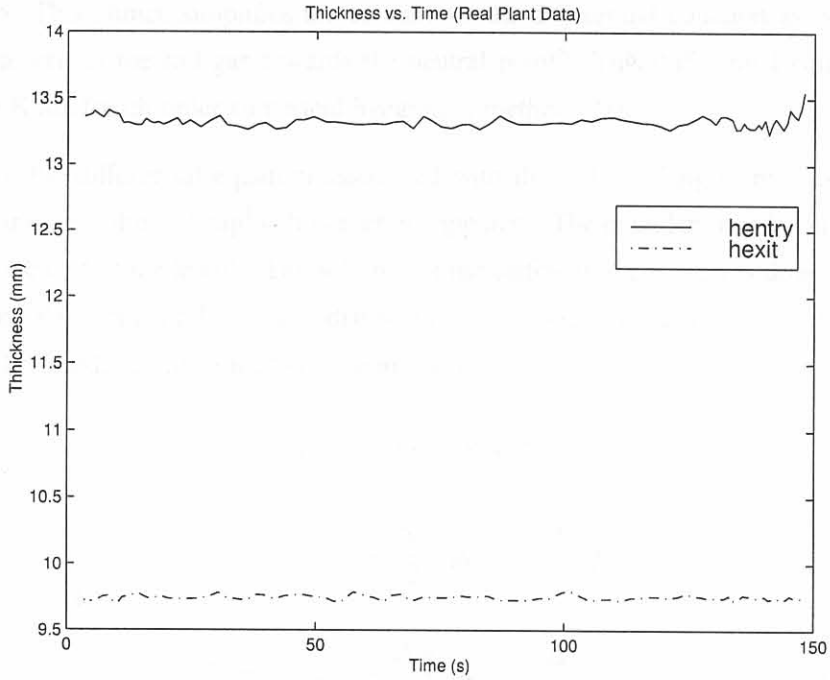

Figure 4.2: Typical entry and exit thicknesses to and from the roll gap vs. the measured time for pass 3.

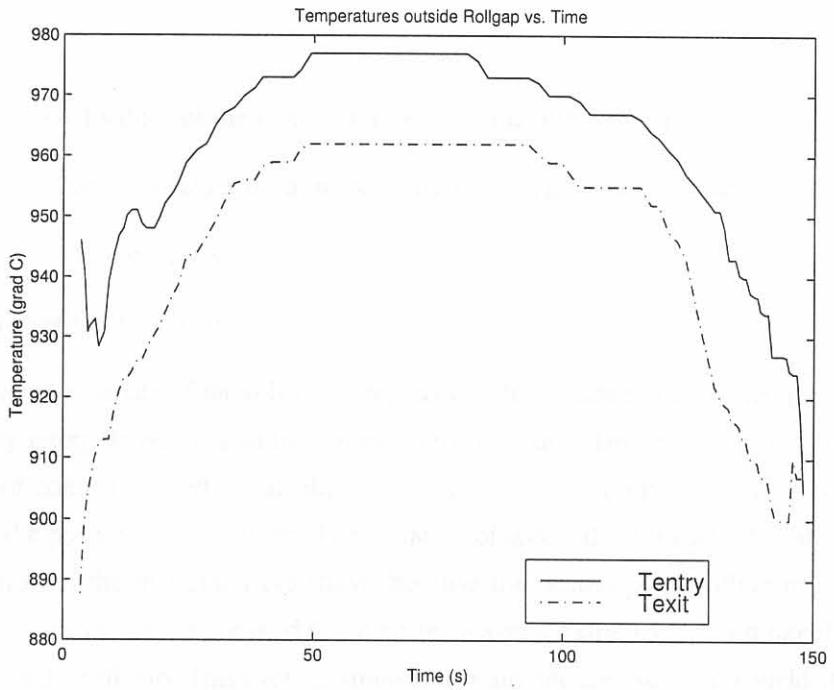

Figure 4.3: Typical entry and exit temperatures to and from the roll gap vs. the measured time for pass 3.

The coordinate system of the roll gap model is chosen such that x_{rg}[5] is increasing towards the entrance of the roll gap. This choice simplifies the solution of the differential equation associated with the length from the exit of the roll gap towards the neutral point[6]. This differential equation is solved using a Runge Kutta fourth order numerical integration method [71].

The solution of the differential equation associated with the roll gap length from the neutral point towards the entrance of the roll gap[7] is however not apparent. The boundary condition of the problem is provided at the end of the length. The solution of the differential equation is done by numerically back-calculating the vertical roll pressure distribution. This back calculation solution is achieved by manipulating the standard Runge Kutta equations as follows:

$$f_1 = f(\phi_{k+1}, p_{k+1}), \tag{4.1}$$

$$f_2 = f(\phi_{k+1} - \frac{\Delta\phi}{2}, p_{k+1} - \frac{\Delta\phi}{2} f_1), \tag{4.2}$$

$$f_3 = f(\phi_{k+1} - \frac{\Delta\phi}{2}, p_{k+1} - \frac{\Delta\phi}{2} f_2), \tag{4.3}$$

$$f_4 = f(\phi_k, y_k), \tag{4.4}$$

$$p_k = p_{k+1} - \frac{\Delta\phi}{6}(f_1 + 2f_2 + 2f_3 + f_4), \tag{4.5}$$

where,

p_k, p_{k+1}: Discretized values of the vertical rolling pressure along the arc of contact;

f_i, $\forall i \in [1, ..., 4]$: Function values used in the numerical integration procedure;

ϕ_k, ϕ_{k+1}: Discretized arc values;

$\Delta\phi$: Angle interval for discretized arc.

In order to have an estimate of the roll gap temperature, the entrance and exit temperature of the roll gap are linearly interpolated to yield the estimated temperature. This estimated roll gap temperature along the arc of contact is used to calculate the yield stress of the material, the friction coefficient, and indirectly the position along the arc. The variation of speed along the arc of contact was not used in the calculation of the material yield stress, because the neutral point rolling mill speed and the associated geometric quantities are used to calculate an average strain and strain rate that the material is subjected to in the roll gap. This average strain and strain rate are used in the yield stress model see Eq. 3.28.

[5] As defined in table 3.1.

[6] $\frac{dp(\phi)}{d\phi} = 2R' \frac{p(\phi)}{h(\phi)} \left[\frac{sin\phi + \mu cos\phi}{1 - \mu tan\phi}\right] - 2R' \frac{(p(\phi) - k(\epsilon, \dot{\epsilon}, \theta))}{h(\phi)} sin\phi.$

[7] $\frac{dp(\phi)}{d\phi} = 2R' \frac{p(\phi)}{h(\phi)} \left[\frac{sin\phi - \mu cos\phi}{1 + \mu tan\phi}\right] - 2R' \frac{(p(\phi) - k(\epsilon, \dot{\epsilon}, \theta))}{h(\phi)} sin\phi.$

As was previously remarked in chapter 2, the neutral point shifts with the application of tension to the strip. A suitable equation was not found in the literature that defines the neutral point position as a function of the applied strip tensions. In order to evaluate the tension interactions with the roll gap model the modelling of the movement of the neutral point is fundamental in the calculation of the frictional forces in the roll gap.

The solution of the two differential equations are independent. At a certain point (neutral point) the solution of these two differential equations equate and the movement of the neutral point is thus solved numerically. In chapter 5 the effects of varying the applied strip tensions and the draft on the specific roll force are also highlighted using some illustrative figures.

4.3.2 Physical constants

In table 4.2 the roll radius as well as an average value for the roll radius and length of the arc of contact are shown. It was found that the logged data and the roll gap model simulation was not in agreement and the roll gap model was tuned to yield adequate roll force simulation. Two tuning parameters, α_{YS} and α_{RF}, were used. α_{YS} was used to tune the yield stress model to agree with calculated values in the database applicable to the Steckel Mill under investigation. After this step the roll force was tuned by adjusting, α_{RF}, and good agreement was achieved. In table 4.3 the yield stress model parameters and the tuning factors are shown.

Table 4.2: Roll gap model parameters

Variable	Value
R	375 mm
R'	403 mm
L_p	50 mm

Table 4.3: Yield stress model parameters and tuning factors. The yield stress model parameters are used in Eq. 3.28

Variable	Value
k_{fo}	2800
k_f	0.0024
k_{fspeed}	0.0165
α_{YS}	0.925
α_{RF}	0.716

4.3.3 Flow chart

In figure 4.4 the roll gap model flow chart is shown. The roll gap model has as its inputs the draft, main mill drive speed, exit and entrance temperatures, and the exit and entrance tensions that are outputs from the tension model. These variables are used to calculate the yield stress and friction coefficient along the arc of contact in order to find the vertical rolling force pressure along the arc of contact. It can be seen that the two independent differential equations are solved independently and when these solutions equate the neutral point is obtained. This array is combined and then integrated over the arc of contact to yield the rolling force. This rolling force is then used to calculate the deformed roll radius. This deformed roll radius is updated with an iterative Gauss-Seidel scheme and this loop terminates when the normalized error between two iterative steps is less than 0.1%. The Gauss-Seidel iterative scheme is described in more detail in section 4.4.2 where the tension model is discussed.

Once the neutral point is found, the velocity and thickness change along the arc of contact are calculated. The output of the roll gap model is the specific roll force, length of the arc of contact, and the entrance and exit velocities of the roll gap. These outputs are used as inputs for the other models in the mill simulator. The specific rolling force is used in the stand model. The length of the arc of contact is used in the main simulator loop to simulate the transport delay across the roll gap. The two speeds are used as inputs to the tension model.

4.4 Tension Model

4.4.1 Solution methodology

The implemented tension models are integrators with large gains. Classical control system theory [72] states that the bandwidth ($rad.s^{-1}$) is equal to the gain of the pure capacitive process. This gain is highly dependent on the constants of the system and is largely influenced by Young's modulus of the strip. In [73], Young's modulus for Stainless Steel grade 304, E_{ss}, is given as a function of temperature. Using the tabulated values in [73] an interpolated value of $E_{ss}|_{\theta=970°C} = 106 \times 10^9 Pa$ was found. The model gain is,

$$\frac{E_{ss}A_{cross}}{L_{cf\leftrightarrow rg}} = \frac{106 \times 10^9 wh_i}{6.4}, \forall i \in [1,2], \tag{4.6}$$

where A_{cross} is the cross sectional area of the strip in the width perpendicular to the rolling direction, and h_i is the thickness on either side of the roll gap. These gains determine the bandwidth, and also the simulation time interval of the model required to keep the tension model stable. The rule-of-thumb is to make the simulation frequency 2-10 times larger than the system bandwidth [74]. From Eq. 4.6, it is evident that the simulation frequency of the model lowers when the thickness decreases. This attests that tension control is of increasing importance with decreasing thickness as is the case for cold rolling mills and the latter passes of the rolling schedule for the Steckel Mill process. In order

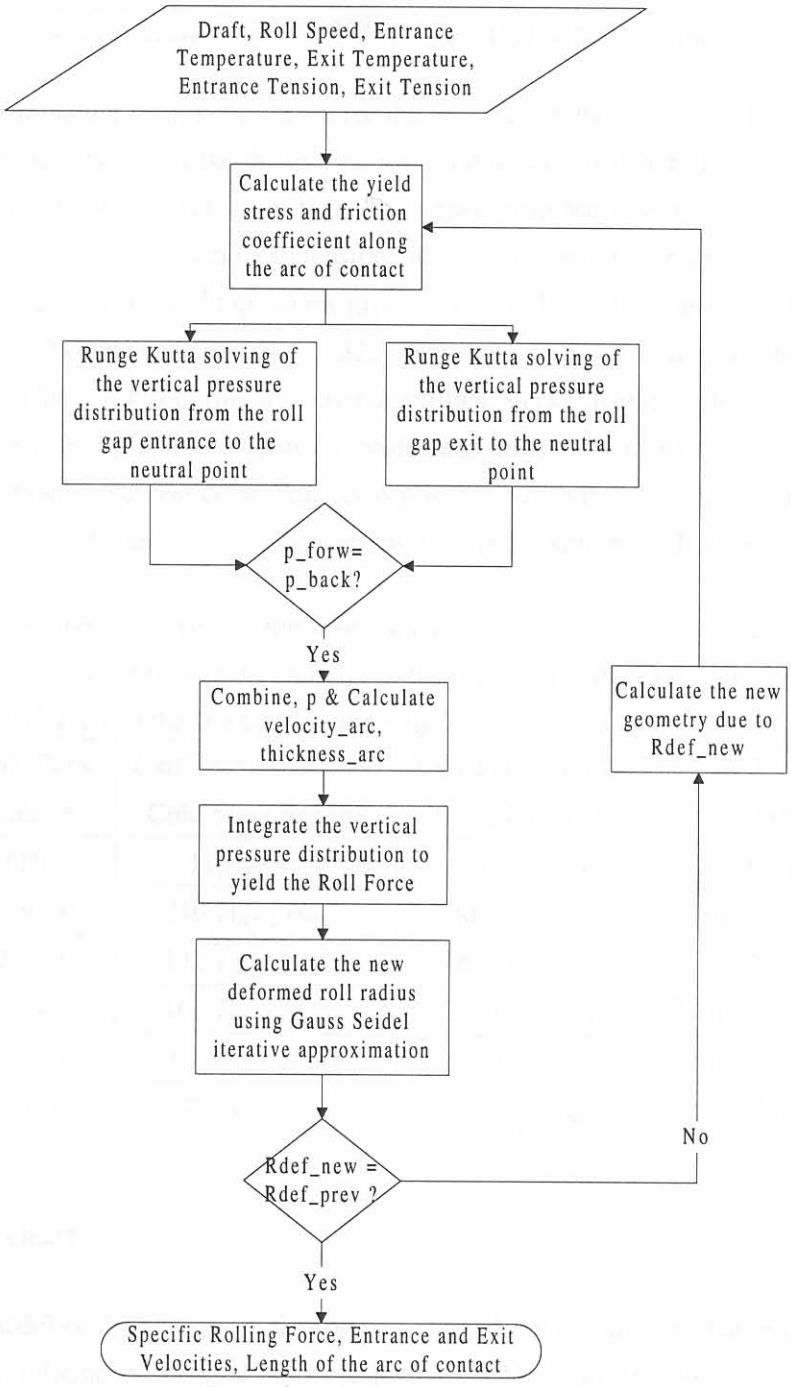

Figure 4.4: Roll gap model flowchart.

to save simulation time, the maximum allowable simulation time interval was chosen to correspond to a sampling frequency twice the bandwidth of the integrator model. The maximum simulation time intervals that can be used for the tension model simulation, when pass 3 data is used, are,

$$\Delta t_{tension} = \frac{2\pi}{2}\frac{L_{cf\leftrightarrow rg}}{E_{ss}A_{cross}} = \frac{1}{7.38\times 10^{9}h_i} = \begin{cases} 1.04\times 10^{-8}s, \; when\, h_i = 13mm \\ 1.51\times 10^{-8}s, \; when\, h_i = 9mm \end{cases} . \quad (4.7)$$

In chapter 5, simulation results are shown for the specific rolling force as a function of the applied tensions. These results may make the tension setup values obtained from Eq. 3.32 seem low. These setup tension values are in fact larger than the applied strip tensions associated with a multistand hot rolling mill, and are comparable to tension values associated with multistand cold rolling mills. In table 4.4, nominal tension setup values given in [3] for hot rolling and cold rolling of steel are compared to results obtained from Eq. 3.32, when similar strip thickness for both the hot rolling cases are used. Table 4.4 confirms the observation that Steckel Rolling relies on tension more as a secondary deformation process compared to multistand mills. Ultimately the strip can be drawn thin if necking[8] is allowed, but less controllability is possible due to the control effort associated with the acceleration and deceleration of the large inertias associated with the coiler motors and their drums.

Table 4.4: In this table the tension setup values are shown for various cases. The notation xB and xF refers to pass x's tension between the entrance of the roll gap and the back coiler and tension between the exit of the roll gap and the front coiler respectively.

Stand (Pass) Number	**Exit Tension (kN/m) Cold Steel Rolling**	**Exit Tension (kN/m) Hot Steel Rolling**	**Eq. 3.32 (kN/m) Steckel Rolling**
0 (1B)	$11\|_{h=2.2mm}$	$0\|_{h=22mm}$	$108.3\|_{h=22mm}$
1 (1F/2B)	$216.7\|_{h=1.65mm}$	$30.1\|_{h=11.57mm}$	$91.0\|_{h=11.57mm}$
2 (2F/3B)	$142.1\|_{h=0.96mm}$	$23.3\|_{h=6.30mm}$	$77.3\|_{h=6.30mm}$
3 (3F/4B)	$100.7\|_{h=0.61mm}$	$18.7\|_{h=3.97mm}$	$68.2\|_{h=3.97mm}$
4 (4F/5B)	$67.6\|_{h=0.41mm}$	$18.3\|_{h=2.95mm}$	$62.9\|_{h=2.95mm}$
5 (5F)	$17.1\|_{h=0.30mm}$	$5\|_{h=2.5mm}$	$60.2\|_{h=2.5mm}$

4.4.2 Flow chart

The tension model could be expressed as an explicit and implicit model. The explicit model is obtained by reformulating the integral model (Eqs. 3.33, 3.34) as an equivalent state-space differential equation model. The explicit model makes it difficult to solve for the implicit behaviour between the tensions applied to the roll gap model and the output velocities of the roll gap model. These velocities are in turn used as inputs to the tension model. Such an iterative process can be solved by using an iterative solution procedure such as Gauss-Seidel iteration.

[8] When the strip tension stress is larger that the material yield stress the strip deforms plastically. This deformation is manifested in a thickness and a less obvious width reduction of the sheet.

In this dissertation the tension model is kept unchanged in its integral format (Eqs. 3.33, 3.34). The input is the draft in the middle of the sheet, $\delta(z = 0, t = t_0)$, at any given time instance, which is an integer multiple of the main loop's simulation time interval, Δt_{Main}. In order to keep the tension loop stable it was found that, $\Delta t_{tension} < \Delta t_{Main}$, and that the tension loop must be solved at a higher frequency than the rest of the models.

It can be argued that due to these differences in the bandwidth of the tension processes and the rest of the simulator, that the tension models are faster than the rest of the processes, and could therefore be omitted from this study. Although there is some truth in this statement, this dissertation is an initial investigation into the tension and gauge interactions and no applicable article in the literature, where the effect of tension deviations on the thickness control loop of a Steckel Mill Process is investigated, could be found. However, statements are made in [3] that tension deviations influence the gauge control system of a single stand rolling mill adversely, and that Steckel Mills relies largely on a drawing process, which implies that the application of large tensions to the strip occurs.

In figure 4.5 two loops are apparent. The outer loop is the time loop that is simulated for time $t = t_0 + n\Delta t_{tension}, \forall t_0 \leq t \leq t_0 + \Delta t_{Main}$, where n is the simulation counter. The inner loop accounts for the iterative solution of the tension as a function of the exit and entrance speeds of the roll gap. The execution of this loop is stopped after the Gauss-Seidel filtered tension answer, $T_i; \forall i \in [1, 2]$,

$$T_i = \alpha T_{i_{new}} + (1 - \alpha) T_{i_{previous}}, \tag{4.8}$$

has stabilized to within a 0.1% error of the normalized tension differences between two iterative steps. This normalized error is expressed as,

$$error_T = \frac{|T_1 - T_{1_{previous}}|}{T_{1_{previous}}} + \frac{|T_2 - T_{2_{previous}}|}{T_{2_{previous}}}, \tag{4.9}$$

where $T_{i_{new}}$ is the current calculated tension due to speed deviations obtained from the roll gap model after $T_{i_{previous}}$ was applied to the roll gap model. This new tension value is filtered in order to ensure convergence and to negate possible divergent oscillating. Before the execution of the next iterative step, $T_{i_{previous}}$ is set equal to the current T_i.

The tension loop executes rapidly if $\alpha = 0.95$. A safety factor of 15 loop iterations is set as the maximum number of iterative steps. After the completion of the loop the tension value is used in the rest of the simulator at the timing instance of the main loop.

4.5 Stand Model

4.5.1 Solution Methodology

Separation of variables

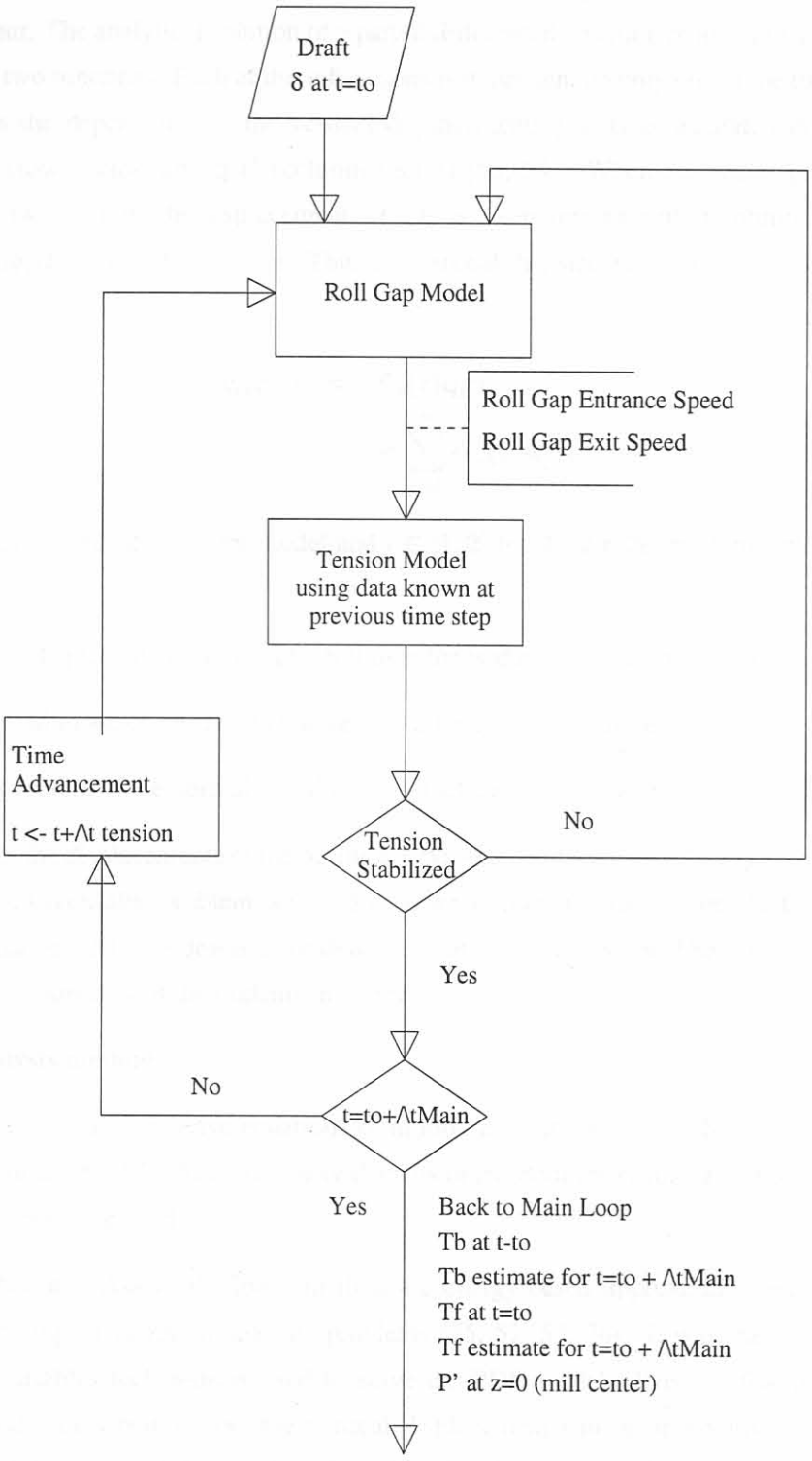

Figure 4.5: Flow Diagram used in the solution of the tension model

There are different ways of solving a partial differential equation model [75, 51, 53, 54, 7] such as depicted in chapter 3. It was decided to use an analytical approximate method [75] to solve the vertical displacements of the rollers as a function of time and space in order to simulate the strip crown behaviour. The analytical solution of a partial differential equation requires that the variable be separated into two functions. Each of these functions is dependent on only one of the two independent variables, thus the dependence of the vertical displacements $y(z,t)$ is separated into two infinite vectors, $\Phi(z)$ (row vector) and $\mathbf{q}(t)$ (column vector) [53, 54]. When the vector product is taken between these two vectors, the displacement, $y(z,t)$ is a superposition of an infinite number of the products $\phi_j(z)q_j(t)$ $(\forall j \in [0,1,2,...])$. Thus the vertical displacements of the stand model can be expressed as:

$$\begin{aligned} y_i(z,t) &= \Phi_i(z)\mathbf{q}_i(t) \\ &= \sum_{j=0}^{\infty} \phi_{i_j}(z)q_{i_j}(t), \end{aligned} \tag{4.10}$$

where $i \in [1,2,3,4]$ for the 4 roller model and $i \in [1,2]$ for the 2 roller pack model. The variables are,

$y_i(z,t)$: Vertical displacement in time of a roll over the width of the rolling mill stand.

$\Phi_i(z)$: The natural mode of vibration (row vector) for a continuous system.

$\mathbf{q}_i(t)$: Column vectors of the normal coordinates, which are continuous functions of time.

The solution for the displacements of the beams can be obtained by solving the Eigenvalue problem of the system. The Eigenvalue problem is solved to generate ordinary and independent sets of ordinary differential equations that will describe the dynamic motion of the system. The calculated eigenvalues are the natural frequencies of the undamped system.

Vibration analysis method

The more common ways to derive equations of motion are with the aid of Newtonian dynamics or Lagrange dynamics [54, 53]. Although more degrees of freedom are required to describe a system if Newtonian dynamics are used.

The Raleigh-Ritz and Assumed Modes method are energy-based approximate analytical methods used for the solving of vibration analysis problems [75, 52, 53, 76]. It was stated earlier that the separation of variables technique is used to solve the PDE model. It is not feasible to calculate the infinite modes of vibration, but the vertical displacement can be approximated by taking the superposition of the products of a finite number of modes of vibration and their accompanying normal coordinates.

The approximate vertical displacement is expressed as,

$$y_i(z,t) \approx \sum_{j=0}^{2p} \phi_{i_j}(z) q_{i_j}(t), \ \forall i \in [1,2,3,4], \tag{4.11}$$

where p is the number of accurate natural modes of vibration.

For the Assumed Modes and the Rayleigh Ritz method the number of modes ($2p$) is chosen two times larger than the predominant spatial modes (p) [75].

Each roller has $2p$ number of assumed modes. Application of the Assumed Modes method only requires that the assumed modes be generated for one element. The same modes can be used for the other roller elements. The assumed modes must satisfy the boundary values given in equations 3.64, 3.65, 3.66, 3.67, 3.69, 3.70, 3.71 and 3.72. From these equations it can be seen that each of the roller elements have the same boundary value structure[9]. In this work the choice of the assumed modes is motivated by the results obtained by Pederson [59], where the first two natural modes of vibration were calculated using Galerkin's method[10]. In this dissertation four assumed modes were developed although not all of these modes are used in the implemented simulator. When the number of assumed modes increase with one, the number of states of the stand model increases with 2 for each roller. The generated assumed modes[11] for one roller are shown in figure 4.6 and are given as,

$$\Psi_i = \begin{bmatrix} \psi_{i_1} & \psi_{i_2} & \psi_{i_3} & \psi_{i_4} \end{bmatrix}, \ \forall i \in [1,2,3,4], \tag{4.12}$$

where the first assumed modes is,

$$\psi_{i_1}(z) = 4.25\left(\frac{2z}{l_i}\right)^3 - 1.28\left(\frac{2z}{l_i}\right) - 0.5, \tag{4.13}$$

the second assumed mode,

$$\psi_{i_2}(z) = 0.15\left(\frac{2z}{l_i}\right)^4 - 0.3\left(\frac{2z}{l_i}\right)^2 + 1.0, \tag{4.14}$$

the third assumed mode,

$$\psi_{i_3}(z) = -2.81\left(\frac{2z}{l_i}\right)^5 - 5.38\left(\frac{2z}{l_i}\right)^3 + 2.06\left(\frac{2z}{l_i}\right) - 0.5, \tag{4.15}$$

and the fourth assumed mode is,

$$\psi_{i_4}(z) = 7.11\left(\frac{2z}{l_i}\right)^6 - 14.22\left(\frac{2z}{l_i}\right)^4 + 7.11\left(\frac{2z}{l_i}\right)^2. \tag{4.16}$$

[9] $y_i^{(1)}\Big|_{z=\frac{\pm l_i}{2}} = 0$ and $y_i^{(3)}\Big|_{z=\frac{\pm l_i}{2}} \neq 0$, $\forall i \in [1,2,3,4]$, where $^{(n)}$ signifies a nth order differentiation of space (z).

[10] Galerkin's method is another approximate analytical method used for solving PDE models [75].

[11] The normal structure of the natural modes of vibration for a simple beam is [59, 60, 53], $\phi_i(z) = c_{i1}cos\beta_i z + c_{i2}sin\beta_i z + c_{i3}cosh\beta_i z + c_{i4}sinh\beta_i z$.

The coupled assumed modes of vibration for the four roller model are, $\mathbf{\Psi} = \begin{bmatrix} \Psi_1 & \Psi_2 & \Psi_3 & \Psi_4 \end{bmatrix}$, and for the two roll pack, $\mathbf{\Psi} = \begin{bmatrix} \Psi_1 & \Psi_2 \end{bmatrix}$, where $\mathbf{\Psi}$ is a row vector.

Taking the assumed modes of the approximate method into consideration, an estimate of the vertical displacement, $\widehat{y_i}$, can be expressed as,

$$\widehat{y_i}(z,t) = \sum_{j=1}^{2p} \psi_{i_j}(z) q_{i_j}(t) = \Psi_i(z)\mathbf{q}_i(t), \ \forall i \in [1,2,3,4]. \tag{4.17}$$

The spatial solution, $\mathbf{\Phi}(z)$, of the stand model is obtained by solving the Eigenvalue problem of the system. When the Eigenvalue problem is solved, the system can be decoupled, and a set of ordinary differential equations for the normal time coordinates $\mathbf{q}(t)$, is obtained. The relationship between the assumed modes and the natural modes of vibrations is [54, 75],

$$\mathbf{\Phi}(z) = \mathbf{\Psi}(z)\mathbf{U}, \tag{4.18}$$

where $\mathbf{U}$ is the modal matrix of the system [54].

For the purposes of the simulator it was decided to concentrate on the two roll pack model, because the four roller model increases the complexity of the mill simulator and increases the simulation time. Other reasons for this choice are given in section 3.5.6.

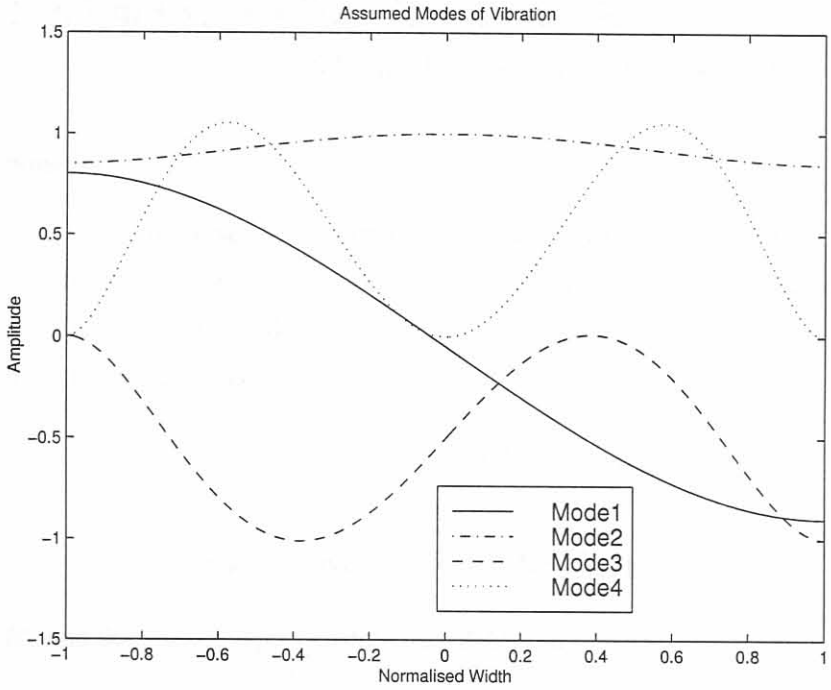

Figure 4.6: Assumed Modes for a roller element

4.5.2 Two Roller model

4.5.2.1 Model equations

Roll Packs

In order to avoid confusion with the indices in this section and the indices used in chapter 3, the indices of the two roll packs, namely $_{12}$ and $_{34}$ are renamed as $_1$ and $_2$ respectively.

When Eq. 4.17 is substituted into Eqs. 3.63 and 3.68, while a fourth order spatial derivative as well as a second and first derivative of time are done, for the estimated vertical displacement of each roller[12],

$$\rho A_1 \Psi_1 \ddot{\mathbf{q}}_1 + EI_1 \Psi_1^{(4)} \mathbf{q}_1 + \beta_{strip} \Psi_1 \dot{\mathbf{q}}_1 + k_{strip} \Psi_1 \mathbf{q}_1 = +k_{strip} \Psi_2 \mathbf{q}_2 + \beta_{strip} \Psi_2 \dot{\mathbf{q}}_2 + P', \quad (4.19)$$

$$\rho A_2 \Psi_2 \ddot{\mathbf{q}}_2 + EI_2 \Psi_2^{(4)} \mathbf{q}_2 + \beta_{strip} \Psi_2 \dot{\mathbf{q}}_2 + k_{strip} \Psi_2 \mathbf{q}_2 = +\beta_{strip} \Psi_1 \dot{\mathbf{q}}_1 + k_{strip} \Psi_1 \mathbf{q}_1 - P'. \quad (4.20)$$

Premultiplying Eq. 4.19 and Eq. 4.20 with $\Psi_1^T(z)$ and $\Psi_2^T(z)$ respectively yields,

$$\begin{aligned} \Psi_1^T \rho A_1 \Psi_1 \ddot{\mathbf{q}}_1 + \Psi_1^T EI_1 \Psi_1^{(4)} \mathbf{q}_1 + \Psi_1^T \beta_{strip} \Psi_1 \dot{\mathbf{q}}_1 + \Psi_1^T k_{strip} \Psi_1 \mathbf{q}_1 = \\ +\Psi_1^T \beta_{strip} \Psi_2 \dot{\mathbf{q}}_2 + \Psi_1^T k_{strip} \Psi_2 \mathbf{q}_2 + \Psi_1^T P', \end{aligned} \quad (4.21)$$

$$\begin{aligned} \Psi_2^T \rho A_2 \Psi_2 \ddot{\mathbf{q}}_2 + \Psi_2^T EI_2 \Psi_2^{(4)} \mathbf{q}_2 + \Psi_2^T \beta_{strip} \Psi_2 \dot{\mathbf{q}}_2 + \Psi_2^T k_{strip} \Psi_2 \mathbf{q}_2 = \\ +\Psi_2^T \beta_{strip} \Psi_1 \dot{\mathbf{q}}_1 + \Psi_2^T k_{strip} \Psi_1 \mathbf{q}_1 - \Psi_2^T P'. \end{aligned} \quad (4.22)$$

Discrete Components

The interactions between the discrete elements associated with the hydraulic jacks, the work roll chock-bearing combinations as well as the forces (these forces work in tandem and are taken as the same force, $J(t)$) that can be exerted by the hydraulic jacks in order to apply positive or negative work roll bending, are expressed as,

$$M_{sJT} \ddot{y}_{sJT} + K_{sJ} y_{sJT} = J(t) + K_{sJ} y_{sJB}, \quad (4.23)$$

$$M_{sJB} \ddot{y}_{sJB} + K_{sJ} y_{sJB} = -J(t) + K_{sJ} y_{sJT}, \quad (4.24)$$

where $s \in [L, R]$, and the generic representations are defined as:

M_{sJT}, M_{sJB}: The masses of the top and bottom work roll chock-bearing combinations.

K_{sJ}: The hydraulic stiffness of the hydraulic actuators and unmodelled stiffness lumped together to form a discrete spring on either side of the mill.

[12]The notation applies $\gamma^{(n)}(\tau) = \frac{\partial^n \gamma}{\partial \tau^n}$, thus $^{(n)}$ denotes an $n^{(th)}$ order spatial derivative of the displacement variable.

y_{sJT}, y_{sJB}: The vertical displacements of the lumped discrete elements M_{sJT}, M_{sJB} (also see figure 3.3).

The interactions between the discrete elements associated with the back-up chock-bearing combinations and the hydraulic actuators and load cells are expressed as,

$$M_{sT}\ddot{y}_{sT} = -F_{HAs}, \tag{4.25}$$

$$M_{sB}\ddot{y}_{sB} + K_{sB}y_{sB} = 0, \tag{4.26}$$

where $s \in [L, R]$, and the generic representations are defined as:

M_{sT}, M_{sB}: The masses of the top and bottom back-up roll chock-bearing combinations.

K_{sB}: The stiffness of the load cells on either side of the mill.

F_{HAs}: The thrust force of the hydraulic actuators.

y_{sB}, y_{sT}: The vertical displacements of the lumped discrete elements M_{sT}, M_{sB} (also see figure 3.3).

The displacements at the end of the rollers and the displacement of the discrete elements are the same displacement and provide the connecting relationship between the discrete and the continuous systems. These displacements are expressed as,

$$y_{LT}(t) = y_{LJT}(t) = y_1(\frac{-l_1}{2}, t) \approx \Psi_1(\frac{-l_1}{2})\mathbf{q}_1(t), \tag{4.27}$$

$$y_{RT}(t) = y_{RJT}(t) = y_1(\frac{l_1}{2}, t) \approx \Psi_1(\frac{l_1}{2})\mathbf{q}_1(t), \tag{4.28}$$

$$y_{LB}(t) = y_{LJB}(t) = y_2(\frac{-l_2}{2}, t) \approx \Psi_2(\frac{-l_2}{2})\mathbf{q}_2(t), \tag{4.29}$$

$$y_{RB}(t) = y_{RJB}(t) = y_2(\frac{l_2}{2}, t) \approx \Psi_2(\frac{l_2}{2})\mathbf{q}_2(t). \tag{4.30}$$

When the above relationships are substituted into equations 4.23, 4.24, 4.25 and 4.26. The resulting eight equations of motion are premultiplied with $\Psi_1^T(\frac{-l_1}{2})$, $\Psi_1^T(\frac{l_1}{2})$, $\Psi_2^T(\frac{-l_2}{2})$ and $\Psi_2^T(\frac{l_2}{2})$ consecutively. The following equations result,

$$\Psi_1^T(\frac{-l_1}{2})M_{LT}\Psi_1(\frac{-l_1}{2})\ddot{\mathbf{q}}_1 = \Psi_1^T(\frac{-l_1}{2})F_{HAL}, \tag{4.31}$$

$$\Psi_1^T(\frac{l_1}{2})M_{RT}\Psi_1(\frac{l_1}{2})\ddot{\mathbf{q}}_1 = \Psi_1^T(\frac{l_1}{2})F_{HAR}, \tag{4.32}$$

$$\Psi_2^T(\frac{-l_2}{2})M_{LB}\Psi_2(\frac{-l_2}{2})\ddot{\mathbf{q}}_2 + \Psi_2^T(\frac{-l_2}{2})K_{LB}\Psi_2(\frac{-l_2}{2})\mathbf{q}_2 = 0, \tag{4.33}$$

$$\Psi_2^T(\frac{l_2}{2})M_{RB}\Psi_2(\frac{l_2}{2})\ddot{\mathbf{q}}_2 + \Psi_2^T(\frac{l_2}{2})K_{RB}\Psi_2(\frac{l_2}{2})\mathbf{q}_2 = 0, \tag{4.34}$$

$$\Psi_1^T(\frac{-l_1}{2})M_{LJT}\Psi_1(\frac{-l_1}{2})\ddot{\mathbf{q}}_1 + \Psi_1^T(\frac{-l_1}{2})K_{JL}\Psi_1(\frac{-l_1}{2})\mathbf{q}_1 = \Psi_1^T(\frac{-l_1}{2})K_{JL}\Psi_2(\frac{-l_1}{2})\mathbf{q}_2 + \Psi_1^T(\frac{-l_1}{2})J, \tag{4.35}$$

$$\Psi_1^T(\frac{l_1}{2})M_{RJT}\Psi_1(\frac{l_1}{2})\ddot{\mathbf{q}}_1 + \Psi_1^T(\frac{l_1}{2})K_{JR}\Psi_1(\frac{l_1}{2})\mathbf{q}_1 = \Psi_1^T(\frac{l_1}{2})K_{JR}\Psi_2(\frac{l_2}{2})\mathbf{q}_2 + \Psi_1^T(\frac{l_1}{2})J, \tag{4.36}$$

$$\Psi_2^T(\frac{-l_2}{2})M_{LJB}\Psi_2(\frac{-l_2}{2})\ddot{\mathbf{q}}_2 + \Psi_2^T(\frac{-l_2}{2})K_{JL}\Psi_2(\frac{-l_2}{2})\mathbf{q}_2 = \Psi_2^T(\frac{-l_2}{2})K_{JL}\Psi_1(\frac{-l_1}{2})\mathbf{q}_1 - \Psi_2^T(\frac{-l_2}{2})J, \tag{4.37}$$

$$\Psi_2^T(\frac{l_2}{2})M_{RJT}\Psi_2(\frac{l_2}{2})\ddot{\mathbf{q}}_2 + \Psi_2^T(\frac{l_2}{2})K_{JR}\Psi_2(\frac{l_2}{2})\mathbf{q}_2 = \Psi_2^T(\frac{l_2}{2})K_{JR}\Psi_1(\frac{l_1}{2})\mathbf{q}_1 - \Psi_2^T(\frac{l_2}{2})J. \tag{4.38}$$

The total stand model in terms of the assumed modes is obtained when equations associated with the top roll pack and equations associated with the bottom roll pack are summed respectively. In the following sections the whole stand model is manipulated to yield a linear state-space matrix model.

4.5.2.2 Mass, stiffness and damping elements

In order to express the stand model in linear matrix notation, the mass, stiffness and damping matrices of each element have to be computed.

Continuous Masses

The mass matrix of each continuous mass roller are expressed as $\mathbf{M}_{ij} \in \Re^{2p\times 2p}, \forall i,j \in [1,2]$. The matrix elements of the estimated mass matrices associated with the rollers are obtained, when the following integrals are done over the width of the rollers:

$$m_{i_h j_g} = \begin{cases} \int_{\frac{-l_i}{2}}^{\frac{l_i}{2}} \psi_{i_h}\rho A_i \psi_{j_g} dz, \ \forall i = j \ and \ i \in [1,2] \\ 0, \ \forall i \neq j \end{cases}, \tag{4.39}$$

where $h, g \in [1, ..., 2p]$.

Discrete bearing mass elements

The matrices for the discrete mass elements are constructed as follows,

$$\mathbf{M}_{dsi} = \Psi_i(z)^T M_{s\chi}\Psi_i(z), \in \Re^{2p\times 2p}, \tag{4.40}$$

$$\mathbf{M}_{dJsi} = \Psi_i(z)^T M_{Js\chi}\Psi_i(z), \in \Re^{2p\times 2p}, \tag{4.41}$$

where s, i, j, χ are indices and $s \in [L, R]$. When $s = L \Rightarrow z = -\frac{l_i}{2}$, $s = R \Rightarrow z = \frac{l_i}{2}$. When $i = 1 \Rightarrow \chi = T$, and when $i = 2 \Rightarrow \chi = B$.

Bending Stiffness of Roller Elements

After the substitution of the assumed vertical displacement into the PDE-model as shown in equations 4.21 and 4.22, the bending stiffness of a roller pack needs to be calculated as,

$$k_{i_g i_h} = \int_0^{l_i} \psi_{i_g} EI_i \psi_{i_h}^{(4)} dz. \tag{4.42}$$

But in [75] it is shown that the assumed bending stiffness of a beam is calculated as,

$$k_{i_g i_h} = \int_0^{l_i} \psi_{i_g}^{(2)} EI_i \psi_{i_h}^{(2)} dz, \tag{4.43}$$

where the latter equation is obtained by following a Lagrangian dynamic approach. The discrepancy between the order of spatial differentiation of the assumed modes between Eq. 4.43 and Eq. 4.42, can be clarified by observing from [54] that the natural bending stiffness of a beam is calculated as,

$$k_{i_g i_h} = \int_0^{l_i} \phi_{i_g}^{(2)} EI_i \phi_{i_h}^{(2)} dz, \tag{4.44}$$

but if the true vertical displacement, $y = \Phi \mathbf{q}$, is substituted into the PDE model (Eqs. 3.63 and 3.68) the bending stiffness would be calculated as,

$$k_{i_g i_h} = \int_0^{l_i} \phi_{i_g} EI_i \phi_{i_h}^{(4)} dz, \tag{4.45}$$

When integration by parts is done twice on Eq. 4.45 the following is yielded,

$$\int_{\frac{-l}{2}}^{\frac{l}{2}} \phi(x)\phi^{(4)}(x)dx = \phi(x)\phi^{(3)}(x)|_{\frac{-l}{2}}^{\frac{l}{2}} - \phi^{(1)}(x)\phi^{(2)}(x)|_{\frac{-l}{2}}^{\frac{l}{2}} + \int_{\frac{-l}{2}}^{\frac{l}{2}} \phi^{(2)}(x)\phi^{(2)}(x)dx, \tag{4.46}$$

and it can be shown that $\int_{\frac{-l}{2}}^{\frac{l}{2}} \phi(z)\phi^{(4)}(z)dz = \int_{\frac{-l}{2}}^{\frac{l}{2}} \phi^{(2)}(z)\phi^{(2)}(z)dz$, but $\int_{\frac{-l}{2}}^{\frac{l}{2}} \psi(z)\psi^{(4)}(z)dz$ is not necessarily equal to $\int_{\frac{-l}{2}}^{\frac{l}{2}} \psi^{(2)}(z)\psi^{(2)}(z)dz$. The relationship (see Eq. 4.18) between the assumed modes and the natural modes of vibration ensures that the real bending stiffness will be computed after the solution of the Eigenvalue problem. Thus Eq. 4.43 is used in the calculation of the assumed bending stiffness of a roll pack. Thus,

$$k_{i_h i_g} = \begin{cases} \int_0^{l_i} \psi_{i_k}^{(2)}(z) EI_i(z) \psi_{j_g}^{(2)}(z)dz, \ \forall i = j \ and \ i \in [1,2] \\ 0, \ \forall i \neq j \end{cases}, \tag{4.47}$$

where $h, g \in [1, 2]$.

Elastic Recovery of Strip

From Eqs. 4.21 and 4.22 it is seen that the elastic recovery of the strip is modelled as a distributed spring element. The matrix elements can be calculated as,

$$k_{strip_{i_h j_g}} = \int_{-\frac{w}{2}}^{\frac{w}{2}} \psi_{i_h}(z) k_{strip}(z) \psi_{j_g}(z)dz, \tag{4.48}$$

where $k_{strip_{i_h j_g}} \in \mathbf{K}_{strip_{ij}}$, and the elastic recovery stiffness matrix is expressed as,

$$\mathbf{K}_{strip} = \begin{bmatrix} \mathbf{K}_{strip_{11}} & -\mathbf{K}_{strip_{12}} \\ -\mathbf{K}_{strip_{21}} & \mathbf{K}_{strip_{22}} \end{bmatrix} \in \Re^{2p \times 2p} \tag{4.49}$$

Load Cell Discrete Spring Elements

From Eqs. 4.33 and 4.34 the discrete stiffness matrix associated with the load cells is calculated as,

$$\mathbf{K}_{ds2} = \Psi_2(z)^T K_{sB} \Psi_2(z) \in \Re^{2p \times 2p}, \tag{4.50}$$

where $s \in [L, R]$ and $\mathbf{K}_{ds2} \in \Re^{2p \times 2p}$. When $s = L \Rightarrow z = -\frac{l_i}{2}$, $s = R \Rightarrow z = \frac{l_i}{2}$.

Hydraulic Jacks Springs elements

From Eqs. 4.35-4.38 the discrete stiffness matrix associated with the hydraulic jack springs is calculated as,

$$\mathbf{K}_{Jdijs} = \Psi_i(z)^T K_{Js} \Psi_j(z), \tag{4.51}$$

where $s \in [L, R]$ and $\mathbf{K}_{Jdijs} \in \Re^{2p \times 2p}$. When $s = L \Rightarrow z = -\frac{l_i}{2}$, $s = R \Rightarrow z = \frac{l_i}{2}$. When $i = 1 \Rightarrow \chi = T$, and when $i = 2 \Rightarrow \chi = B$.

Strip/Work Roll Damping

From Eqs. 4.21 and 4.22 it is seen that the damping is also modelled as a distributed parameter. The damping matrix elements are calculated as,

$$C_{i_h j_g} = \int_{-\frac{w}{2}}^{\frac{w}{2}} \psi_{i_h}(z) \beta_{strip}(z) \psi_{j_g}(z) dz, \tag{4.52}$$

where $C_{i_h j_g} \in \mathbf{C}_{ij} \in \Re^{2p \times 2p}$.

Total Stand Model

When the above matrices are summed the assumed modes mass and stiffness matrices are obtained as,

$$\widehat{\mathbf{M}} = \begin{bmatrix} \mathbf{M}_{11} + \mathbf{M}_{dL1} + \mathbf{M}_{dR1} & \mathbf{0} \\ +\mathbf{M}_{dJL1} + \mathbf{M}_{dJR1} & \\ \mathbf{0} & \mathbf{M}_{22} + \mathbf{M}_{dL2} + \mathbf{M}_{dR2} \\ & +\mathbf{M}_{dJL2} + \mathbf{M}_{dJR2} \end{bmatrix} \in \Re^{4p \times 4p}, \tag{4.53}$$

$$\widehat{\mathbf{K}} = \begin{bmatrix} \mathbf{K}_{11} + \mathbf{K}_{strip_{11}} + \mathbf{K}_{Jd11L} & -\mathbf{K}_{strip_{12}} - \mathbf{K}_{Jd12L} - \mathbf{K}_{Jd12R} \\ +\mathbf{K}_{Jd11R} & \\ -\mathbf{K}_{strip_{21}} - \mathbf{K}_{Jd21L} - \mathbf{K}_{Jd21R} & \mathbf{K}_{22} + \mathbf{K}_{strip_{22}} + \mathbf{K}_{Jd22L} \\ & +\mathbf{K}_{Jd22R} + \mathbf{K}_{dL2} + \mathbf{K}_{dR2} \end{bmatrix} \in \Re^{4p \times 4p}. \tag{4.54}$$

The assumed damping matrix of the stand model is expressed as,

$$\widehat{\mathbf{C}} = \begin{bmatrix} \mathbf{C}_{11} & -\mathbf{C}_{12} \\ -\mathbf{C}_{21} & \mathbf{C}_{22} \end{bmatrix} \in \Re^{4p \times 4p}. \tag{4.55}$$

Taking Eq. 4.18 into account the coupled stand model equations of motion can be expressed as,

$$\widehat{\mathbf{M}}\mathbf{U}\ddot{\mathbf{q}} \; + \widehat{\mathbf{C}}\mathbf{U}\dot{\mathbf{q}} + \; \widehat{\mathbf{K}}\mathbf{U}\mathbf{q} = \mathbf{B}\mathbf{u} \tag{4.56}$$

4.5.2.3 Discretization

The continuous mass rollers were discretized into 50 discrete elements with 51 nodes. The distance between two nodes is expressed as Δ_z, which is equal to 8cm. Using these discrete nodes the integrals can be solved using Boole's numerical integration method [71] or normal Euler numerical integration. The areas and second moments of inertias were diagonalized[13] and the assumed modes were evaluated at each node[14].

Different values of p was experimented with but in the final simulator p was taken as one. In [59] a total of 2 vibration modes were used and in [40] three modes of vibration are used as the rollers are large and stiff elements, which limit high order spatial bending modes.

4.5.2.4 Solution

The modal matrix is solved from the general Eigenvalue problem,

$$(\widehat{\mathbf{K}} - \omega^2\widehat{\mathbf{M}})\mathbf{U} = 0, \tag{4.57}$$

where $\mathbf{U} \in \Re^{4p \times 4p}$.

The decoupled equation of motion of the stand is written as,

$$\mathbf{U}^{\mathrm{T}}\widehat{\mathbf{M}}\mathbf{U}\ddot{\mathbf{q}} \; + \mathbf{U}^{\mathrm{T}}\widehat{\mathbf{C}}\mathbf{U}\dot{\mathbf{q}} + \; \mathbf{U}^{\mathrm{T}}\widehat{\mathbf{K}}\mathbf{U}\mathbf{q} = \mathbf{U}^{\mathrm{T}}\mathbf{B}\mathbf{u} \tag{4.58}$$

where $\mathbf{M} = \mathbf{U}^{\mathrm{T}}\widehat{\mathbf{M}}\mathbf{U}$, $\mathbf{K} = \mathbf{U}^{\mathrm{T}}\widehat{\mathbf{K}}\mathbf{U}$, $\mathbf{C} = \mathbf{U}^{\mathrm{T}}\widehat{\mathbf{C}}\mathbf{U}$ and $\mathbf{q} = \begin{bmatrix} q_{1_1} & q_{1_2} & q_{2_1} & q_{2_2} \end{bmatrix}^T \in \Re^{2(2p)\times 1}$[15].

The decoupled normal coordinate system is expressed as,

$$\begin{bmatrix} \dot{\mathbf{q}} \\ \ddot{\mathbf{q}} \end{bmatrix} = \begin{bmatrix} \mathbf{I}_{2p\times 2p} & 0 \\ -\mathbf{M}^{-1}\mathbf{K} & -\mathbf{M}^{-1}\mathbf{C} \end{bmatrix} \begin{bmatrix} \mathbf{q} \\ \dot{\mathbf{q}} \end{bmatrix} + \begin{bmatrix} 0 \\ \mathbf{M}^{-1}\mathbf{U}^{\mathrm{T}}\mathbf{B} \end{bmatrix} \mathbf{u} \tag{4.59}$$

where $\mathbf{B}$ and $\mathbf{u}$ are the input matrix and input vector respectively. In section 4.7 these variables are defined.

[13] $A_i(z) = diag\{A\} \in \Re^{51\times 51}$, $I_i(z) = diag\{I\} \in \Re^{51\times 51}$, where $i \in [1, 2]$.

[14] $\Psi_i \in \Re^{51\times 2p}$

[15] The notation $q_{\#roll_{\#assumed\ mode}}$ applies.

The natural modes of vibration of the stand model are calculated by using the calculated modal matrix and the assumed modes vector as shown in Eq. 4.18. In figures 4.7, 4.8, 4.9 and 4.10 the natural modes of vibration for the two roller pack case, where the number of assumed modes is 3 and 4, are shown. In figures 4.11 and 4.12 the natural modes of vibration for two different cases when the number of assumed modes is 2 are shown. The distinguishing factor between these two cases is whether the hydraulic jacks were modelled or not, e.g. $K_{sJ} = 0$ (figure 4.11) or $K_{sJ} = 8e10\frac{N}{m}$ (figure 4.12).

The discretized vertical displacements are calculated as,

$$\mathbf{y} = \begin{bmatrix} y_{1_{\Delta_z}} \\ y_{2_{\Delta_z}} \end{bmatrix} = \begin{bmatrix} \Phi_1 & \Phi_2 \end{bmatrix} \begin{bmatrix} \mathbf{q}_1 \\ \mathbf{q}_2 \end{bmatrix}, \tag{4.60}$$

where $y_{1_{\Delta_z}}, y_{2_{\Delta_z}} \in \Re^{51\times 1}$.

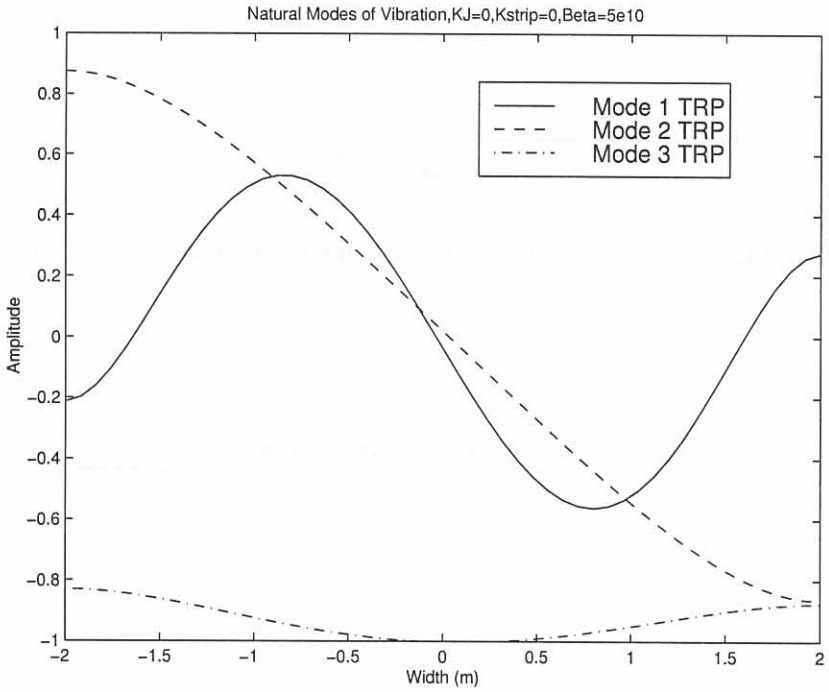

Figure 4.7: Natural modes of vibration for 3 assumed modes of Top Roll Pack.

4.5.2.5 Flowchart

The solution of the stand model only requires matrix operations and a Runge Kutta time integration. The Runge Kutta procedure is used on the total simulator nonlinear state-space model. This will be discussed in section 4.7.

4.5.3 Physical constants

Roller Weights

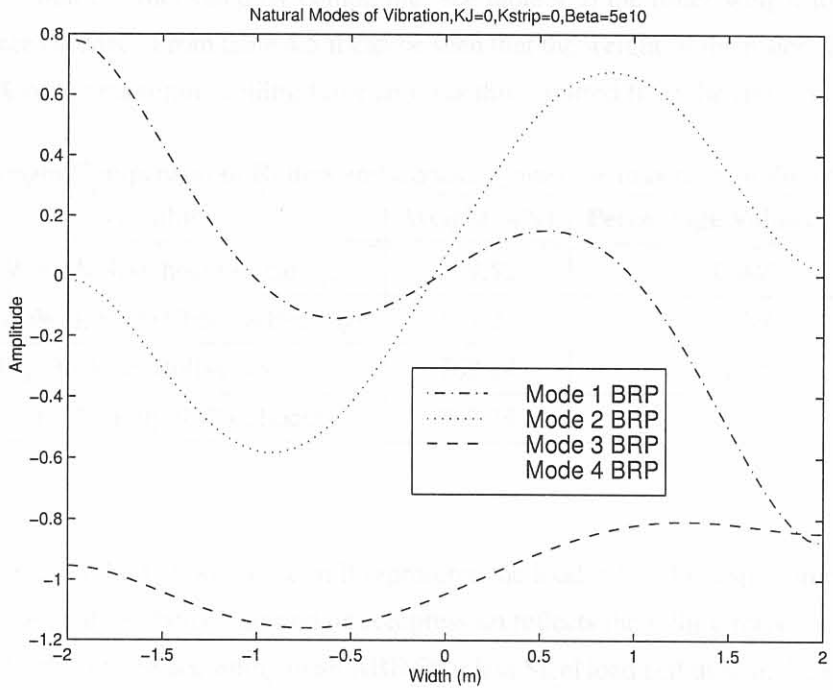

Figure 4.8: Natural modes of vibration for 3 assumed modes of Bottom Roll Pack.

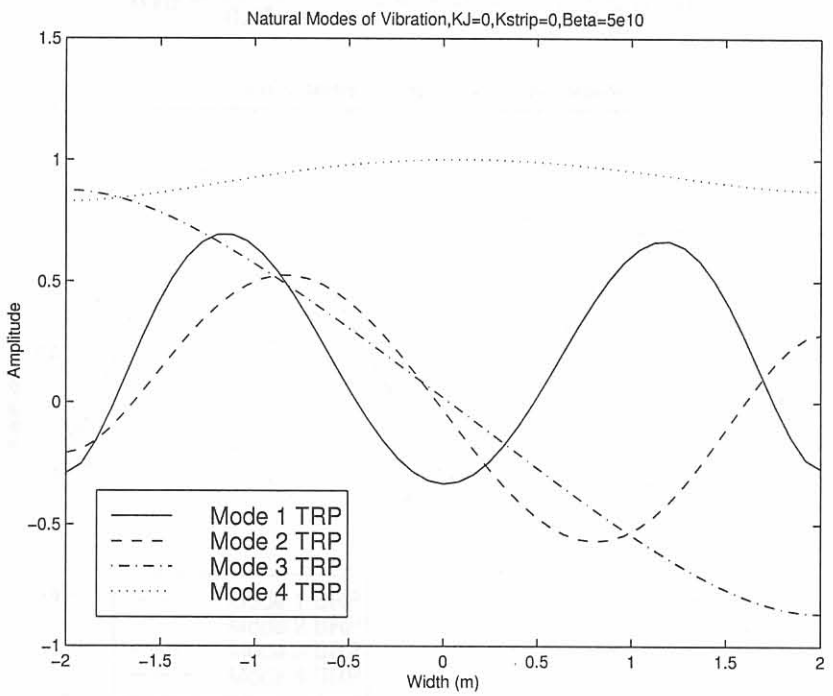

Figure 4.9: Natural modes of vibration for 4 assumed modes of Top Roll Pack.

In chapter 3 the weight of the rollers was not taken into consideration when the model was derived. This modelling choice is motivated by comparing (see table 4.5) the roller weight to the maximum mill rolling force (40MN). From table 4.5 it can be seen that the weight of the roller elements in total is less than 5 % of the maximum rolling force and was thus omitted from the stand model derivation.

Table 4.5: Weight Comparison of Rollers and Chocks against the maximum rolling force, 40MN.

Variable	Weight (kN)	Percentage Value of F_{limit}
Top Work Roll+Chocks+Bearings	179.52	0.449
Bottom Work Roll+Chocks+Bearings	194.24	0.486
Top Back-up Roll+Chocks	762.24	1.91
Bottom Back-up Roll+Chocks	762.24	1.91

Load cells

The discrete spring at the bottom of the mill represents the load cell. The displacement of this hard spring models the load cell behaviour and its compression reflects the rolling force in the mill. It was decided to model this spring according to an ABB Stainless Steel load cell used in the industry for roll force measurement in hot rolling mills. The rectangular load cell, type PFVL 101V, of the Millmate Roll Force System range was chosen [77]. The spring compression at nominal load is not to exceed 0.05mm and if nominal load is taken as half the mill force limit on either side of the mill, the spring constant is found to be,

$$K_{sB} = \frac{0.5F_{limit}}{0.05mm} = 400 \times 10^9 N/m, \forall s \in [L, R]. \tag{4.61}$$

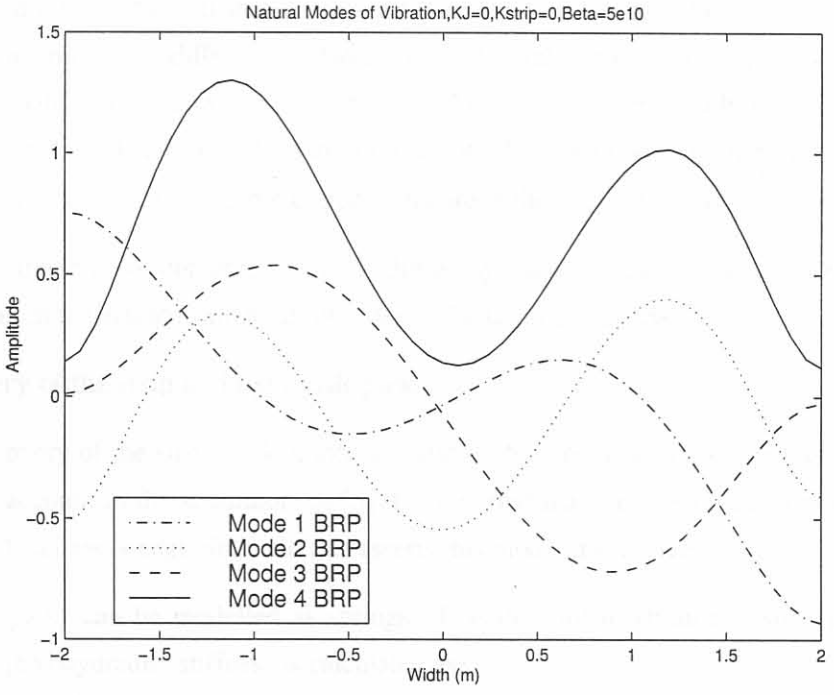

Figure 4.10: Natural modes of vibration for 4 assumed modes of Bottom Roll Pack.

Damping

In [8] damping for the HAGC system is provided between the strip and the working rolls. It is reported in [78] that this damping is dependent on the length of the arc of contact in the roll gap. R-M Guo showed in [8] that there is a contradiction with the statements in [78] and practical data obtained in [8]. In the absence of a correction to this damping equation defined in [78], the same equation will be used namely,

$$\beta_{strip}(t).w = \frac{w.k(\epsilon,\dot{\epsilon},\theta)|_{x_{rg}=0}}{\omega_{main}(t)} \left[\frac{N}{m.s^{-1}}\right], \tag{4.62}$$

where $k(\epsilon,\dot{\epsilon},\theta)|_{x_{rg}=0}$ ($\approx 280MPa$) is the yield stress of the material at the delivery side of the roll gap, $\omega_{main}(t)$ is the main mill drive angular velocity and w is the strip width (1.4m). From the logged data, concentrating only on the similarly identified strips, damping coefficients for pass 1, $\beta_{strip}|_{pass1} = 1.48 \times 10^8$, and pass 3, $\beta_{strip}|_{pass3} = 1.18 \times 10^8 N.m^{-1}.s$, were calculated. However with these damping coefficients a non-bumpless start of the simulation from the chosen steady state resulted. In chapter 5 section 5.3.2, simulation results for a $\beta_{strip}|_{pass3} = 1 \times 10^8 N.m^{-1}.s$ are compared to other values for the distributed friction coefficient.

The nearly steady state point could be maintained by increasing β_{strip}. The general observation was that the mill oscillation could not completely be damped out. Time simulations in [40] also exhibited such oscillatory behaviour and in this investigation [40] damping was only modelled between the strip and the work rolls. In chapter 5 damping ratios for the mill stand model with different β_{strip} and K_J are shown and discussed. An investigation of the damping found in the mill stand might prove beneficiary for the long term research program.

From the logged data of the exit thickness (see figure 4.2) it is not possible to draw conclusions of these oscillations, due to the difference between the high oscillation period frequency, when $\beta_{strip} = 5e10N.m^{-1}.s$, with an oscillating period of roughly 2.6ms and the time resolution of the logged data is 0.4 seconds. The oscillation periods of the 3 modes of vibration in [40] fall in the range of 3ms-4ms. The amplitude of oscillation is not that extreme and are in the order of $2\mu m$.

It needs to be stressed that damping in the nonlinear hydraulic actuator was not modelled and that maybe damping in the actuator might absorb these vibration oscillations.

Elastic recovery of the strip and hydraulic jacks

The elastic recovery of the strip is taken into account in the model derivation, but as a first iteration not taken into account in the simulator. In [3] it is reported that the elastic recovery of the strip for hot rolling applications is negligible and this asserts this modelling choice.

The hydraulic jacks can be modelled as springs. It is difficult to attain realistic values for these springs, but in [65] hydraulic stiffness is calculated as,

$$K_J = \frac{A\beta_o}{h_2}, \tag{4.63}$$

where A is the working area of the actuator, $\beta_o = 1.38GPa$ is the oil's bulk modulus and $\overline{h_2}$ is the average exit thickness of the roll gap assuming the hydraulic jacks coincide on the same vertical yz plane as the exit from the roll gap. The actuator working area is calculated by taking the four bending cylinders per bending block, of which 2 bending blocks per mill side are fitted. A bending cylinder has a full bore side diameter of 210mm. Using Eq. 4.63, the hydraulic stiffness is calculated as $K_J|_{pass3} \approx 40 \times 10^9 N/m$.

It is found that using this magnitude for the bending stiffness coupled the upper and lower roll packs to such an extent that the first natural mode of vibration was dominant for both roll packs. The vibration behaviour of the lower roll pack should be dominated by the second spatial mode of vibration, according to the results obtained by Pederson [59]. This roll pack should only exhibit an increasing/decreasing amount of bending as the rolling force increases/decreases. The displacements at the end of the roll pack should reflect these force deviations by increasing the compression of the load cell spring or reducing it respectively. Taking this statement into consideration and the fact that the elastic recovery of the strip is limited, the upper and lower roll packs are completely decoupled by making $k_{strip} = 0$ and $K_{Js} = 0, \forall s \in [L, R]$.

In figures 4.11 and 4.12 the effect of the jack springs are compared according to the natural modes of vibrations obtained. When the jack springs are large the asymmetrical behaviour between upper and lower roll packs are accentuated in figure 4.12 when compared to 4.11.

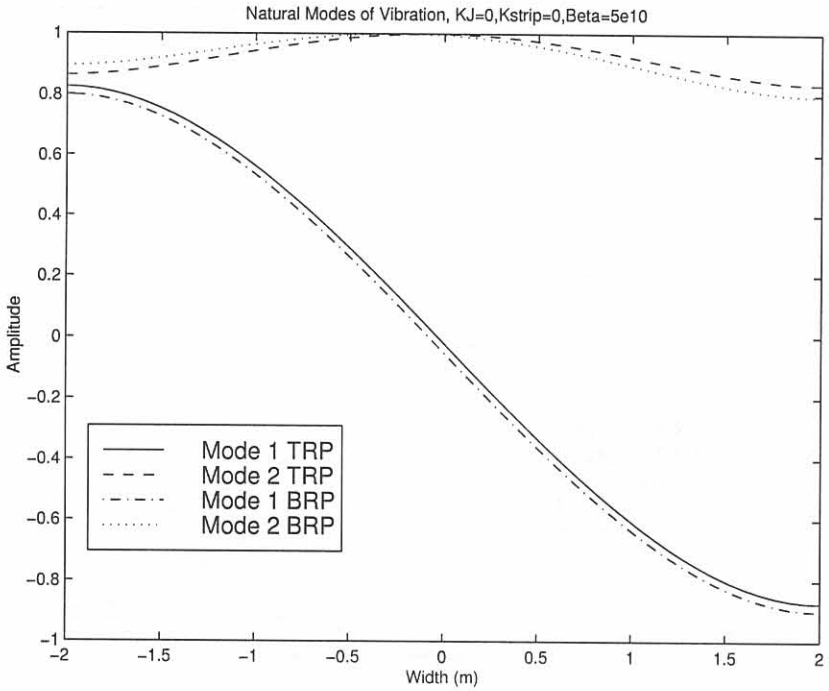

Figure 4.11: Natural modes of vibration for $K_{Js} = 0$ and $\beta_{strip} = 5 \times 10^{10} N.m^{-1}.s$.

4.5.4 Mill Stretch Model

Tests are conducted by plant personnel on the mill under study in order to calculate the mill spring curves for either side of the rolling mill. The test conducted on the mill can be described as follows:

The top roll pack is placed in contact with the bottom roll pack, without a strip in the roll gap. Once the rollers are in place the top roll pack is pressed against the roll pack with a measured force, $F_{test_s} \approx 730Tons$, and at this force level the initial mill stretch $y_{stretch_{test_s}}$ (where $s \in [L, R]$) is logged. The force is then increased until a total rolling force of roughly 30MN is measured (15MN per side). The mill stretch curves (see figure 3.4) are calculated using the values shown in table 4.6.

In [65] the structural stiffness of a rolling mill is given as $16.65 \times 10^6 lb/in = 2.93 \times 10^9 N/m$ and in [59] the structural stiffness of the investigated plate mill is $2.02 \times 10^9 N/m$. These values are in accordance with the calculated values (see table 4.6) for the Steckel Mill under consideration.

Table 4.6: Mill stretch model values

Side	F_{test_s} (MN)	$y_{stretch_{test_s}}$ (mm)	K_{sT} (N/m)
$s = L$ (OS)	7.217	2.774	3.388×10^9
$s = R$ (DS)	7.190	2.765	3.413×10^9

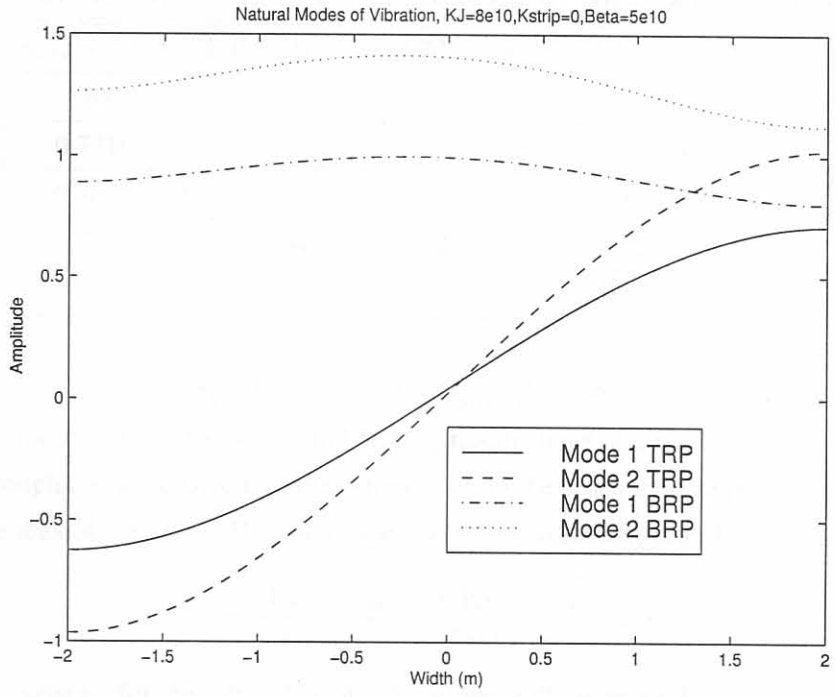

Figure 4.12: Natural modes of vibration for $K_{Js} = 80 \times 10^9 N/m$ and $\beta_{strip} = 5 \times 10^{10} N.m^{-1}.s$.

4.6 Hydraulic actuator model

Data of the implemented plant actuators for the Steckel mill under consideration are not available. Information of the physical constants and dimensions of such actuators had to be extracted from articles [8, 64, 65, 79] and a servovalve manufacturer brochure [68]. This procedure was deemed necessary in order to get a true reflection of the physical system.

4.6.1 Physical constants

Different types of servovalves are used in the rolling mill environment. The Steckel Mill, under investigation, uses a servovalve with a natural frequency, f_s, of 51Hz[16]. This value agrees with the operating frequency range for servovalves, 60 - 100 Hz, listed by Guo [8]. Using this specified frequency range as a criteria, the Moog Servovalve D661-range was identified from [68].

Table 4.7 relates values for different hydraulic systems found in the literature as well as values of the D661 servovalve. All the listed values were converted into SI Units in order to compare them and to motivate choices for the simulator.

Table 4.7: Comparison of hydraulic system parameters.

Variable	Bhowal [64]	Guo [8]	Ginzburg [65]	Huzyak [79]	Moog D661 [68]
q_0 ($\frac{m^3}{s}$)	6.67×10^{-4}	1.45×10^{-3}	4.70×10^{-3}	1.58×10^{-3}	1.33×10^{-3}
I_0 (mA)	20	-	30	20	10
A_1 (m^2)	0.7310	-	0.6243 m^2	0.6243	-
A_2 (m^2)	0.1639	-	-	0.1698	-
P_s (MPa)	25	31.04	27.59	27.59	35
P_t (MPa)	6	-	-	-	5

Cylinder flow is calculated using, $Q = A\vartheta = K_{v_s} x_{v_s} \sqrt{\frac{\Delta P}{\rho}}$, where the term incorporating the pressure difference has the units of velocity, and $K_{v_s} x_{v_s}$ has the units of area. The rated flow of the valve has to pass through the servovalve into the cylinder. From the brochure data [68] this area is taken as the spool drive area of 1.35 cm^2. Using this approach the value of K_{v_s} can be calculated as,

$$K_{v_s} = \frac{A_{spool\ drive}}{x_{v_s max}} = \frac{1.35cm^2}{3mm} = 0.045m.$$

The hydraulic systems, for the left and right sides of the mill, were modelled using the values summarized in Table 4.8.

It is assumed that the response of the second order transfer function servovalve model is critically damped. This assumption can be motivated by referring to time response curves [68]. Once the spool

[16]Personal correspondence with M. Lewis.

movement is larger than 100% the flow, associated with a certain pressure drop, can not exceed the maximum flow, and a stroke greater than 100% will not reflect this limitation. This phenomena was incorporated as a hard constraint on the stroke length of $\pm 3mm$ in the mill simulator.

The thrust force capability of the modelled actuators are given in table 4.9, and a physical constraint of 40MN (20MN on each side of the mill) is applied. The modelled actuators are therefore capable of handling these large rolling forces (20MN).

4.7 Dynamic Simulator

The dynamic simulator consists of two dynamic models. The two models are the tension model and a combination of the hydraulic actuator models and the stand model. The tension model is simulated at a higher sampling rate than the rest of the simulator. The combination of the hydraulic actuator models and the stand model is expressed as a non linear state-space model. This nonlinear state-space

Table 4.8: Hydraulic Model System Parameters

Variable	Value
q_0	$1.5 \times 10^{-3}\ \frac{m^3}{s}$
I_0	± 10 mA
A_1	$0.74\ m^2$
A_2	$0.16\ m^2$
P_{high}	35 MPa
P_{low}	5 MPa
w_v	$2\pi \times 51\ \frac{rad}{s}$
ζ_v	1
K_{leak}	1×10^{-9}
K_{v_s}	0.045 m
$x_{v_{s_{max}}}$	3×10^{-3} m
K_{c_s}	1.5
τ_{i_s}	1×10^{-2}

Table 4.9: Thrust force capability.

P_{s1} (MPa)	P_{s2} (MPa)	F_{HA_s} (MN)
5	5	2.9
5	35	-1.9
35	5	25.1
35	35	20.3

model is solved using a fourth order fixed time step Runge Kutta method [71].

The spatial modelling of the rollers provides the simulator with the draft deviation across the width of the sheet. This deviation is used to solve the roll gap model at some of the 51 discretized nodes in order to yield varying specific rolling forces across the width of the strip. It is assumed that the strip is very ductile at 1000°C and that the strip does fill the whole roll gap. The simulator is not able to account for strip with an entering negative (concave) crown, because the strip will not fill the whole roll gap along the curvature of bended rolls. In the simulator the spatial dynamic draft is calculated utilizing the following equation,

$$\begin{aligned}\delta(z,t) &= h_{1_{setup}} - h_{2_{setup}} - (\delta h_1(t) - \delta h_2(z,t)) \\ &= \delta_{setup} - (\delta h_1(t) - (y_1(z,t) - y_2(z,t))), \quad where \ \tfrac{-w}{2} \leq z \leq \tfrac{w}{2}.\end{aligned} \tag{4.64}$$

$\delta h_1(t)$ is taken as the measured entrance thickness deviation at the center of the strip. $\delta h_2(z,t)$ is evaluated over the width of the strip.

In figure 4.13 the flow chart of the mill simulator is shown. This high level flow chart shows how the various models are used in the mill simulator.

The nonlinear state-space model of the simulator will be expressed for the two roll pack system with two assumed modes per roller. The assignment of states for the nonlinear state-space model is as follows[17]:

$$\mathbf{x} = \begin{bmatrix} \mathbf{x}_a & \mathbf{x}_b \end{bmatrix}^T, \tag{4.65}$$

$$\mathbf{x}_a = \begin{bmatrix} x_1 & x_2 & x_3 & x_4 & x_5 & x_6 & x_7 & x_8 \end{bmatrix}^T = \begin{bmatrix} q_{1_1} & q_{1_2} & q_{2_1} & q_{2_2} & \dot{q}_{1_1} & \dot{q}_{1_2} & \dot{q}_{2_1} & \dot{q}_{2_2} \end{bmatrix}^T, \tag{4.66}$$

where $q_{i_j}, \forall i,j \in [1,2]$ were defined in section 4.5.2.4.

The state assignments associated with the hydraulic actuators are,

$$\begin{aligned}\mathbf{x}_b = &\begin{bmatrix} x_9 & x_{10} & x_{11} & x_{12} & x_{13} & x_{14} & x_{15} & x_{16} & x_{17} & x_{18} \end{bmatrix}^T = \\ &\begin{bmatrix} x_{v_L} & \dot{x}_{v_L} & P_{L1} & x_{v_R} & \dot{x}_{v_R} & P_{R1} & P_{L2} & P_{R2} & x_L & x_R \end{bmatrix}^T,\end{aligned} \tag{4.67}$$

and the input vector of the dynamic simulator is,

$$\mathbf{u} = \begin{bmatrix} x_{11} & x_{15} & x_{14} & x_{16} & P'(z) \end{bmatrix}^T. \tag{4.68}$$

The flows of the hydraulic actuator models expressed as functions of the states are as follows:

$$Q_{L1} = \begin{cases} K_{v_L} x_9 \sqrt{\frac{2}{\rho_o}(P_s - x_{11})}, & when \ x_9 \geq 0 \\ K_{v_L} x_9 \sqrt{\frac{2}{\rho_o}(x_{11} - P_t)}, & when \ x_9 < 0 \end{cases}, \tag{4.69}$$

[17] All of the variables have previously been defined in chapter 3.

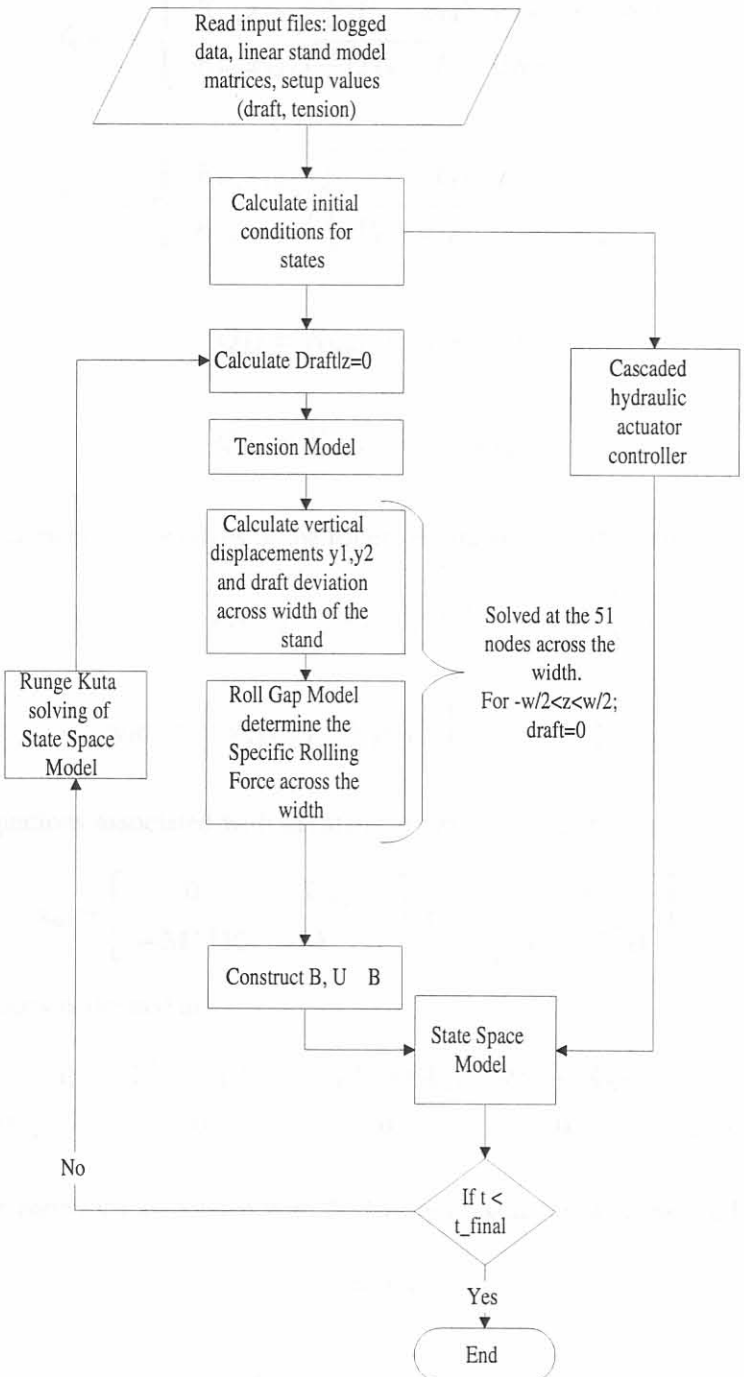

Figure 4.13: Mill simulator flowchart

$$Q_{L2} = \begin{cases} K_{v_L} x_9 \sqrt{\frac{2}{\rho_o}(x_{15} - P_t)}, & when\ x_9 \geq 0 \\ K_{v_L} x_9 \sqrt{\frac{2}{\rho_o}(P_s - x_{15})}, & when\ x_9 < 0 \end{cases}, \tag{4.70}$$

$$Q_{R1} = \begin{cases} K_{v_R} x_{12} \sqrt{\frac{2}{\rho_o}(P_s - x_{14})}, & when\ x_{12} \geq 0 \\ K_{v_R} x_{12} \sqrt{\frac{2}{\rho_o}(x_{14} - P_t)}, & when\ x_{12} < 0 \end{cases}, \tag{4.71}$$

$$Q_{R2} = \begin{cases} K_{v_R} x_{12} \sqrt{\frac{2}{\rho_o}(x_{16} - P_t)}, & when\ x_{12} \geq 0 \\ K_{v_R} x_{12} \sqrt{\frac{2}{\rho_o}(P_s - x_{16})}, & when\ x_{12} < 0 \end{cases}, \tag{4.72}$$

$$Q_{Ll} = K_{leak_L}(x_{11} - x_{15}), \tag{4.73}$$

$$Q_{Rl} = K_{leak_R}(x_{14} - x_{16}), \tag{4.74}$$

The vertical displacements at the edges of the rollers as functions of the states are,

$$y_{LT} = \begin{bmatrix} \phi_{1_1}(\frac{-l_1}{2}) & \phi_{1_2}(\frac{-l_1}{2}) \end{bmatrix} \begin{bmatrix} x_1 & x_2 \end{bmatrix}^T; \tag{4.75}$$

$$y_{RT} = \begin{bmatrix} \phi_{1_1}(\frac{l_1}{2}) & \phi_{1_2}(\frac{l_1}{2}) \end{bmatrix} \begin{bmatrix} x_1 & x_2 \end{bmatrix}^T; \tag{4.76}$$

The linear state equations associated with the stand are expressed as follows,

$$\dot{\mathbf{x}}_a = \begin{bmatrix} \mathbf{0} & \mathbf{I}_{2\times 2} \\ -\mathbf{M}^{-1}\mathbf{K} & -\mathbf{M}^{-1}\mathbf{C} \end{bmatrix} \mathbf{x}_a + \begin{bmatrix} \mathbf{0} \\ \mathbf{M}^{-1}\mathbf{U}^{\mathbf{T}}\mathbf{B} \end{bmatrix} \mathbf{u}, \tag{4.77}$$

where the input matrix is defined as,

$$\mathbf{B} = \begin{bmatrix} -\Psi_1^T(\frac{-l_1}{2})A_{L1} & \Psi_1^T(\frac{-l_1}{2})A_{L2} & -\Psi_1^T(\frac{l_1}{2})A_{R1} & \Psi_1^T(\frac{l_1}{2})A_{R2} & \Delta_z\Psi_1(z)^T \\ \mathbf{0} & \mathbf{0} & \mathbf{0} & \mathbf{0} & -\Delta_z\Psi_2(z)^T \end{bmatrix}. \tag{4.78}$$

The nonlinear state equations associated with the hydraulic systems are expressed as,

$$\dot{x}_9 = x_{10}, \tag{4.79}$$

$$\dot{x}_{10} = -2\zeta_{v_L}\omega_{v_L}x_{10} - \omega_{v_L}^2 x_9 + \omega_{v_L}^2 I_{c_L}, \tag{4.80}$$

$$\dot{x}_{11} = \frac{Q_{L1} - Q_{Ll} + A_{L1}\dot{y}_{L1} - \frac{A_{L1}A_{L2}}{K_{LT}\Delta}(Q_{L2} - Q_{Ll} + A_{L2}\dot{y}_{LT})}{\frac{V_{L1}(x_{17})}{\beta_o} + \frac{A_{L1}^2}{K_{LT}} - \frac{(A_{L1}A_{L2})^2}{K_{LT}^2\Delta}}, \tag{4.81}$$

$$\dot{x}_{12} = x_{13}, \tag{4.82}$$

$$\dot{x}_{13} = -2\zeta_{v_L}\omega_{v_L}x_{13} - \omega_{v_L}^2 x_{12} + \omega_{v_L}^2 I_{c_R}, \tag{4.83}$$

$$\dot{x}_{14} = \frac{Q_{R1} - Q_{Rl} + A_{R1}\dot{y}_{R1} - \frac{A_{s1}A_{s2}}{K_{sT}\Delta}\left(Q_{R2} - Q_{Rl} + A_{R2}\dot{y}_{RT}\right)}{\frac{V_{R1}}{\beta_o} + \frac{A_{R1}^2}{K_{RT}} - \frac{(A_{R1}A_{R2})^2}{K_{RT}^2\Delta}}, \tag{4.84}$$

$$\dot{x}_{15} = \frac{-Q_{L2} + Q_{Ll} - A_{L2}\dot{y}_{LT} + \frac{x_{11}A_{L1}A_{L2}}{K_{LT}}}{\left(\frac{V_{L2}}{\beta_o} + \frac{A_{L2}^2}{K_{LT}}\right)}, \tag{4.85}$$

$$\dot{x}_{16} = \frac{-Q_{R2} + Q_{Rl} - A_{R2}\dot{y}_{RT} + \frac{x_{14}A_{R1}A_{R2}}{K_{RT}}}{\left(\frac{V_{R2}}{\beta_o} + \frac{A_{R2}^2}{K_{RT}}\right)}, \tag{4.86}$$

$$\dot{x}_{17} = \frac{\dot{x}_{11}A_{L1} - \dot{x}_{15}A_{L2}}{K_{LT}} - \dot{y}_{LT}, \tag{4.87}$$

$$\dot{x}_{18} = \frac{\dot{x}_{14}A_{R1} - \dot{x}_{16}A_{R2}}{K_{RT}} - \dot{y}_{RT}, \tag{4.88}$$

It needs to be stressed that most of these states are not defined as small signal variables and reflect total state values for some state variables. The states associated with the linear stand model are expressed as small signal deviation state values. The states associated with the hydraulic actuators are not expressed as small signal state variables.

4.8 Conclusion

In this chapter the solution methodologies for each of the models identified in chapter 3 were discussed. These models were incorporated into a mill simulator and the chapter ended with the expression of the nonlinear state space model associated with the hydraulic actuator and stand model combination. The tension model can not operate independently and uses the roll gap model in order to solve the implicit relationship between the tensions and the roll gap speeds as well as the time advancement of the tension simulation. The tension model is solved at a specific time instance using the draft value at the middle of the strip. These tension values are used in the solution process of the nonlinear state-space model of the stand and actuators combination. In the following chapter, simulation results and the system identification for control purposes will be shown.

Chapter 5

Simulation results

5.1 Introduction

The mill simulator is constructed out of various models implemented in a C++ environment. The simulator consists of different models as discussed in chapter 3 and 4. Not all of these models can function independently. The roll gap model functions as an independent unit, and as was remarked in section 4.8 the tension and roll gap model form an integrated unit. The nonlinear state space combination of the hydraulic systems and the rolling mill stand also function as an independent unit, which uses the roll gap model in order to provide simulated behaviour of the strip in the roll gap.

As part of the initial investigation a linear control model will be identified by doing System Identification (SID) on the nonlinear mill simulator at a specific operating point. The choice of this operating point is discussed in section 4.2.2.

The input-output (I/O) relationships of the plant/simulator are shown in figure 5.1. The controlled and manipulated variables as well as the plant external plant disturbance, entrance thickness are indicated. The use of these variables in the identification process of a linear plant model, will be discussed in the latter part of this chapter.

The implicit and nonlinear behaviour of the Steckel hot rolling process were discussed in chapters 3 and 4. An algebraic linearization might prove insufficient to capture implicit process behaviour, for example the influence of the deformed roll radius on the calculation of P' in the roll gap model. SID as a means of obtaining models for real plant processes is not uncommon in the industry [15, 80] where the practical data, obtained from the application of step tests or Pseudo Random Binary Signals (PRBS) to the plant, are analysed. This SID approach was also successfully used for the identification of linear models for controller design. Examples of the application of SID to nonlinear plant simulators to find linear models, are the dissertation by F.R. Camisani-Calzolari [23], where speed disturbance rejection controllers for the secondary cooling zone in a continuous caster were

designed, and various rolling mill projects [21, 81]. To algebraically linearize the total rolling process model, which exhibits a number of iterative loops as part of the numerical solution method, can be time consuming and less accurate in comparison to the application of step tests and the use of SID.

5.2 Roll gap model simulations

In this section three figures (figures 5.2, 5.3 and 5.4) are discussed. The results were obtained from three separate simulations of the roll gap model. The settings for these simulations are shown in table 5.1 and will now be further discussed.

Table 5.1: Settings of the input variables of the roll gap model.

Case	$\delta(mm)$	$T_1(MN)$	$T_2(MN)$
1	3	0	0
2	3	5	0
1	3	0	5

In figure 5.2 the vertical roll pressure as a function of the length of the arc of contact is shown, as obtained from simulations conducted using the roll gap model. The shape of the function resembles

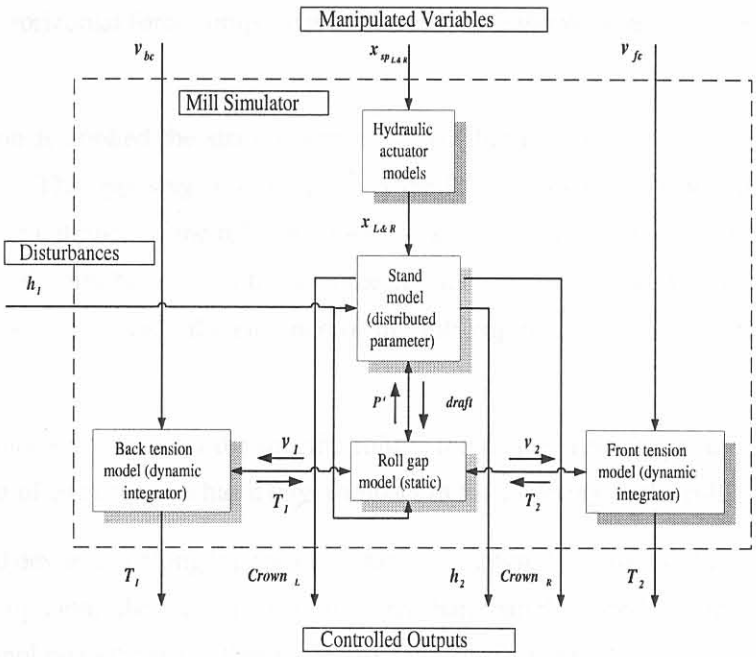

Figure 5.1: The I/O relationship of the plant/simulator. In this figure the manipulated variables of the two hydraulic actuators are treated as one manipulated variable. It is noteworthy to mention that h_1 is not the only modelled disturbance that can result in exit gauge deviations, but T_1 and T_2 can also adversely influence the exit thickness. The latter two variables are plant outputs as well as internal disturbances in the simulator.

a hill (friction hill [28, 2, 44]). The pinnacle of this friction hill corresponds to the neutral point as discussed in section 4.3.1. With no applied strip tension the neutral point is almost in the middle of the arc of contact. When tension is applied to the strip it is seen that the neutral point shifts accordingly. The application of front tension moves the neutral point towards the entrance of the roll gap. This is in agreement with statements in [2], and the neutral point can be moved to the exit of the roll gap by applying back tension to the strip.

When back tension is applied to the strip, the friction forces work towards the exit of the roll gap trying to draw the strip through the roll gap. The application of back tension hinders the delivery of strip from the roll gap and a larger friction force working towards the exit of the roll gap is needed to pull the strip through the roll gap. This larger friction force is obtained when the neutral point shifts towards the exit of the roll gap resulting in a longer length of the arc of contact. This longer arc of contact is subjected to the frictional forces working from the roll gap entrance towards the roll gap exit, thus pulling the strip through the roll gap. In [2] it is stated that the tension lowers the friction component of the rolling force. This is the case and can be explained by way of the vertical pressure distribution curve along the arc of contact. This friction hill can be split up into two areas, the first area resembles a rectangular area and the second area is almost triangular in shape. This triangular area resembles the part of the rolling force that is associated with the frictional forces. When tension is applied this triangle area decreases as can be seen in figure 5.2. But it was stated earlier in the paragraph that a larger friction force along the arc of contact is needed to pull the strip through the roll gap. Thus the horizontal force component increases, while the vertical force component decreases P'.

When front tension is applied the strip is almost pulled through the roll gap due to the actions of the applied tension. The opposing reaction force is the friction force that works from the exit of the roll gap towards the entrance of the roll gap along the arc of contact. Thus when the front tension is increased the neutral point has to shift towards the entrance of the roll gap in order to create a larger frictional force working towards the entrance of the roll gap that opposes the effect of the applied front tension.

Both cases of applied tension lower the specific rolling force (see previous paragraph and figure 5.2), but the application of back tension has a larger impact in the lowering of the rolling force [2].

In figure 5.3 speed deviations along the arc of contact are shown. With the application of front tension the speed of the strip along the arc of contact is larger than than the speeds when no tension and only back tension are applied to the strip. This increase can be attributed to the drawing of the strip through the roll gap. The speed along the arc of contact is smaller compared to the other 2 cases (no tension and only front tension applied), when back tension is applied to the strip.

In figure 5.4 half the thickness deviation along the arc of contact for the three cases[1] are shown. It

[1] i) No applied tension; ii) Applied front tension; iii) Applied back tension

appears that the thickness difference due to the application of tension is small. This is expected due to the fact that the magnitude of the applied tension was limited in order to prevent the tension in the strip from exceeding the yield stress of the material. Larger thickness reduction due to the application of tension can be expected, when the applied tension exceeds the yield stress of the material resulting in necking[2] of the strip.

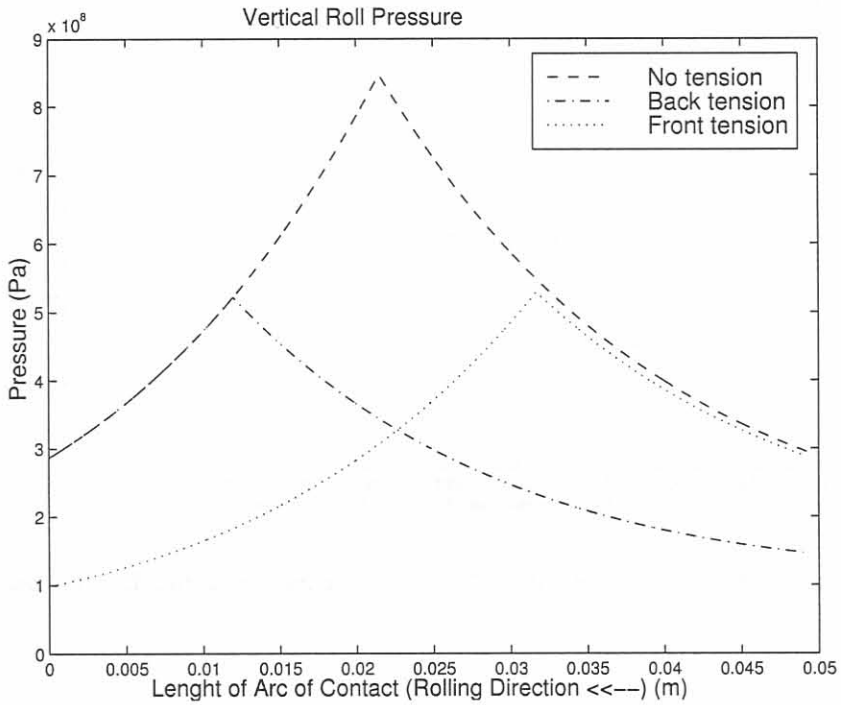

Figure 5.2: Vertical pressure distribution vs. roll gap distance as a function of the applied strip tensions.

In figures 5.5, 5.6, 5.7, and 5.8[3] the draft and the applied tensions are varied in order to investigate how close to the physical limit of the mill the chosen operating point (see section 4.2.2) of the mill simulator is.

From figure 5.8 it can be seen that when the tensions are kept fixed an increase of 2mm in the draft taken is possible. It needs to be stressed that although the mill is capable to handle such an increase the mill frame stretch may be excessive.

From figures 5.5 and 5.6 it can be seen that when the draft increases the specific rolling force increases. The converse is true for increases in the applied strip tensions as can be seen in especially figure 5.7, and also in figures 5.5 and 5.6. The elastic deformation range of the tension process was taken to correspond to 0-200MPa, which is smaller than the calculated yield stress (280MPa) at a draft of 3mm. From figure 5.8 it can be seen that, for a draft of 3mm and applied tensions fixed at their setup values, the specific rolling force is well below the physical limit of the mill.

[2]See section 3.4.2 for a description of necking.

[3]Note that in this section $T_b = T_1$ and $T_f = T_2$ as defined in chapter 3 section 3.4.2.

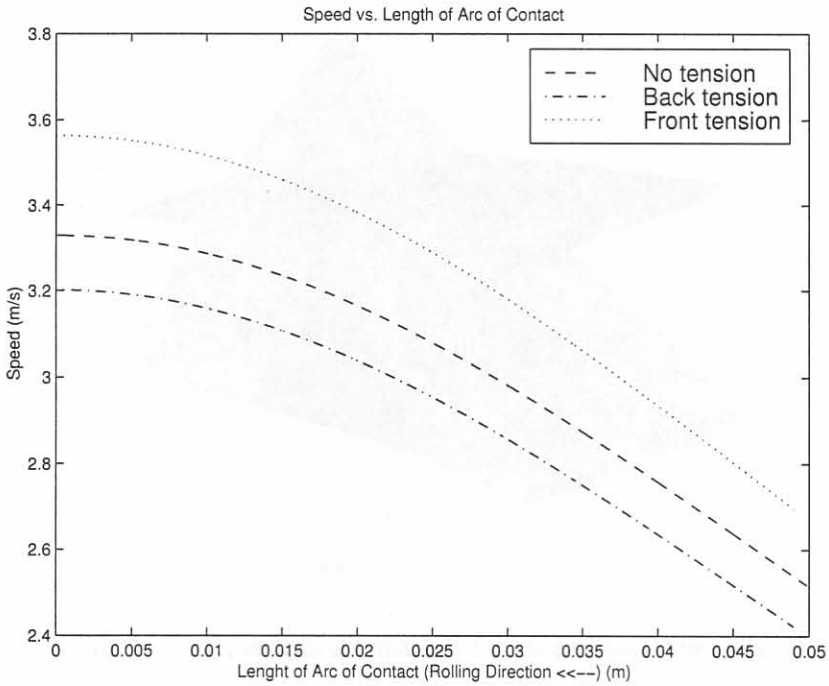

Figure 5.3: Velocity along the arc of contact vs. the length of the arc of contact.

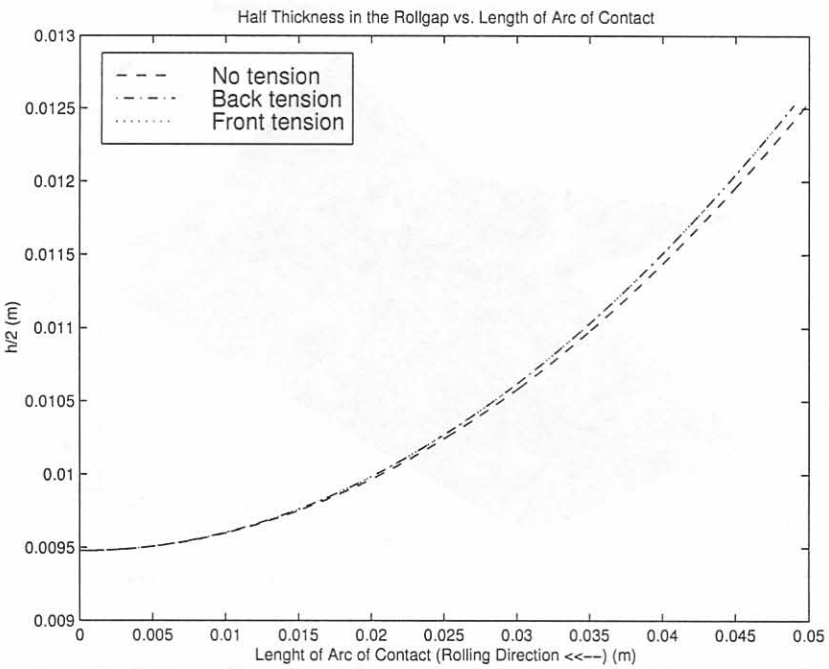

Figure 5.4: Half thickness variation through the roll gap as a function of the length of the arc of contact

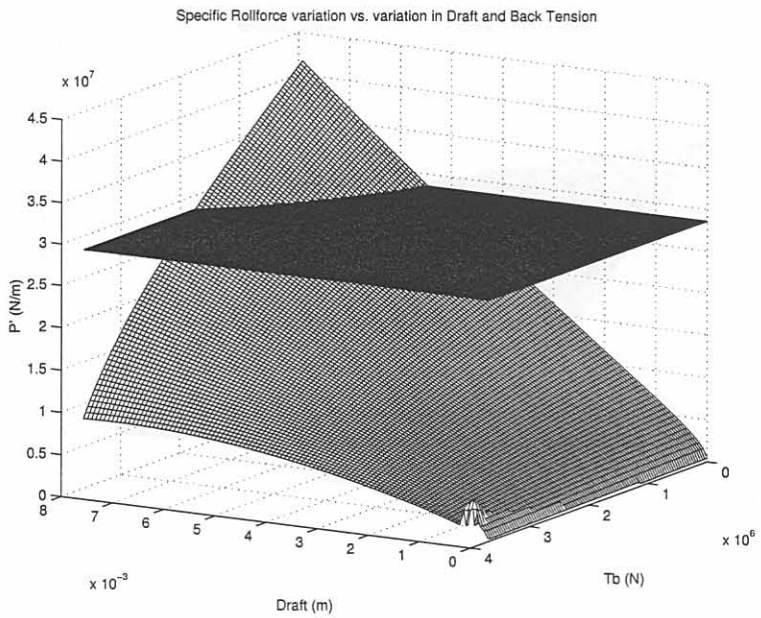

Figure 5.5: The Specific Rolling Force as a function of draft and back tension applied to the rolling mill, when the front tension is kept constant at its setup value ($P' = f(\delta, T_b)|_{T_{f_{setup}}}$). The Physical Mill Limit ($\frac{40MN}{w}|_{w=1.3m} \approx 2.8 \times 10^7 \frac{N}{m}$) is also shown.

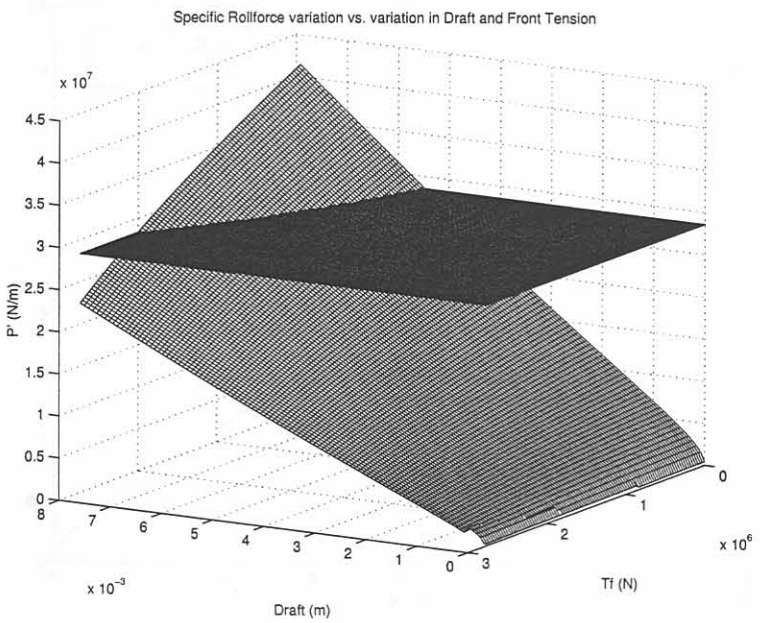

Figure 5.6: The Specific Rolling Force as a function of draft and front tension applied to the rolling mill, when the back tension is kept constant at its setup value ($P' = f(\delta, T_f)|_{T_{b_{setup}}}$). The Physical Mill Limit ($\frac{40MN}{w}|_{w=1.3m} \approx 2.8 \times 10^7 \frac{N}{m}$) is also shown.

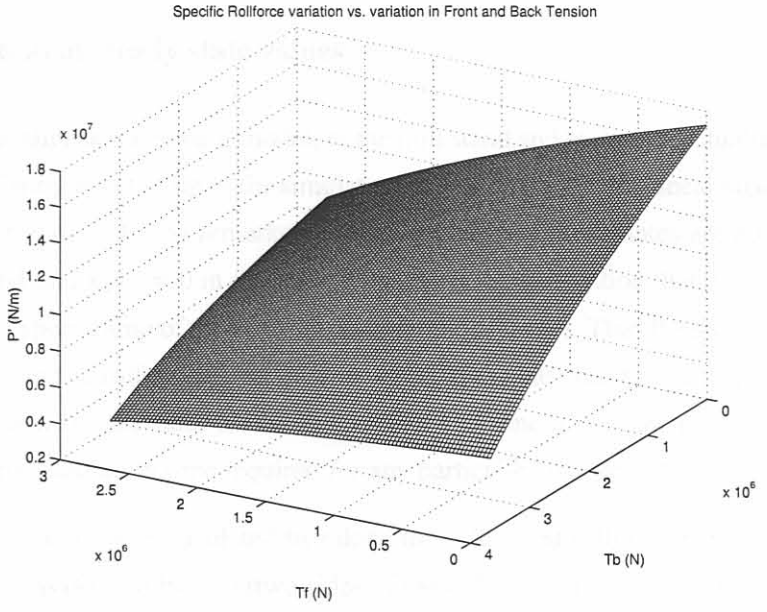

Figure 5.7: The Specific Rolling Force as a function of the applied tensions, when the draft is kept constant at 3mm ($P' = f(T_b, T_f)|_{\delta=3mm}$).

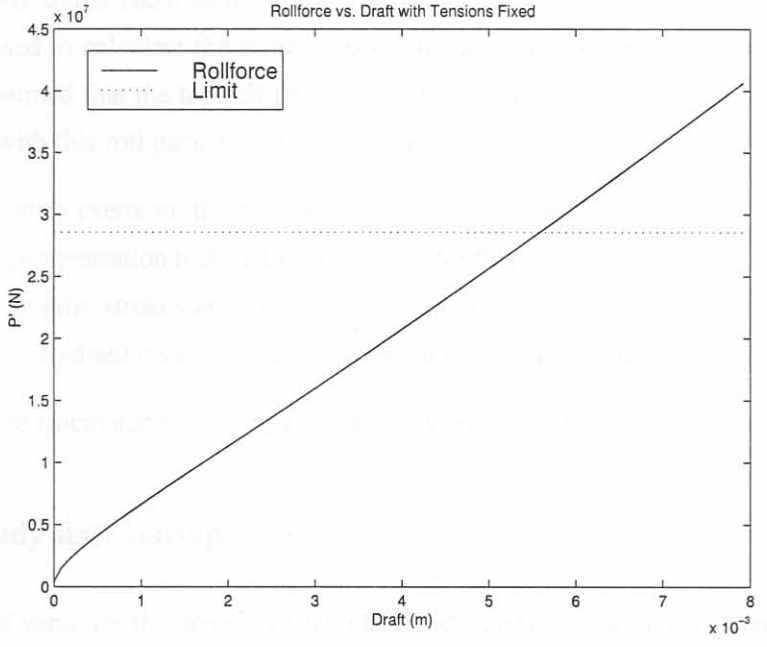

Figure 5.8: The Specific Rolling Force as a function of draft taken, when the tensions are kept constant at their setup values ($P' = f(\delta)|_{T_{b_{setup}}, T_{f_{setup}}}$). The Physical Mill Limit ($\frac{40MN}{w}|_{w=1.3m} \approx 2.8 \times 10^7 \frac{N}{m}$), the horizontal line, is also shown.

5.3 Nonlinear state-space model

5.3.1 Calculation of steady state values

The states of the nonlinear state-space model, of the mill stand and hydraulic actuators, was calculated in order to have a bumpless start up of the simulator. In section 4.7 the nonlinear state-space equations of the simulator are given. It was remarked earlier that most of these states are not defined as small signal variables and that $\mathbf{x}(0) \neq 0$ in general. It is noteworthy to mention that the simulator is started on the acceleration speed ramp of the mill drive synchronous motor. Thus the simulation is not started before commencement of rolling, but rather after a part of the pass has been completed. This start-up procedure is not ideal and the state vector at that instant of time is unknown. This methodology was induced by the long simulation time required for any particular simulation[4].

The states at steady state were calculated by taking the calculated rolling force at $t = 0$. This calculated rolling force was divided by two (two sides of the mill) to yield the shearing forces at the edges of the top roll pack. In the steady state these shearing forces has to equal the thrust forces of the hydraulic actuators. From these thrust forces the pressures in the cylinder chambers can be calculated, by setting the leakage flow between the main chamber and the secondary chamber to zero (e.g. steady state). This implies that the pressures of the main and secondary chambers are equal.

The shearing forces at the edges of the bottom roll pack compresses the load cells. These compressions are calculated and is taken as the vertical displacement of the bottom roll pack. The vertical displacement is used to calculate the initial states associated with the vertical displacements of this roll pack. It is assumed that the top roll pack does not have an initial vertical displacement, and the states associated with this roll pack are all taken as zero.

The force that the strip exerts on the rollers causes the mill to stretch excessively. A static BISRA-Davy gaugemeter compensation is done to compensate for this mill stretch, and the steady state values of the dynamic hydraulic strokes are increased with the relevant compensation quantities, on either side of the mill. The hydraulic strokes are varied around these steady state values.

The states that were calculated for anticipated bumpless simulation start up are shown in table 5.2.

5.3.2 Non steady state startup

The magnitudes of variables that have not been identified satisfactory were discussed in section 4.5.3. The magnitudes are the hydraulic stiffness of the hydraulic jacks (K_J) and the damping between the strip and the work rolls (β_{strip}), which influence the dynamic behaviour of the mill stand, and

[4] An Intel ®Pentium II 400MHz personal computer was used to complete the simulations for this dissertation. Multi-tasked simulations under Windows NT ®ran in excess of 48 hours, which makes it very time consuming to experiment with process parameters.

ultimately the whole process behaviour. A comparison was made between different model scenarios, where the damping coefficient and the hydraulic spring constants, were experimented with. In table 5.3 a representative comparison is made between three different scenarios.

When $K_J = 40e9\frac{N}{m}$, the damping ratios associated with the dominant eigenvalues of the stand model increase and the vibration oscillations decays more rapidly. These increased ratios limit the oscillatory nature of the stand model. The main difference between the models with different β_{strip} is classified according to the degree of bumpless simulation startup. Complete bumpless transfer can not be achieved, because at the time instance when the simulation is started the mill speed is still increasing. In figure 5.10 ($\beta_{strip} = 1e8\frac{N}{m^2.s^{-1}}$) it can be seen that the draft changes quite drastically from the calculated initial state when compared to the model cases where $\beta_{strip} \geq 5e10\frac{N}{m^2.s^{-1}}$ (see figure 5.9).

5.4 System Identification

The proposed controlled variables of the system are the centerline exit thickness of the strip from the roll gap, the tension in the strip whilst rolling on either side of the roll gap, and the thickness profile of the strip. The manipulated variables available are the hydraulic cylinder strokes on both sides of the mill frame and the coiler furnace motor speeds. The hydraulic actuators can function independently or as a combined unit. In figure 5.1 the I/O relationship of the simulator are shown with the manipulated and controlled variables indicated. The linearized plant can be expressed as transfer functions in the

Table 5.2: Calculated states for bumpless simulation start up. The units of the states are not shown.

State	Value
$x_1, x_2, x_5, x_6, x_7, x_8, x_9, x_{10}, x_{12}, x_{13}$	0
x_3	1.84×10^{-6}
x_4	-3.12×10^{-5}
x_7	-3.12×10^{-5}
$x_{11}, x_{14}, x_{15}, x_{16}$	2.15×10^{7}
x_{17}	3.68×10^{-3}
x_{18}	3.65×10^{-3}

Table 5.3: Comparison of the damping ratios (ζ), natural frequencies (ω_n and f_n), and natural period (T_n) for different cases of K_J and β_{strip}.

$K_J(\frac{N}{m})$	$\beta_{strip}(\frac{N}{m^2.s^{-1}})$	ζ	$\omega_n(rad.s^{-1})$	$f_n(Hz)$	$T_n(s)$
0	5e10	1.7700e-009	3.8030e+001	6.0526e+000	1.6522e-001
		1.7700e-009	3.8030e+001	6.0526e+000	1.6522e-001
		1.0000e+000	1.1883e-003	1.8912e-004	5.2876e+003
		1.0000e+000	7.6827e-002	1.2227e-002	8.1783e+001
		6.6661e-003	2.3712e+003	3.7739e+002	2.6498e-003
		6.6661e-003	2.3712e+003	3.7739e+002	2.6498e-003
		1.0000e+000	1.7224e+005	2.7412e+004	3.6480e-005
		1.0000e+000	6.4953e+005	1.0338e+005	9.6734e-006
0	1e8	8.7562e-007	3.8030e+001	6.0526e+000	1.6522e-001
		8.7562e-007	3.8030e+001	6.0526e+000	1.6522e-001
		1.0000e+000	5.9442e-001	9.4605e-002	1.0570e+001
		1.0000e+000	5.6895e+001	9.0551e+000	1.1044e-001
		2.5896e-002	3.3267e+003	5.2946e+002	1.8887e-003
		2.5896e-002	3.3267e+003	5.2946e+002	1.8887e-003
		1.0000e+000	1.1845e+002	1.8851e+001	5.3046e-002
		1.0000e+000	1.2954e+003	2.0616e+002	4.8505e-003
40e9	1e8	8.9491e-003	3.8063e+001	6.0580e+000	1.6507e-001
		8.9491e-003	3.8063e+001	6.0580e+000	1.6507e-001
		5.7559e-002	7.4109e+002	1.1795e+002	8.4783e-003
		5.7559e-002	7.4109e+002	1.1795e+002	8.4783e-003
		2.4562e-002	3.5074e+003	5.5823e+002	1.7914e-003
		2.4562e-002	3.5074e+003	5.5823e+002	1.7914e-003
		1.0000e+000	4.6337e+002	7.3747e+001	1.3560e-002
		1.0000e+000	2.2118e+003	3.5203e+002	2.8407e-003

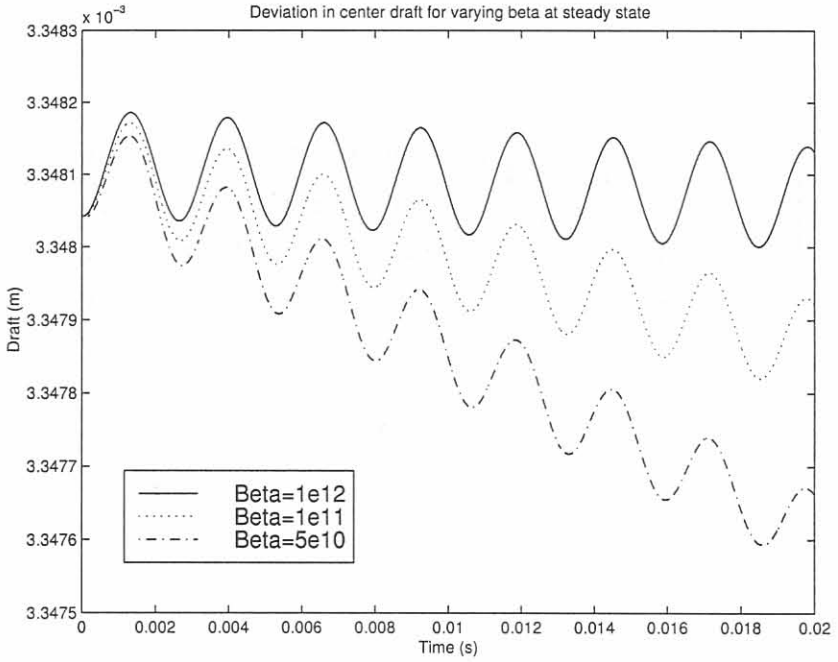

Figure 5.9: Steady state comparison of the draft deviation for $\beta_{strip} \in [5e10, 1e11, 1e12] \frac{N}{m^2.s^{-1}}$ and $K_J = 0 \frac{N}{m}$.

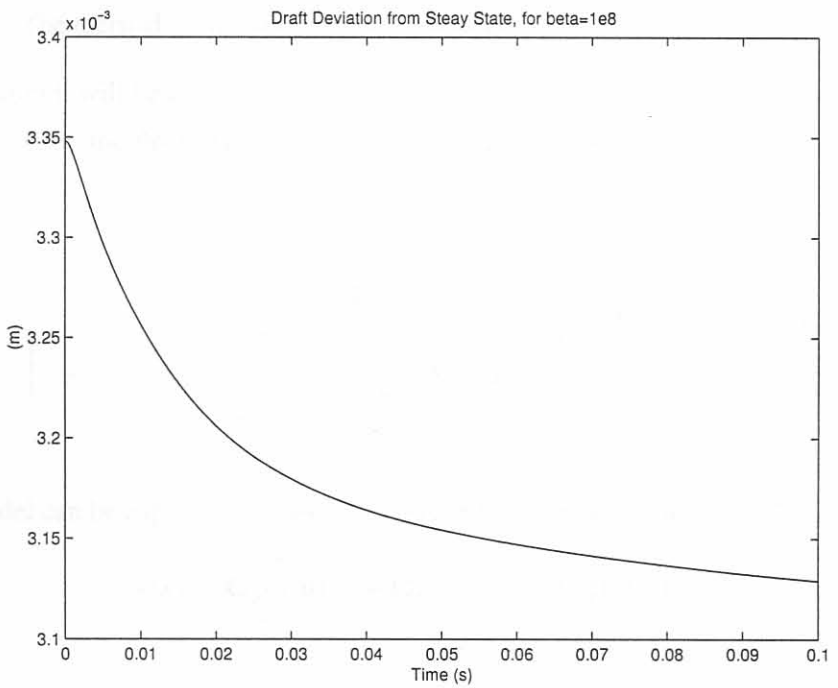

Figure 5.10: Steady state comparison of the draft deviation for $\beta_{strip} = 1e8 \frac{N}{m^2.s^{-1}}$ and $K_J = 0 \frac{N}{m}$.

Laplace transform format as follows:

$$\begin{bmatrix} \delta h_2(s) \\ \delta T_1(s) \\ \delta T_2(s) \\ \delta Cr_L(s) \\ \delta Cr_R(s) \end{bmatrix} = \begin{bmatrix} g_{11}(s) & g_{12}(s) & g_{13}(s) & g_{14}(s) \\ g_{21}(s) & g_{22}(s) & g_{23}(s) & g_{24}(s) \\ g_{31}(s) & g_{32}(s) & g_{33}(s) & g_{34}(s) \\ g_{41}(s) & g_{42}(s) & g_{43}(s) & g_{44}(s) \\ g_{51}(s) & g_{52}(s) & g_{53}(s) & g_{54}(s) \end{bmatrix} \begin{bmatrix} \delta x_{sp_L}(s) \\ \delta x_{sp_R}(s) \\ \delta v_{bc}(s) \\ \delta v_{fc}(s) \end{bmatrix} + \widehat{\mathbf{G}_d}(s) \begin{bmatrix} \delta h_1(s) \\ input\ hardness \\ \mu \\ \delta T_1(s) \\ \delta T_2(s) \\ Cr_{thermal\ rolls} \\ Bearing\ oil\ film \\ Roll\ eccentricity \\ v_{roll} \\ \theta \\ \vdots \end{bmatrix} \tag{5.1}$$

where,

$\widehat{\mathbf{G}_d}(s)$: A matrix containing disturbance transfer functions;

$g_{ij}(s)$: The transfer function between the i^{th} output and j^{th} input;

δCr_L: Strip thickness crown on the left side of the mill;

δCr_R: Strip thickness crown on the right side of the mill

$Cr_{thermal\ rolls}$: The thermal crown build up on the rollers[5].

As a first iteration it will be assumed, similarly to [81], that the hydraulic actuators function jointly. The calculated centerline thickness control signal is applied to each of the actuators.

The reduced model is[6],

$$\begin{bmatrix} \delta h_2(s) \\ \delta T_1(s) \\ \delta T_2(s) \end{bmatrix} = \begin{bmatrix} g_{11}(s) & g_{12}(s) & g_{13}(s) \\ g_{21}(s) & g_{22}(s) & g_{23}(s) \\ g_{31}(s) & g_{32}(s) & g_{33}(s) \end{bmatrix} \begin{bmatrix} \delta x_{sp_{L\&R}}(s) \\ \delta v_{bc}(s) \\ \delta v_{fc}(s) \end{bmatrix} + \begin{bmatrix} g_{d11}(s) & g_{d12}(s) & g_{d13}(s) \\ g_{d21}(s) & 0 & g_{d23}(s) \\ g_{d31}(s) & g_{d32}(s) & 0 \end{bmatrix} \begin{bmatrix} \delta h_1(s) \\ \delta T_1(s) \\ \delta T_2(s) \end{bmatrix} \tag{5.2}$$

The above model can be expressed in standard transfer function model notation [72],

$$\mathbf{y}(s) = \mathbf{G}_p(s)\mathbf{u}(s) + \mathbf{G}_d(s)\mathbf{d}(s) + \mathbf{G}_w(s)\mathbf{w}(s), \tag{5.3}$$

with,

[5]The rest of the variables are either defined in chapter 3 and 4 or are self explanatory.

[6]Only the first row of the disturbance transfer function matrix is considered of importance and the transfer functions $g_{d21}(s), g_{d23}(s), g_{d31}(s), g_{d32}(s)$ will not be identified in this dissertation. It can be argued that the transfer functions $g_{d23}(s), g_{d32}(s) \approx 0$, because the tensions are connected via a static roll gap model.

$\mathbf{y}(s) = \begin{bmatrix} \delta h_2(s) & \delta T_1(s) & \delta T_2(s) \end{bmatrix}^T = \begin{bmatrix} y_1(s) & y_2(s) & y_3(s) \end{bmatrix}^T$: The controlled variable vector;

$\mathbf{u}(s) = \begin{bmatrix} \delta x_{sp_{L\&R}}(s) & \delta v_{bc}(s) & \delta v_{fc}(s) \end{bmatrix}^T = \begin{bmatrix} u_1(s) & u_2(s) & u_3(s) \end{bmatrix}^T$: The manipulated variable vector;

$d(s) = \begin{bmatrix} \delta h_1(s) & \delta T_1(s) & \delta T_2(s) \end{bmatrix}^T$: The measured disturbance vector;

The linear plant model is obtained by applying step tests to one of the three manipulated inputs whilst the other two inputs are kept at their steady state operating points. In the following section the design of these step tests is discussed.

5.4.1 Design and results from the step tests

It was decided to use step tests to identify the linear models. The reason being the ease of their application to the simulator. The application of a PRBS signal might be preferred in industry, because the average energy inserted into the system is zero. The design of a PRBS signal, that capture the necessary dynamics by ensuring that the first zero of the $(\frac{sin(j\omega)}{j\omega})$ frequency envelope of the periodic square wave signal [82] is greater than the plant bandwidth, is difficult in the absence of a given plant bandwidth. Ballpark estimates of the plant bandwidth can however be found from the literature.

When the SID steps are applied to the simulator, the main mill drive speed is forced constant in the simulator at the desired point of linearization in order to eliminate possible dynamic effects on the controlled outputs due to main mill drive speed deviations.

5.4.1.1 Combined hydraulic strokes, $\delta x_{L\&R}$

From figures 5.5, 5.6, and 5.8 it can be seen that another 2 mm of draft increase is permitted before the physical limit of the mill is reached[7]. The linear model that will be identified is for regulation purposes, and it is not anticipated that such a large draft increase will be required, when the mill setup is adapted during the execution of a rolling schedule. A large increase in the mill draft might not even be obtainable due to the significant amount of mill stretch. The magnitude of the hydraulic stroke step was chosen as $1mm$, and from figure 5 in [18] where it is shown that when a supervisory GPC[8]-controller is used to regulate the rolling process after a 1mm hydraulic stroke disturbance was applied. When the controller was switched on after 4 seconds the manipulated stroke was rarely larger than 1mm. Grimble and Katebi [18] state that when the hydraulic stroke was larger than 1mm it was excessive and in this dissertation a dynamic stroke increase range of 1mm was used in the identification of a linear model for process regulation purposes.

[7] It should be stressed that these figures were obtained from simulations using the roll gap and tension model unit of the simulator and the dynamic effects of the rolling mill stand are not reflected in these results.

[8] Generalized Predictive Control.

In figure 5.11 a zoomed plot of the hydraulic strokes of both actuators are shown. When this 2nd order response is approximated as a 1st order response a time constant of $\tau = 83ms$ can be calculated, which corresponds to a bandwidth of 12Hz. This bandwidth corresponds to a benchmark value of 15Hz [1] for hydraulic systems. From figure 20 of [8] it can be concluded that the hydraulic actuators' bandwidth fall into the specified operation range for a double acting position mode hydraulic actuator.

In figure 5.12 the cascaded controlled servovalve-spool strokes are shown. Note the hard limit of $|3mm|$ imposed on the spool stroke movement. This hard limit was introduced by reasoning that the cylinder flow can not increase if the spool opening is already at a maximum. Thus if the gain of the cascaded PI stroke position controllers of the hydraulic systems are tweaked as such that the servovalve spools' limits are readily attained for larger required strokes, the system response will be slower than anticipated due to the flow saturation.

In figures 5.13-5.15 different comparison plots of the exit gauge are shown. In figure 5.13 the supposed steady state evolution of the exit gauge are shown at the strip center and end points. The deviation away from the steady state is attributed to non bumpless start-up as well as the forcing of the strip on the rollers, which is not compensated for.

In figure 5.14 the steady state evolution is compared to the exit gauge response when a combined hydraulic stroke increase of $1mm$ is applied. The relative difference between these two responses is large and constitute the dynamic behaviour due to a hydraulic stroke increase. It is important to note the order with which the thickness decreases compared to the input step of $1mm$. From this figure it can be seen that the thickness decreased with a mere $|300\mu m|$, and the rest of the $1mm$ stroke is

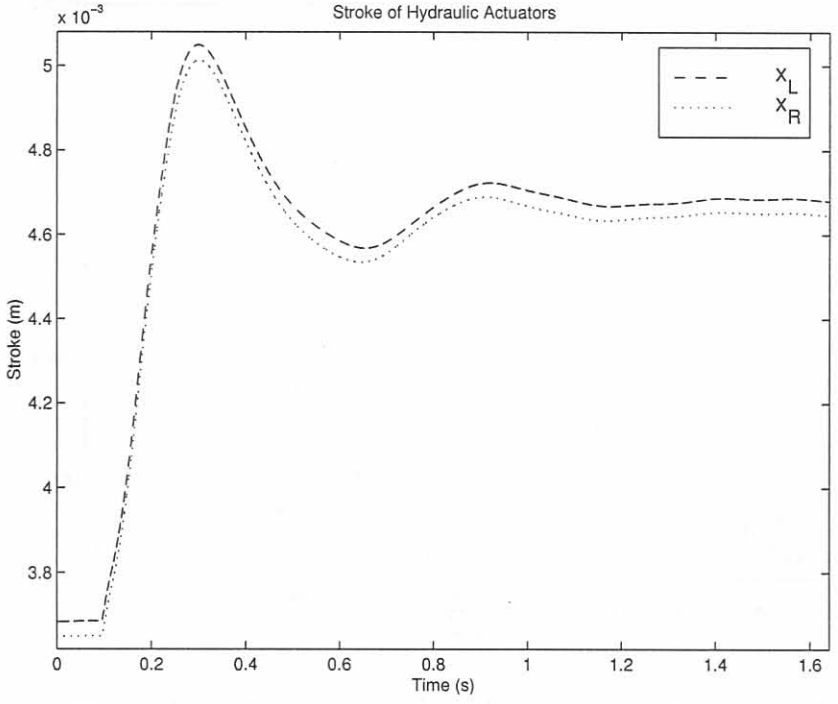

Figure 5.11: Hydraulic strokes, after a step input of 1mm was done in the hydraulic stroke at 92.6ms.

embedded in the mill stretch.

In figure 5.15 a three dimensional view of the exit thickness are shown, after the application of a

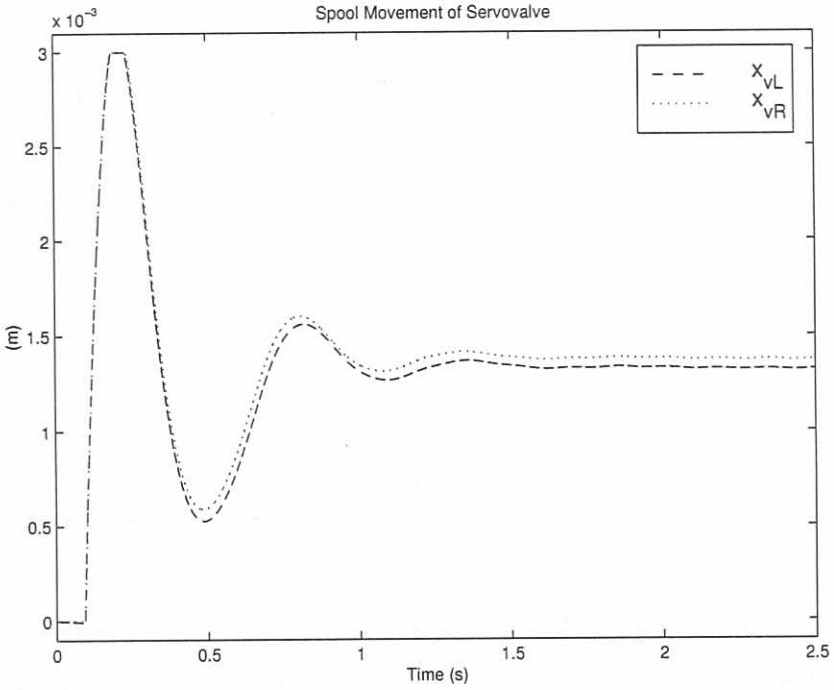

Figure 5.12: Servovalve spool stroke, after a step input of 1mm was done in the hydraulic stroke at 92.6ms.

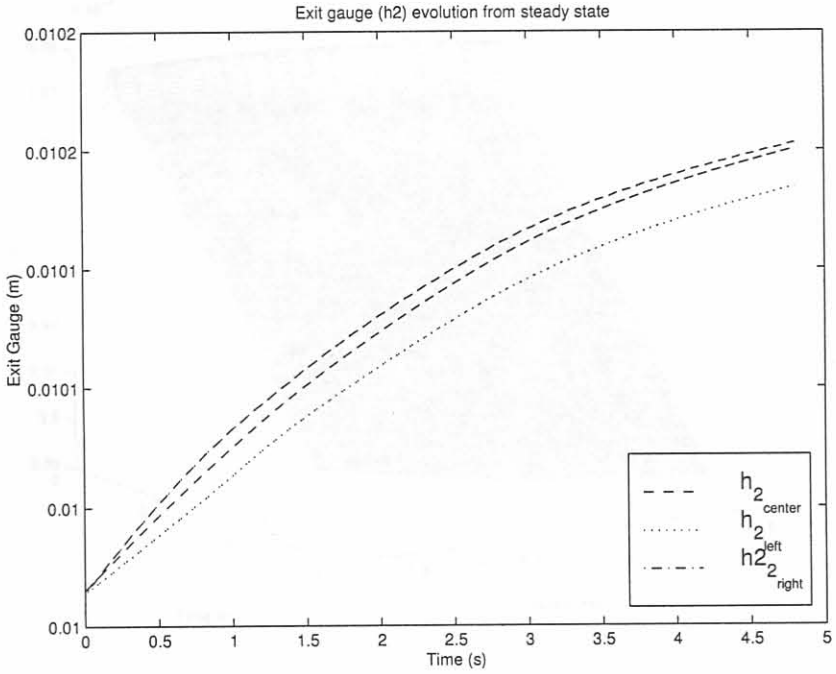

Figure 5.13: Exit gauge at the center and end points of the strip, at supposed steady state (i.e. the manipulated variables are kept zero).

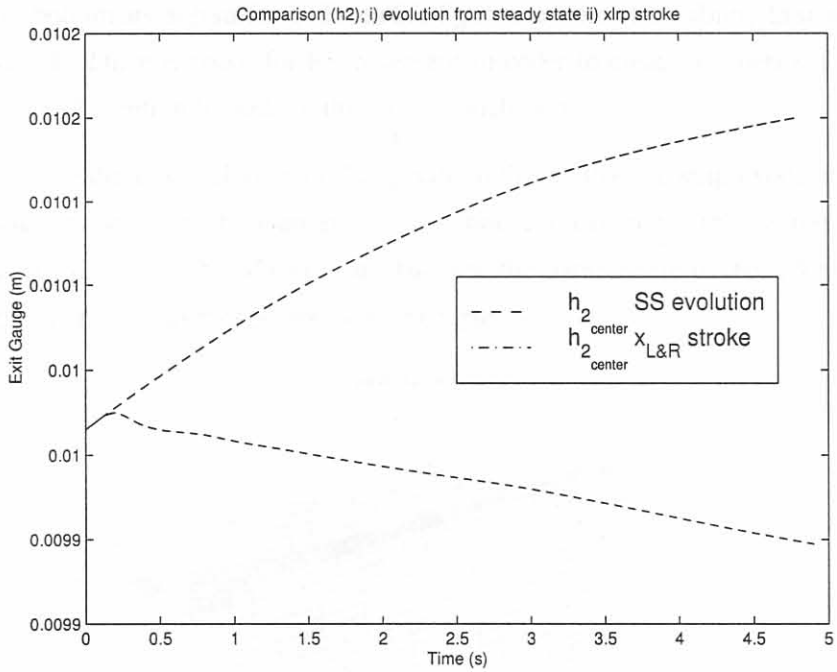

Figure 5.14: A comparison plot of the exit gauge at the center of the strip, between the output obtained when a step input of 1mm was done in the hydraulic stroke at 92.6ms, and the steady state evolution.

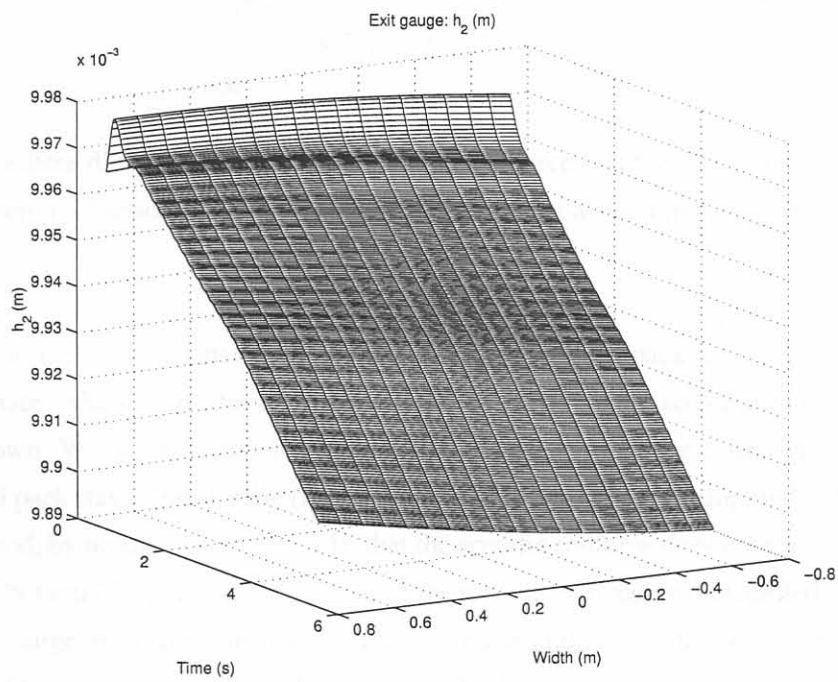

Figure 5.15: A three dimensional view of the exit gauge as a function of space and time, after a step input of 1mm was done in the hydraulic stroke at 92.6ms.

hydraulic stroke setpoint change was made at 92.6ms. The plotted thickness deviations does not reflect the strip's bottom and top surfaces. From this figure the simulator's ability to simulate thickness crown is displayed. There is room for improvement in order to create a superior thickness crown simulator and special mention is made of this in the conclusions.

In figure 5.16 a three dimensional view of the specific rollforce that the strip exerts onto the two roll packs as a function of space and time are shown in response to the 1mm stroke step that was applied. The function is not very smooth and this is attributed to the static nature of the roll gap model. This function is highly nonlinear as was pointed out in chapter 3.

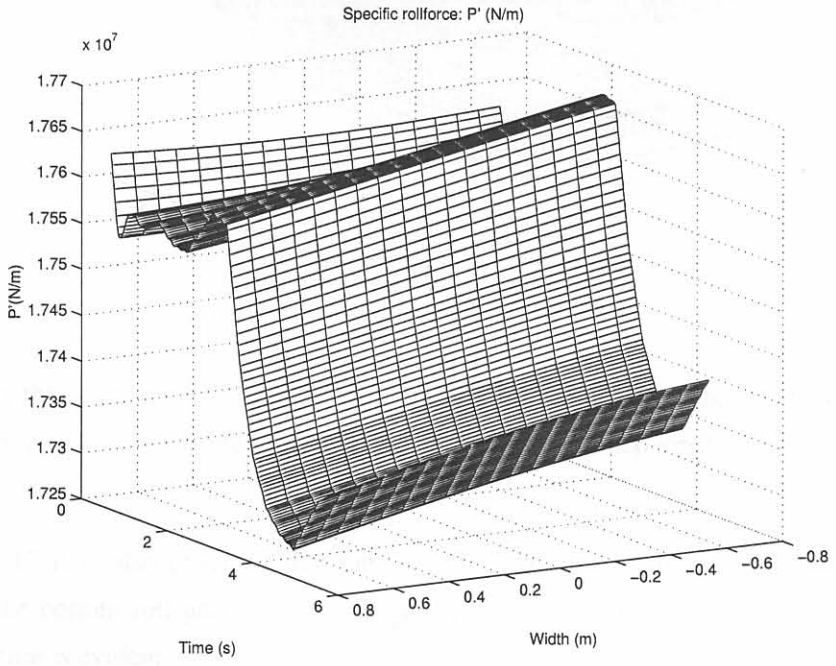

Figure 5.16: A three dimensional view of the specific rollforce that the strip exerts onto the two roll packs as a function of space and time, after the application of a step input of $1mm$ in the hydraulic stroke at 92.6ms.

In figure 5.17 a three dimensional view of the top and bottom roll pack deviation movements from their steady state values, after the application of a hydraulic stroke setpoint change was made at 92.6ms, is shown. When the deviational movements of the roll packs are compared it is evident that the bottom roll pack stays almost static (ignoring the high frequency small amplitude vibrations). This can be explained, by noting from figure 5.16 that the specific rollforce does change over time but not by much. The bottom (K_{LB} and K_{RB}) springs of the mill stand model was modelled as measurement load cells with large associated stiffnesses. This therefore implies that the movement of the bottom roll pack should be minimimal. Note that figure 5.17 reflects the small signal movement of the roll packs and does not imply that the one roll pack moves through the other roll pack. It can be seen from this figure that while the bottom roll pack movement stays almost static, the top roll pack movement is dictated by the hydraulic stroke. The draft deviation from the setup draft is the difference between

the deviation movements of the roll packs, when the input thickness is fixed.

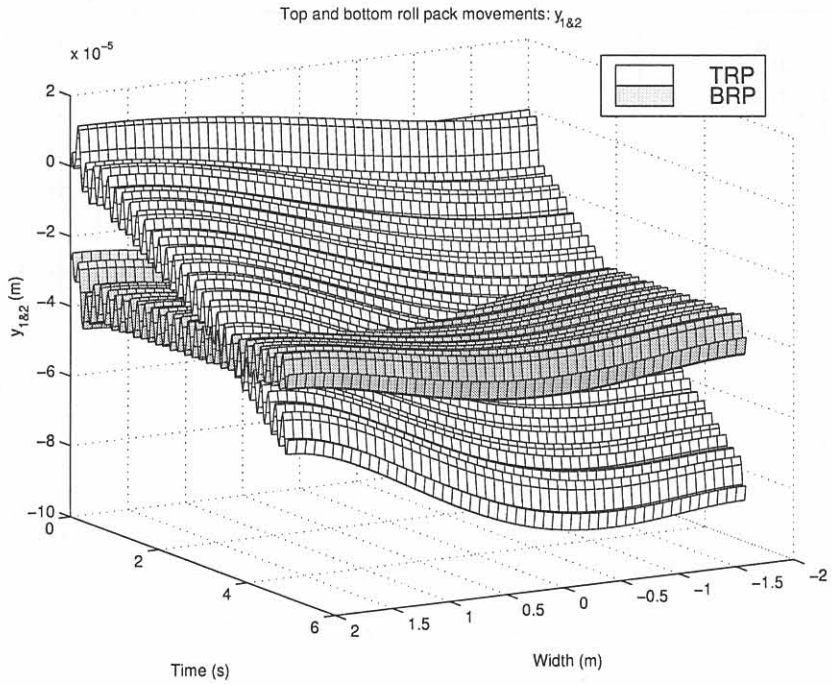

Figure 5.17: A three dimensional view of the deviation movement from the steady state of the two roll packs as functions of space and time, after the application of a step input of $1mm$ in the hydraulic stroke at 92.6ms.

From figure 5.17 it is also observed that the second mode of vibration is the dominant mode of vibration for the bottom roll pack. For the top roll pack a combination of the first and the second mode of vibration is evident.

5.4.1.2 Speed steps, $\delta v_{bc}, \delta v_{fc}$

The speed steps were calculated in order to have the maximum effect on the centerline gauge. This entails increasing the tension, on either side to a maximum stress value of $200MPa \Rightarrow [3.72MN\ |_{h_1=13.3mm}, 2.716MN\ |_{h_2=9.7mm}]$ from the setup values of $\approx$ 8MPa. Tension is not permitted to be negative, because negative tensions will not decrease the rolling force and will according to the roll gap model increase the rolling force. This might not be a true reflection of the true rolling process. The tensions are calculated by integrating the speed difference between the coiler and the roll gap speeds. This knowledge is used to calculate the step size of the coiler speed or the time duration of the step using the following relationship,

$$E_{ss}A_{cross_i}L^{-1}_{rg\leftrightarrow cf}\Delta x_i = E_{ss}A_{cross_i}L^{-1}_{rg\leftrightarrow cf}\Delta v_{\kappa c}\Delta t_{step} = 200\times 10^6 A_{cross_i} - T_{i_{setup}}, \qquad (5.4)$$

where $i \in [1,2]$ and correspondingly $\kappa \in [b,f]$. $E_{ss} = 106GPa$ is Youngs' modulus of stainless steel at $970°C$. A_{cross_i} is the cross sectional area of the sheet perpendicular to the rolling direction on either side of the roll gap.

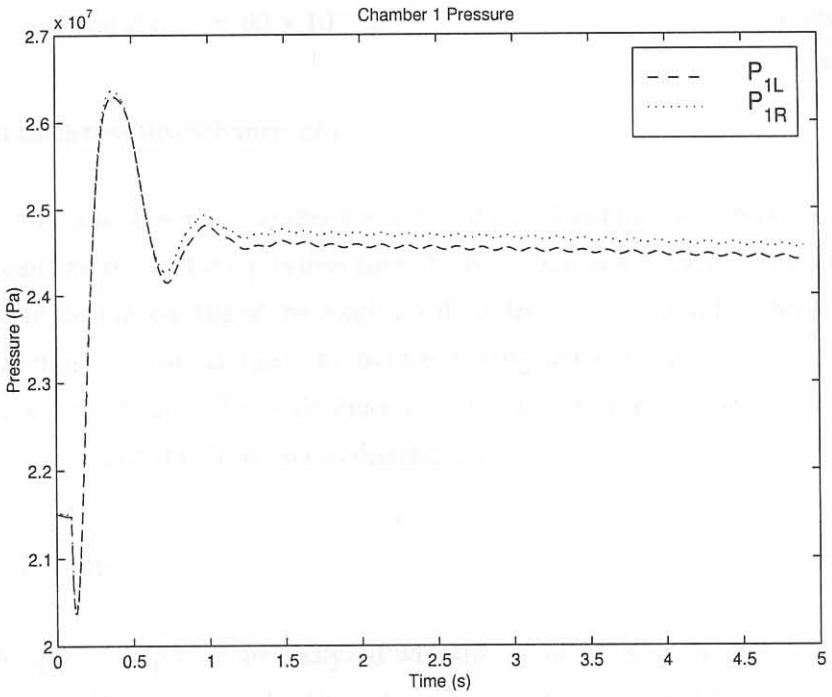

Figure 5.18: Pressure in cylinder chamber 1, after the application of a step input of $1mm$ in the hydraulic stroke at 92.6ms.

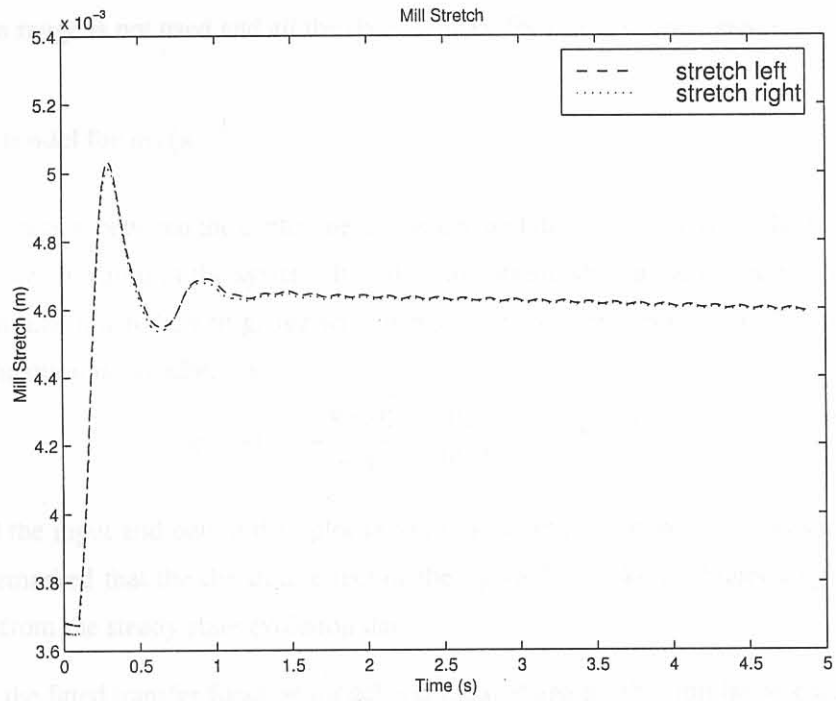

Figure 5.19: Mill stretch, after the application of a step input of $1mm$ in the hydraulic stroke at 92.6ms.

Different values for $\Delta v_{\kappa c}$ and Δt_{step} were experimented with. The two parameters were chosen as, $\Delta v_{\kappa c} = \pm 0.2 m.s^{-1}$ and $\Delta t_{step} = 60 \times 10^{-3} s$.

5.4.1.3 Input thickness disturbance, δh_1

The operating point was chosen on the speed up ramp of pass 3 and the input thickness disturbance is the controlled exit thickness of the previous pass. Thus the entrance thickness deviation will not be so large, and from the logged data of the Steckel Mill under consideration, the absolute value of the thickness deviation is less than $|200|\mu m$. In [64] the investigated hydraulic gauge control system was tested with a maximum input thickness deviation of $|200|\mu m$, which gives justification for the choice of a disturbance step input of $0.2mm$ in this dissertation.

5.4.2 Identification

The data of the applied step tests are analyzed with the aid of the System Identification toolbox of Matlab. ARX (Auto Regression with eXternal input) models were fitted [83]. In this dissertation an exposition of system identification is not given and the interested reader is referred to References [84, 83].

In section 5.3.1 a remark was made about the long duration of any simulation. This places a restriction on the amount of available data suitable for system identification purposes, and in some cases a model validation data range is not used and all the data are used for fitting of the models.

5.4.2.1 The model for $g_{11}(s)$

This transfer function between the centerline exit gauge and the requested hydraulic stroke is the most important transfer function of the system. It will be important when a model based controller is used to predict with how much the exit gauge will change when a change is made in the hydraulic stroke. The transfer function is calculated as,

$$g_{11}(s) = \frac{-8.0865 \times 10^{-2}}{s + 1.9 \times 10^{-1}} e^{-4.15 \times 10^{-3} s}. \tag{5.5}$$

In figure 5.20 the input and output data plot used in the identification of $g_{11}(s)$ is shown. In section 5.4.1.1 it is remarked that the dynamic effect of the hydraulic stroke is obtained by subtracting the step test data from the steady state evolution data.

In figure 5.21 the fitted transfer function model is compared against the simulation data obtained from the nonlinear plant simulator.

The accuracy of the identified transfer function models was done by looking at the autocorrelation function of the error between the model output and the simulation data, and the cross correlation

between this error and the manipulated variable that was stepped. The 99% confidence intervals for these correlation values are computed using the 'resid' command in Matlab's SID toolbox and are displayed as dotted lines on the correlation plots. The computation of these values is done assuming that the error to be white and independent of the stepped manipulated variable [83]. An autocorrelation and cross correlation plot obtained from identifying $g_{11}(s)$ is shown in figure 5.22. From this plot it can be seen that the cross correlation lies in the 99% confidence intervals, but the autocorrelation transgress this 99% confidence level. From this plot and the good correspondence of the time plot (figure 5.21), the transfer function model can be regarded as a good fit to the simulation data.

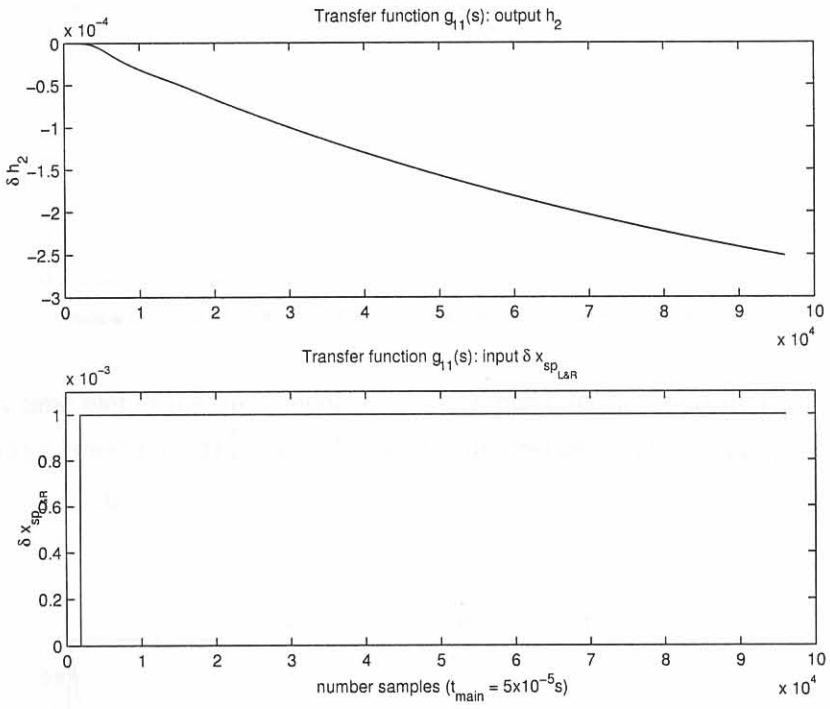

Figure 5.20: I/O data used in the identification of $g_{11}(s)$. (The x axis denotes the number of samples with the sampling interval given as $t_{main} = 5 \times 10^{-5}$)

5.4.2.2 The model for $g_{21}(s)$ and $g_{31}(s)$

The two transfer functions between the tension outputs and the hydraulic stroke setpoint are very similar. It should be noted that the fitting ranges of these two models were taken such that the tensions stayed greater than zero in the simulations. In figure 5.23 the I/O data plot used in the identification of $g_{21}(s)$ is shown. In figure 5.24 the identified transfer function model for $g_{31}(s)$ is compared to the nonlinear plant simulation data. In figure 5.25 the auto- and cross correlation plots of the identified transfer function model for $g_{21}(s)$ are shown. From these figures it can be concluded that the identified models approximate the nonlinear behaviour accurately at the point of linearization. The models are

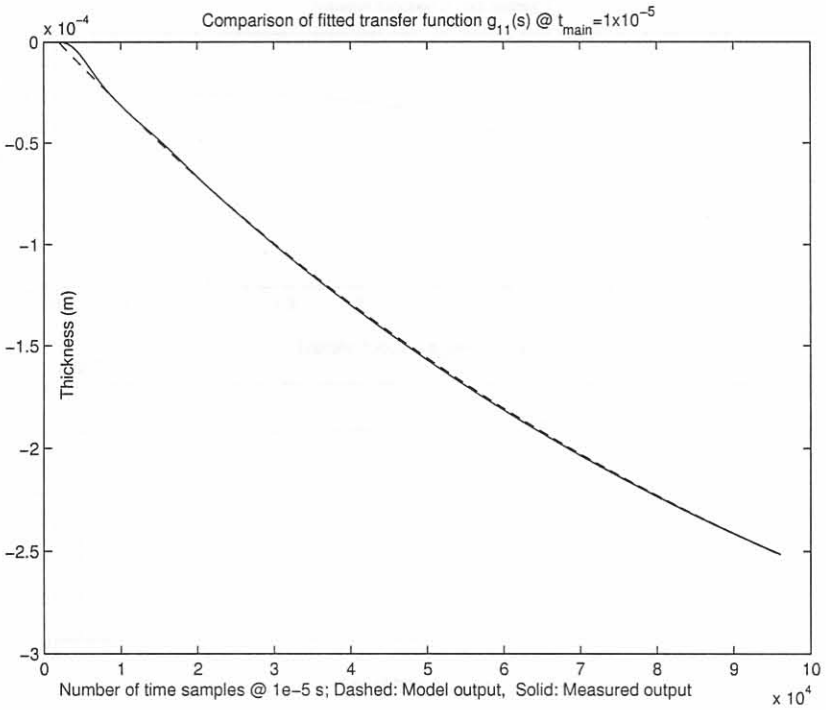

Figure 5.21: A time plot of the fitted model $g_{11}(s)$ compared to the simulation data obtained from the nonlinear plant simulator. (The x axis denotes the number of samples with the sampling interval given as $t_{main} = 5 \times 10^{-5}$)

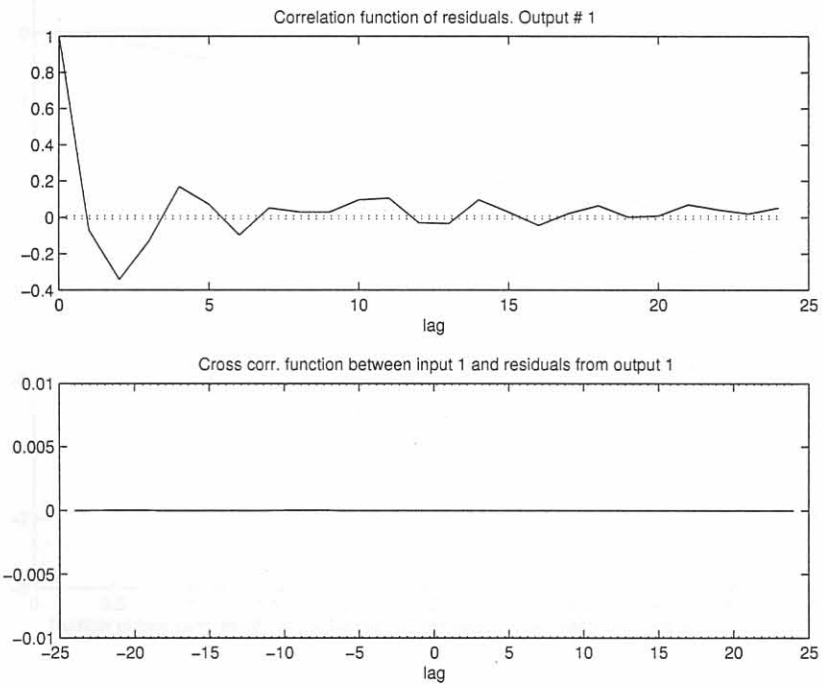

Figure 5.22: Correlation and cross correlation plots of the fitted model for $g_{11}(s)$. The dotted lines indicate the 99% confidence level.

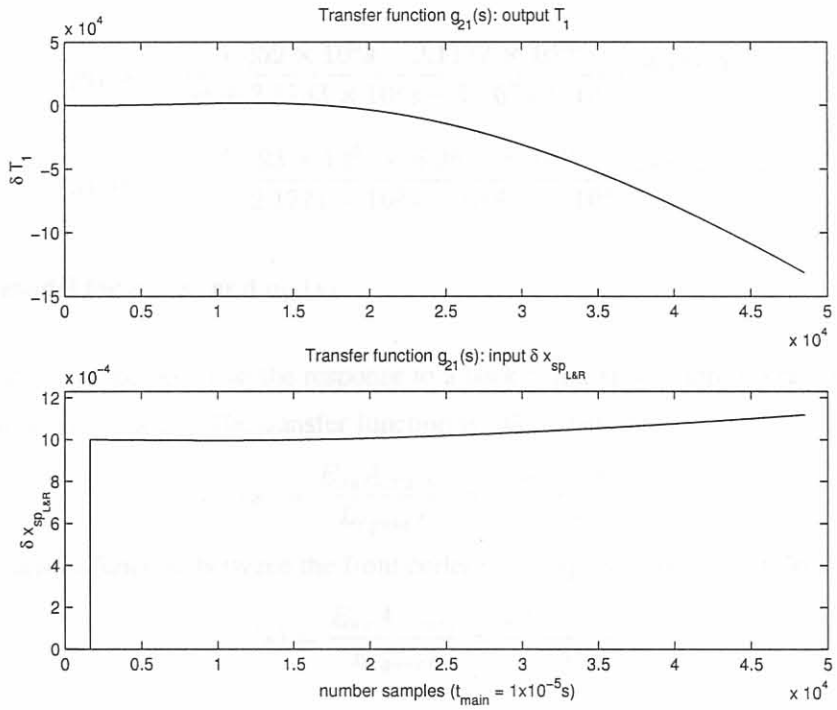

Figure 5.23: I/O data used in the identification of $g_{21}(s)$[10]. (The x axis denotes the number of samples with the sampling interval given as $t_{main} = 5 \times 10^{-5}$)

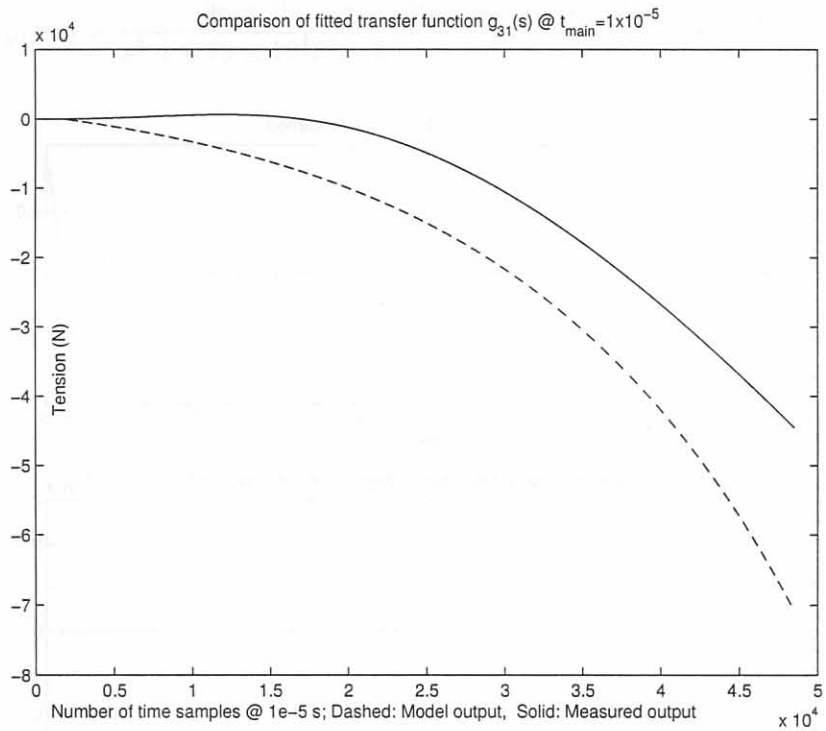

Figure 5.24: A time plot of the fitted model $g_{31}(s)$ compared to the simulation data obtained from the nonlinear plant simulator. (The x axis denotes the number of samples with the sampling interval given as $t_{main} = 5 \times 10^{-5}$)

given as,

$$g_{21}(s) = \frac{1.059 \times 10^5 s - 2.1177 \times 10^{10}}{s^2 + 2.1183 \times 10^2 s - 1.1674 \times 10^3} e^{-0.15 \times 10^{-3} s}. \tag{5.6}$$

$$g_{31}(s) = \frac{3.493 \times 10^5 s - 6.9612 \times 10^{10}}{s^2 + 2.1771 \times 10^3 s - 1.1989 \times 10^4} e^{-0.33 \times 10^{-3} s}. \tag{5.7}$$

5.4.2.3 The model for $g_{22}(s)$ and $g_{33}(s)$

From figure 5.26 it can be seen that the response to a back coiler speed step is a ramp in the tension, signalling a capacitive process. The transfer function is calculated as,

$$g_{22}(s) = \frac{E_{ss} A_{cross_1}}{L_{rg \leftrightarrow cf}} = -\frac{308 \times 10^6}{s}. \tag{5.8}$$

Similarly the transfer function between the front coiler motor speed and the strip front tension is,

$$g_{33}(s) = \frac{E_{ss} A_{cross_2}}{L_{rg \leftrightarrow cf}} = \frac{225 \times 10^6}{s}. \tag{5.9}$$

5.4.2.4 The model for $g_{12}(s)$

The transfer function was calculated as,

$$g_{12}(s) = \frac{7.96 \times 10^{-5} s^2 + 2.017 s - 5.94 \times 10^4}{s^3 + 6.93 \times 10^4 s^2 + 8.54 \times 10^8 s - 3.82 \times 10^{10}} e^{-5 \times 10^{-3} s}. \tag{5.10}$$

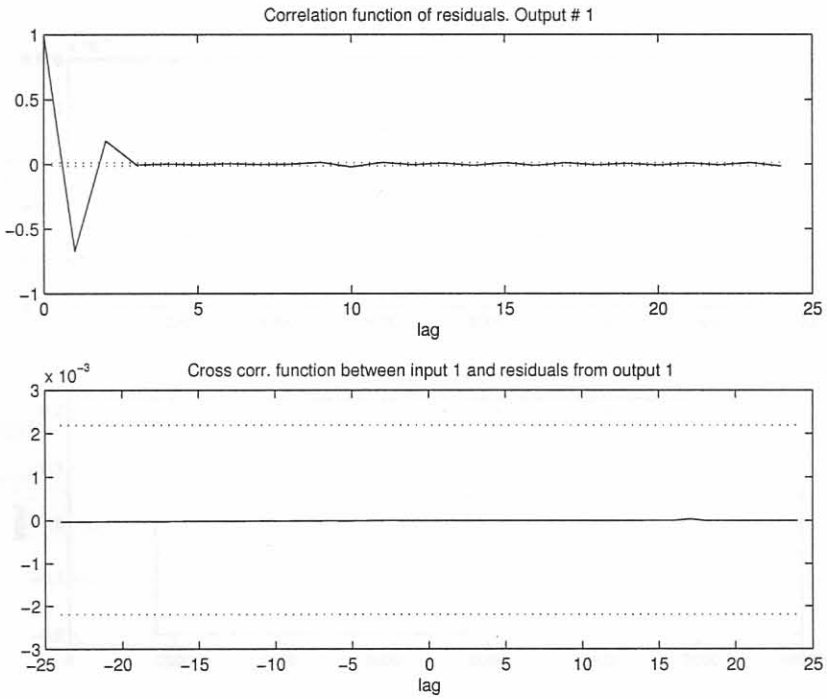

Figure 5.25: Correlation and cross correlation plots of the fitted model for $g_{21}(s)$. The dotted lines indicate the 99% confidence level.

From the time signals (figures 5.27) it can be seen that the speed inputs does influence the thickness output, but not by much. The speed inputs only start to play a role as soon as the tension start to increase above a threshold value when the tension nears the yield stress of the material. In figure 5.31 it can be seen how the application of a step on the back tension influence the centerline thickness.

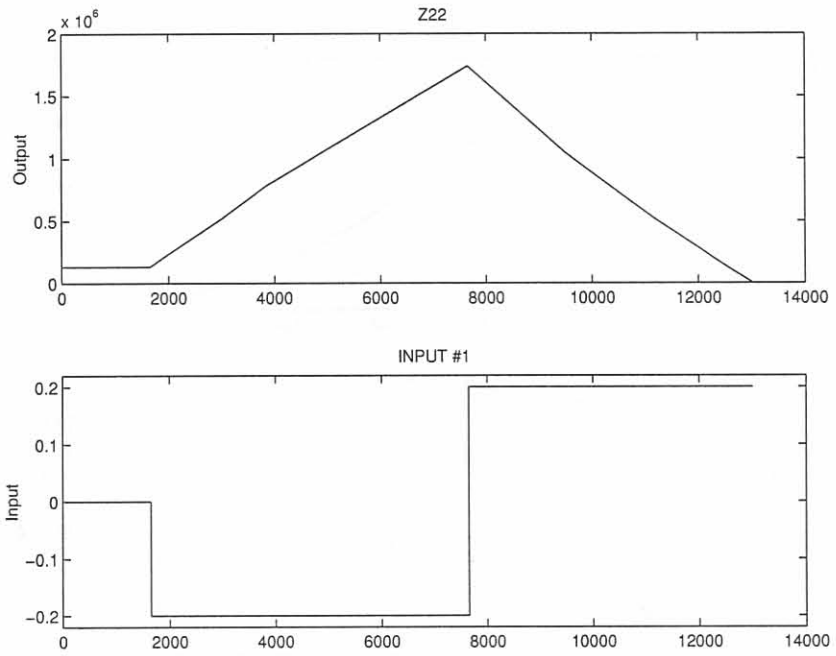

Figure 5.26: The input/output relationship for the derivation of $g_{22}(s)$. (The x axis denotes the number of samples)

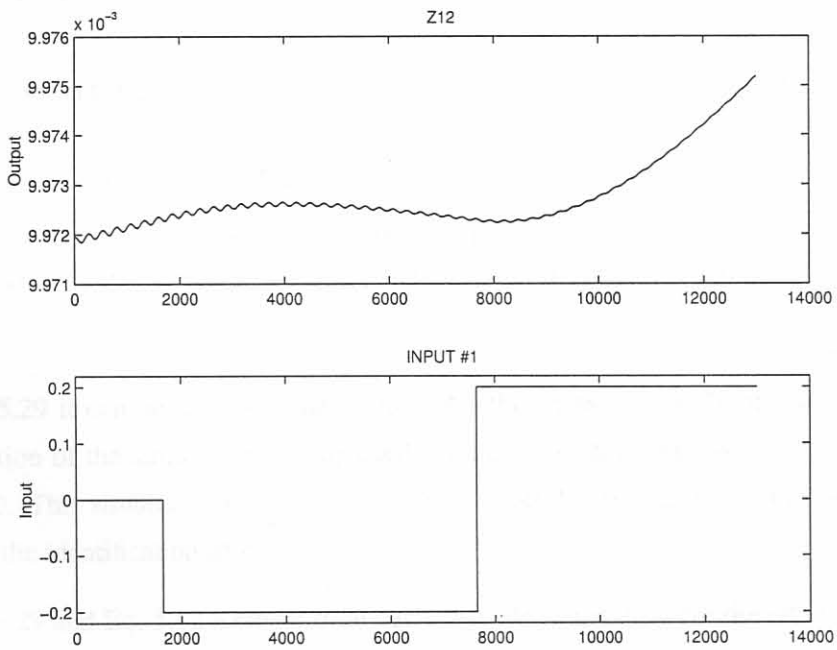

Figure 5.27: The input/output relationship for the derivation of $g_{12}(s)$. (The x axis denotes the number of samples)

5.4.2.5 The model for $g_{32}(s)$

The transfer function was calculated as,

$$g_{32}(s) = \frac{4.294 \times 10^5 s^2 - 6.82 \times 10^{10} s - 1.18 \times 10^{14}}{s^3 + 1.57 \times 10^5 s^2 - 3.19 \times 10^6 s + 2.06 \times 10^8} e^{-3.21 \times 10^{-3} s} \tag{5.11}$$

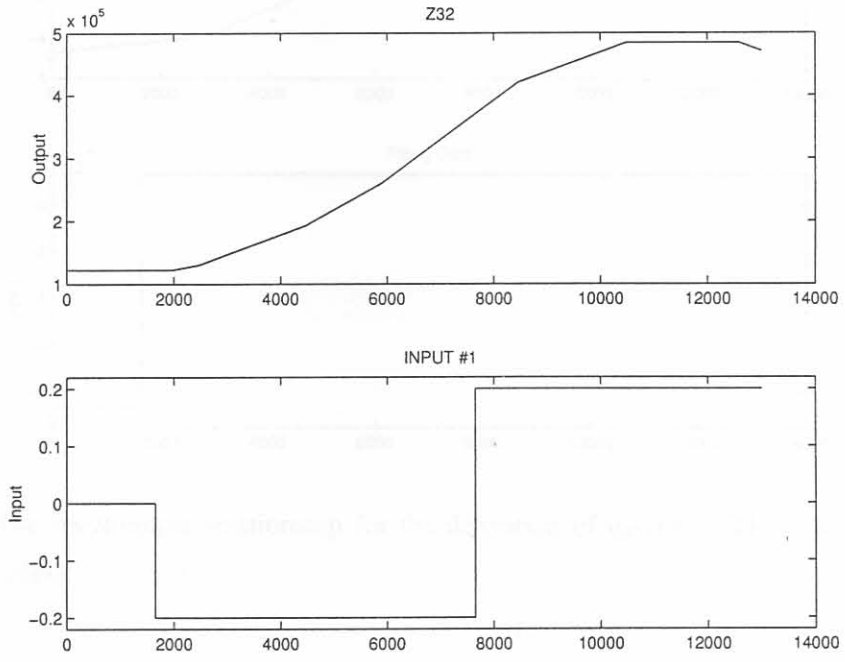

Figure 5.28: The input/output relationship for the derivation of $g_{32}(s)$. (The x axis denotes the number of samples)

5.4.2.6 The model for $g_{d11}(s)$

The transfer function was calculated as,

$$g_{d11}(s) = \frac{-1.06 \times 10^{-3} s^3 - 3.95 \times 10^2 s^2 - 4.18 \times 10^7 s - 3.74 \times 10^{13}}{s^4 + 1.0353 \times 10^5 s^3 + 1.017 \times 10^{11} s^2 + 6.24 \times 10^{14} s - 3.9 \times 10^{14}} . e^{-8.49 \times 10^{-3} s}. \tag{5.12}$$

From figure 5.29 it can be seen that the initial input thickness step of 1mm was too large for the allowed duration of the simulation. An updated simulation with an input step of $|200\mu m|$ is shown in figure 5.30. This simulation run, was however of small duration and the obtained results do not contribute to the identification of $g_{d11}(s)$.

From figure 5.29 and Eq. 5.12 a longer time delay was identified, than for the other transfer function models. This large time delay is associated with the time necessary for the strip to travel through the roll gap (transport time). This time delay is only a fraction of the transport time, and only models the first time instance when the effect of an increased draft is detected. This associated transport time is

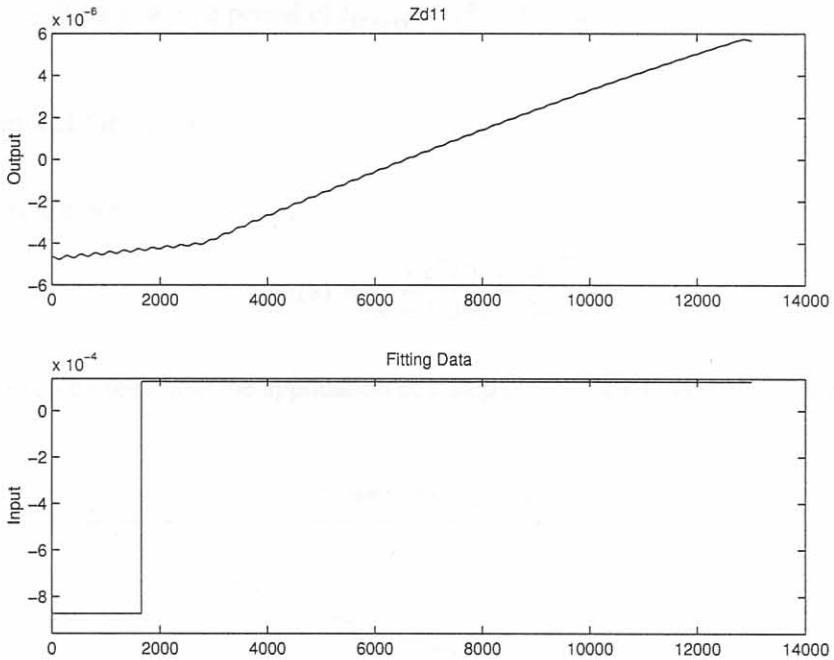

Figure 5.29: The input/output relationship for the derivation of $g_{d11}(s)$. (The x axis denotes the number of samples)

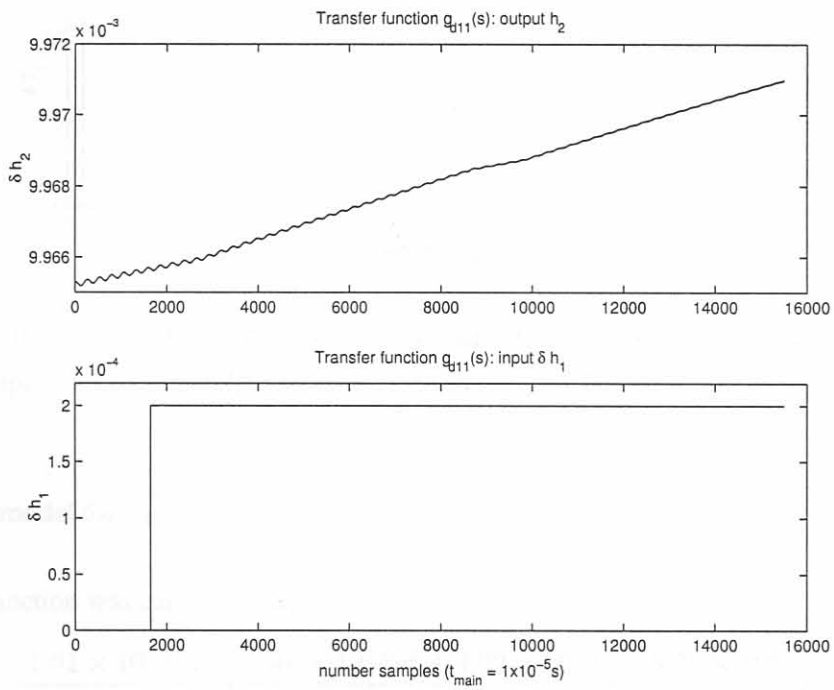

Figure 5.30: The input/output relationship for the derivation of $g_{d11}(s)$. (The x axis denotes the number of samples with the sampling interval given as $t_{main} = 5 \times 10^{-5}$)

calculated by taking the length of the arc of contact, $L_p = 0.05m$, and the operating velocity of the mill is 3.5m/s, resulting in a time period of $t_{travel} = 15 \times 10^{-3}s$.

5.4.2.7 The model for $g_{d12}(s)$

The transfer function was calculated as,

$$g_{d12}(s) = \frac{-5.2779 \times 10^{-11}}{s + 1.964 \times 10^{-1}}. \tag{5.13}$$

In figure 5.31 it can be seen how the application of a step on the back tension influence the centerline thickness.

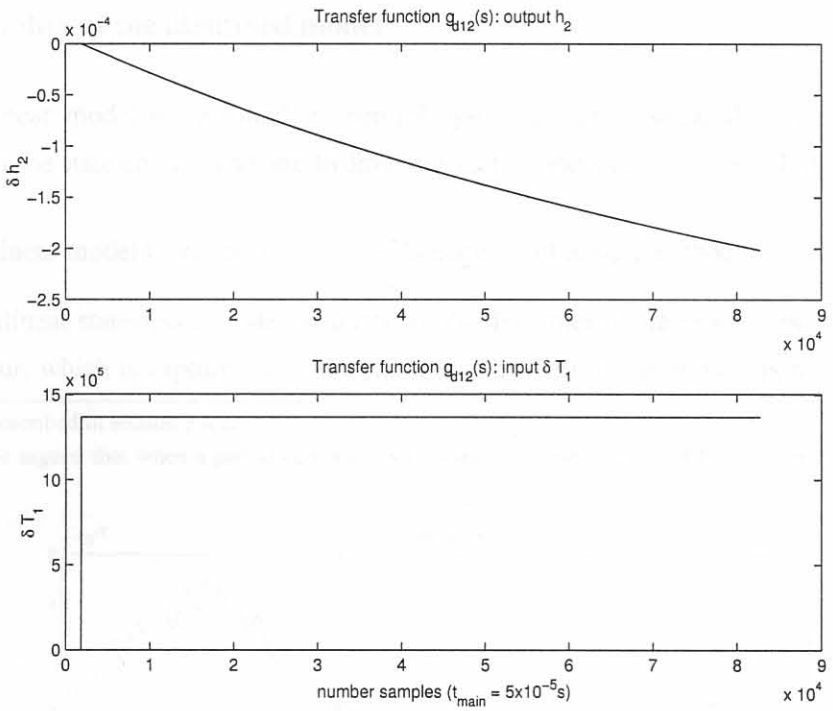

Figure 5.31: The input/output relationship for the derivation of $g_{d12}(s)$. (The x axis denotes the number of samples with the sampling interval given as $t_{main} = 5 \times 10^{-5}$))

5.4.2.8 The model for $g_{d13}(s)$

The transfer function was calculated as,

$$g_{d13}(s) = \frac{1.01 \times 10^{-11}s^3 - 2.46 \times 10^{-6}s^2 + 4.02 \times 10^{-1}s - 9.23 \times 10^3}{s^4 + 8.74 \times 10^4 s^3 + 5.61 \times 10^{10}s^2 + 1.99 \times 10^{14}s + 1.72 \times 10^{16}} e^{-1.28 \times 10^{-3}s}. \tag{5.14}$$

In figure 5.26 it can be seen how the application of a step on the back tension influence the centerline thickness.

From figures 5.31 and 5.32 which were obtained from two different types of simulations, it is evident that if the tension step is small and not of a long duration the influence on the exit gauge is small. On the other hand if a large tension step is applied and held at that value, it can be seen that the influence on the exit gauge can become more of a cumbersome factor. The results obtained from the simulation for the identification of $g_{d12}(s)$ gives justification for investigating the tension and thickness interactions. The simulation results from the identification of $g_{d13}(s)$ was applied for too short time duration and it might be necessary to repeat this experiment to obtain a better result. It also needs to be stressed that the tensions were limited, in order to prevent necking from occuring[11], when necking are modelled and allowed the attainable tension to gauge impact can be larger making tension control a necessity.

5.4.3 Suitability of the identified model

Why is this linear model more suited for control system design, compared to the nonlinear or a linearization of the state-space stand and hydraulic actuator model (e.g. not the whole simulator)?

- With a linear model there are a number of linear control design methods that can be used.
- The nonlinear state-space model accounts for the dynamics of the process, but the the material behaviour, which is captured with the simulation of the roll gap model, is not incorporated[12]

[11] Necking is described in section 3.4.2.

[12] It can also be argued that when a partial derivative with respect to time is taken of Eq. 3.15 a dynamic model can

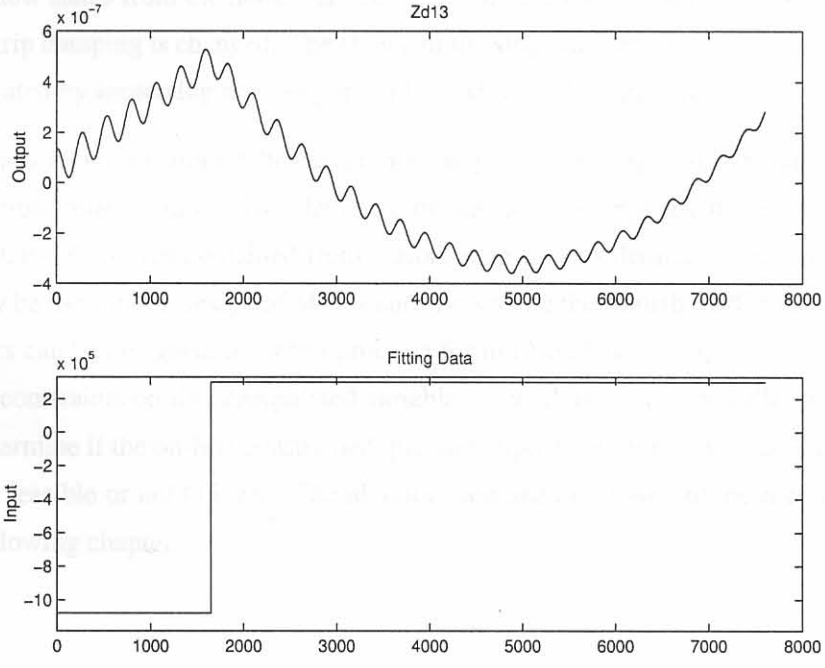

Figure 5.32: The input/output relationship for the derivation of $g_{d13}(s)$. (The x axis denotes the number of samples)

into the non-linear or a linearized version of the state-space model of the stand and the hydraulic actuators.

- The identified MIMO I/O representation does identify the dynamic behaviour of the total simulator, e.g. the dynamic behaviour of the stand and hydraulic actuators and the static interaction of the material with the rollers. This transfer function model can also easily be used with the Matlab MPC toolbox.

- The dimension of the state-space model is large (i.e. 18 states), and when the 4 roller case is of interest or when the higher frequency vibration modes also need to be modelled, the number of states of the simulator increases. This increase can possibly increase the difficulty of designing a state feedback controller in the state space domain.

5.5 Conclusion

In this chapter some simulation results were shown and the system identification process was done in order to yield a linear MIMO plant model that can be used for controller design.

As part of the simulation results, it was shown how the roll gap model unit reacts, in terms of the neutral point movement, when applied tensions to the strip are modelled. Results showed how the specific rolling force change when the draft input and applied tensions were varied. These relationships were compared to the physical limits of the mill.

It was shown how states from the nonlinear state-space model vary at supposedly steady state, when values of the strip damping is changed. The choice of the strip damping that was used in the simulator was also motivated by inspecting the damping ratios and natural frequencies of the stand model.

A linear plant was identified around the chosen operating point and expressed in transfer function notation (input/output relationships). The identification was done by applying the System Identification toolbox of Matlab [83] to data obtained from various step tests as defined in this chapter. The total model can now be used in the design of MPC controllers using the Matlab MPC toolbox [85]. Before such controllers can be designed, a control problem formulation has to be given. An industrial MPC controller has constraints on the manipulated variables as well as on the controlled variables. These constraints determine if the on-line constrained quadratic optimization problem associated with MPC controllers are feasible or not [15, 86]. The identification and discussion of these constraints will be done in the following chapter.

be constructed for the material behaviour. This dynamic model can be incorporated into the nonlinear state-space model, making it more suitable for state-space controller design.

Chapter 6

Control Problem Formulation

6.1 Introduction

In this section an initial control problem is formulated for the Steckel hot rolling mill. The suggested control scheme for the ongoing study is concisely discussed. Limitations on the control inputs are identified taking into account that the proposed control scheme is a supervisory MPC[1] controller. Predictive control methods [86] were investigated and the interested reader is referred to authoritative literature [15, 20, 85, 22, 87, 18, 80, 1] dealing with the theory and application of predictive controllers to industrial processes. In [18] the application of a supervisory GPC[2] controller to a hot rolling mill process is shown, justifying the choice of MPC in this study.

6.2 The Control Problem

6.2.1 Background

It was stated in section 1.1 that current automation projects focuses on the Automatic Gauge Control (AGC) systems, profile and shape control systems, and the control of temperature and the mechanical properties of the strip. Other control systems that are investigated concentrate on the minimizing of head- and tail end strip losses [19].

The profitability of a rolling mill is a function of the mill throughput and the quality of the strip produced [3]. This statement is motivated by the following:

- Throughput improvements: The conventional hot rolling operation has developed significantly during the last thirty years. The main driving force behind this development was to increase the

[1]Model Predictive Control.

[2]Generalized Predictive Control.

output [3]. As an example typical mill output has increased from 2MT per year (before 1960) to 6MT per year (1970-1980) [3].

- Quality improvements: Since 1980 extra emphasis for rolling mill operation has been added. Over capacity of steel production has introduced much more competition and the quality of the produced strip, i.e. dimensional accuracy, surface finish, flatness, and physical properties [4, 5, 3], is used to distinguish strip manufacturers from each other. In more recent years only a few new hot mills have been built, with the emphasis being on revamping existing mills. Current designs therefore concentrate on improving quality and reducing the operation costs.

In order to improve the product quality and the throughput the control engineer has about four dynamic manipulated variables to control: the exit thickness; the tension in the strip whilst rolling; the mechanical properties of the strip; and the shape and profile of the strip.

The mechanical properties of the strip are controlled indirectly by controlling the temperature of the strip to follow a specified temperature versus time profile derived from considering the metallurgy of the strip [5]. The temperature of the strip in the finishing mill is controlled by controlling the rolling speed of the mill and the descaling sprays on either side outside the roll gap. In order to control the final coiling temperature of the strip, the temperature of the strip is controlled to follow a cool down temperature profile. The strip's final pass exit speed from the roll gap and the speed of the strip on the run out table as well as top and bottom water curtain sprays are used as actuators to control the final coiling temperature and the mechanical properties of the strip [25].

The aim of thickness control is to regulate the exit thickness from the roll gap to within the customer specified quality tolerances e.g. strip thickness mean and thickness standard deviation. Modern and advanced control methods can be employed to decrease the thickness standard deviation and decrease the thickness mean closer to the customer's lower thickness bound, resulting in material savings [19]. The thickness controller must be able to reject disturbances such as non-uniform input thickness, hardness variations, input tension variations, output tension variations and friction variations [3] whilst maintaining an uniform output gauge. Normal AGC (Automatic Gauge Controller) systems consist of a BISRA-Davy gaugemeter compensator [27, 1, 21] and a closed loop thickness controller using a delayed[3] X-ray measurement of the output gauge. The measurement transport delay in the feedback loop can make the feedback control system unstable. A Smith Predictor is normally used to compensate for this transport delay.

Potential benefits from the fast actuators on new upgraded mills can be limited if good tension control is not performed. Fast roll gap movements introduced to correct thickness disturbances generate transient tension changes. This results in uncontrolled thickness variations after the roll gap if no tension control is done [3]. Thickness variations not only have an adverse effect on quality and profit

[3]This delay is attributed to the distance that the strip has to travel from the exit of the roll gap to the X-ray device position

but may also lead to mill instability during the rolling of later passes and subsequent cold rolling.

The control of the tensions in the strip whilst rolling are regulator problems [55]. Both tensions are controlled around their associated steady state values that is applied to the strip in order to decrease the rolling load, and effectively increasing the mill's capability to make larger thickness reductions. This increase in reduction capability can ultimately lead to an increase of the throughput of the mill by reducing the number of passes necessary to reach the required exit thickness.

As stated earlier, tension deviations are disturbances for the thickness control loop and therefore these deviations has to be minimized. If these deviations go uncontrolled and the tension in the strip is higher than the yield stress of the material, the strip can deform plastically outside the roll gap and can ultimately tear. The tension deviations can be controlled by controlling the speed of the coiler motors and the rolling mill speed. The large inertias of the motors and their mechanical loads (coiler drums with or without strip wound on it) in conjunction with the limited electric torque of the motors bound the angular acceleration or deceleration of the motors.

It is further assumed that tension is established in the mill before the mill drive is accelerated towards the mill threading speed. Camisani-Calzolari et al. [19] identified a potential economic benefit from speeding up and decelerating the mill optimally. In this investigation the linearized plant was identified on the acceleration ramp of the main mill motor. This is to asses if a modern control method such as MPC can be utilized to decrease losses associated with off-specification head ends. Following the same reasoning, a similar investigation can be conducted on the deceleration ramp of the main mill motor.

The control of shape/flatness and crown/profile fall outside the scope of this dissertation, but the capability exists in the mill simulator to investigate the crown/profile behaviour of the rolling process.

6.2.2 Initial control problem formulation

The simulator was developed in order to reflect the thickness crown evolution of the strip (this includes the centerline gauge) and the tension in the strip whilst rolling. Thus the initial control problem focuses on the control of the centerline exit thickness and tension regulation.

The initial control problem can be stated as follows:

- Thickness control: The exit thickness of the strip has to be regulated within a certain specified thickness range, in the presence of disturbances as was described in section 6.2.1.
- Tension control: The tensions in the strip have to be regulated around their steady state values. The tension deviations have to be negated to limit their influence on the exit thickness.

In section 6.4 specifications for the manipulated variables and the output variables are discussed. In the following section the proposed control method is concisely discussed.

6.3 Model predictive control (MPC)

6.3.1 Background

The most common Model Based Predictive Control (MBPC) methods are MPC (model predictive control) and GPC (generalized predictive control) and some of the lesser known methods are UPC (unified predictive control) [20]. These methods are all related and in this section the background on the development of MPC and GPC are given. The similarities for these two methods are also highlighted.

MPC as it is known today were rediscovered in the late 1970's when the two most influential papers on MBPC, namely "Model Predictive Heuristical Control" (IDCOM - IDentification/COMmand) by Richalet et al. (1978, France) and Dynamic Matrix Control (DMC) by Cutler and Ramarker (1979, USA), were published [15, 87]. The publication of these two papers generated a lot of interest in the field of predictive control at the start of the 1980's [15].

Clarke et al. (1987) published the first comprehensive exposition of Generalized Predictive Control (GPC) [87, 88, 89]. Morari [15] states that although the ideas underlying DMC and GPC are similar the two methods were developed with different objectives in mind. Clarke states in [88] that GPC is an adaptive method that borrows an idea from the Dynamic Matrix Control method of Cutler and Ramarker. Fischer [90] gives a good personal perspective and summary of the different process control methods documented in the literature. He distinguishes between the two methods and their different objectives as is reported in [86]. Although there is not clarity on the definition the similarities are compelling.

Predictive control methods uses an internal model of the process to predict how the plant will react to a certain input vector sequence. The optimization of the control input vector sequence is done in a receding horizon time principle. The internal model and the receding horizon principle will briefly be discussed.

Internal model

The IMC (Internal Model Control) structure was first defined by Garcia and Morari (1982) and referenced in [87]. In figure 6.1 the IMC structure is showed. In this figure HG is the pant, $H\widetilde{G}$ is the internal process model, A^* is the disturbance predictor/filter and G_c^* is the controller. The measured output is given as c and the reference signal is given as R. For a comprehensive exposition of IMC the interested reader is referred to Morari's Robust Process Control book [91].

Receding horizon control

Predictive controllers use a receding horizon principle. At each time step the optimal (or sub-optimal) control sequence is computed in order to minimize a certain performance index subject to constraints on the manipulated and controlled variables. The optimized control law is obtained by procedures

followed in the solving of classical optimal control problems [93] and feasible control problems [94]. What sets the receding horizon approach apart from optimal control is that after the computation of the optimal control sequence only the first control sample of the control law sequence is applied to the plant. The horizon is then shifted onwards with one time sample and the whole optimization is repeated incorporating the new information of plant measurements.

An open-loop optimal strategy [93] would simply assert the optimal set of future controls $\{u\{k+j), j = 0...\}$ while the receding horizon approach makes the MBPC method into a closed-loop feedback control law. Feedback of the current plant output measurement $y(k)$ is via the prediction equations. This feedback is often referred to as the realignment of the process [95].

In figure 6.2 the idea of the receding horizon is displayed graphically. At time k the future control sequence $\{u(k), ..., u(k+N-1)\}$ is optimized in order to minimize a performance index, $J(u,k)$, subjected to input and output constraints. The result of this optimization may differ depending on the structure of the performance index [20]. The different predictive controllers are unified in the aim to compute the optimal control sequence that will force the future control output signal $y(k+j)$ as close to the reference signal $r(k+j)$ [4] without violating any input/output constraints. At time k the first element of the optimized control sequence are applied to the plant and the optimization is restarted with the shifted horizon at time $k+1$ [98].

[4]The reference trajectory is denoted by $w(t)$ in numerous GPC articles [96, 88, 89, 97] and in Soeterboek's book [20]. It was decided to denote the reference trajectory as $r(t)$, which corresponds with classical control notation.

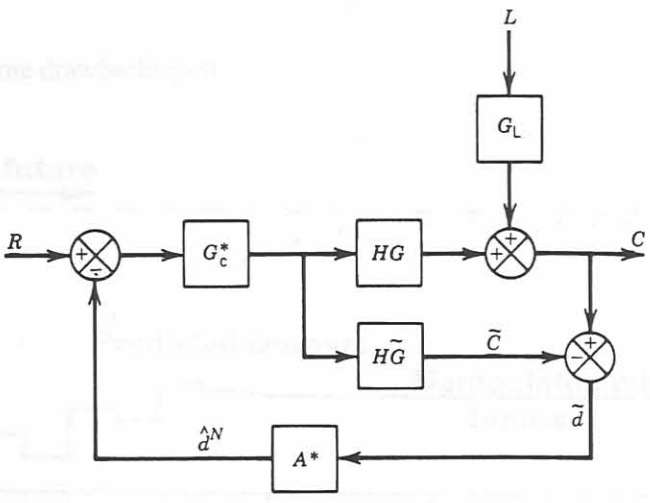

Figure 6.1: IMC Structure (This figure was adopted from [92])

6.3.2 Why MBPC?

MBPC is widely accepted in the process industry and posses many attributes which make MBPC a successful approach to industrial controller design [98, 95]:

- Simplicity: The basic ideas of MBPC do not require complex mathematics and are intuitive.
- Richness: The basic MBPC components e.g. the internal model, the horizons, the objective function etc. can be tailored to the details of the investigated problem.
- Practicality: The practical way in which input and output constraints can be handled in a natural way distinguishes MBPC from other control algorithms. Industrial processes have their limitations in rated capacities, technological requirements and are supposed to deliver outputs within the quality specifications bounds. MBPC can handle these limitations in a systematic way.
- Demonstrabilty: The MPC control concept has worked profitably in many industrial applications even before the theory for MBPC matured to its current state.
- Adaptability: Although not all of the MBPC methods have the ability to adapt the plant model the extension to an adaptive scheme does not seem that difficult. The adaptation of the plant model is a self tuning feature of some MBPC in order to handle structural changes such as actuator failures, changes in system parameters and system structure of the plant.

MBPC does have some drawbacks [98]:

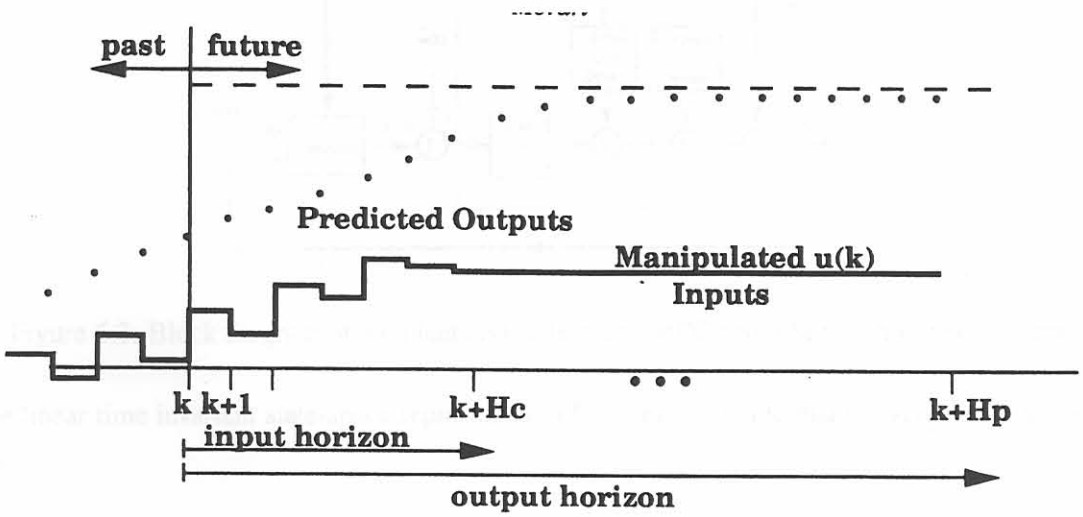

Figure 6.2: The Moving Horizon Approach (This figure is taken from an article by M. Morari in[95] page 24).

- A detailed process model has to be available. Sometimes this model derivation can take up to 80% of the project time[5] .
- The methodology is open and many variations have led to a large number of MBPC methods as will be shown later.
- Theoretical proof of the closed loop plant's stability and robustness are difficult to derive although in practice stability and robustness are easy to obtain.

6.3.3 MPC theory

In this section MPC will be described using the linear time invariant state-space representation of the plant. The equations will be concisely listed according to the notation used in the Matlab MPC toolbox [85]. The interested reader can find the derivations of DMC and MPC in [87, 85, 95].

Although the GPC method is also mentioned the emphasis for this dissertation is on MPC. This is attributed to the following:

- The availability of the Matlab MPC toolbox [85] as a design tool.
- Previous research work conducted by J.G. Bekker[6] [22] on the application of MPC to control the off-gas process of an Electric Arc Furnace.

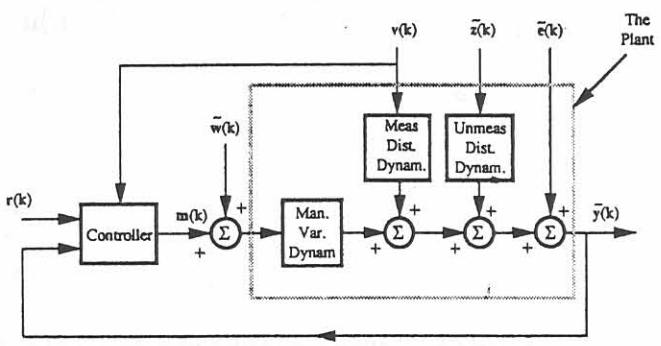

Figure 6.3: Block diagram of the plant and state-space MPC controller with state estimation.

The linear time invariant state-space representation for a multivariable plant is given as (also see fig. 6.3):

$$\mathbf{x}(k+1) = \Phi\mathbf{x}(k) + \Gamma\mathbf{u}(k) + \Gamma_d\mathbf{d}(k) + \Gamma_w\mathbf{w}(k) \tag{6.1}$$

[5]This statement give justification for the development of a nonlinear plant model in this dissertation, and using it to identify a detailed process model.

[6]Previously at the Measurement and Control Group at the University of Pretoria.

$$\begin{aligned}\mathbf{y}(k) &= \overline{\mathbf{y}}(k) + \mathbf{z}(k) \\ &= \mathbf{C}\mathbf{x}(k) + \mathbf{D}_u\mathbf{u}(k) + \mathbf{D}_w\mathbf{w}(k) + \mathbf{z}(k) \end{aligned} \tag{6.2}$$

with,

$\Phi, \Gamma, \Gamma_d, \Gamma_w, \mathbf{C}, \mathbf{D}_u, \mathbf{D}_w$: Discrete state-space coefficient matrices

$\mathbf{x}(k)$: State vector

$\mathbf{u}(k)$: Input vector

$\mathbf{d}(k)$: Measured disturbance vector

$\mathbf{w}(k)$: Unmeasured disturbance vector

$\mathbf{z}(k)$: Measurement noise vector

The unmeasured disturbance and the noise can be deterministic or stochastic of nature. The state estimation for the state can be derived in an analogous way to the LQG procedure [85]. It is assumed that the future disturbances will be zero and the internal model is to estimate the future state of the plant[7]:

$$\mathbf{x}(k+1|k) = \Phi\mathbf{x}(k|k-1) + \Gamma\mathbf{u}(k) + \Gamma_d\widehat{\mathbf{d}}(k) + \Gamma_w\mathbf{w}(k) \tag{6.3}$$

The cost function that needs to be minimized is,

$$J(m,p,\mathbf{Q},\mathbf{R}) = \underset{u(.)}{min}\left[\sum_{i=1}^{p}\mathbf{x}^T(k+i|k)\mathbf{Q}\mathbf{x}(k+i|k) + \sum_{i=1}^{p}\mathbf{u}^T(k+i-1)\mathbf{R}\mathbf{u}(k+i-1)\right] \tag{6.4}$$

with,

m: the control horizon

p: the prediction horizon

$\mathbf{Q}, \mathbf{R}$: Weighting matrices on the states and the inputs respectively.

From Eq. 6.4 it is seen that the states are weighted with a variable gain matrix as opposed to DMC where the tracking error is weighted [87].

6.3.4 Control law computation: On-line optimization

The MPC control method constitute a quadratic optimization problem. A fast convergent optimization algorithm is needed to solve the optimization problem on line. Many of optimization routines can be found in the literature. The routines can be divided into a search based or gradient based method.

[7]Corrections based on measurements are $\mathbf{x}(k|k) = \mathbf{x}(k|k-1) + \mathbf{K}(\mathbf{y}_m(k) - \mathbf{y}(k|k-1))$ [95].

The optimization routine used for the on-line solving of the MPC control law depends on the chosen norm used in the objective function [87]. If the objective function was expressed using a linear norm then Linear Programming will suffice.

In most of the cases the objective function uses the quadratic norm to express the performance index, thus quadratic programming is utilised to solve the quadratic problem. Dantzig's algorithm discussed in [22, 99] is a popular quadratic algorithm used in the Matlab MPC toolbox [85] to simulate the constrained close loop MPC controlled plant. This algorithm was also used by J.G. Bekker [22] in his investigation into the control of the off gas process of an Electric Arc Furnace.

6.3.5 Stability and constraint handling

After the last decade a lot has been done to develop the predictive controller theory [15]. Morari gives a good summary of the current state of the research in [15]. Researchers [100, 101, 102, 103, 104, 105] have showed that by choosing the prediction horizon infinite the stability of the constrained predictive control method can be proven. Other researchers did not make this infinite horizon assumption as documented in [106, 107]. In [86] these key issues are discussed in more detail.

6.3.6 Tuning of Predictive Control algorithms

One of the features that make MBPC methods so attractive is the ease of tuning. Important performance criteria that need to be satisfied with the chosen tuning parameters are good setpoint tracking, sufficient disturbance rejection (regulation behaviour) and robustness against model mismatch. The tuning parameters that can be used to tune a MBPC controller depends on what performance index was implemented [20, 98]. For MPC the following parameters are used to tune the controller:

- m: The control horizon;
- p: The prediction horizon;
- $\mathbf{Q}$: Positive semidefinite output weighting matrix;
- $\mathbf{R}$: Positive definite input weighting matrix

Tuning rules are discussed in [20, 98] and are not repeated here.

Remarks

When $\mathbf{R}$ is the zero matrix the control input vector is not penalized and the resulting control law might tend to bang bang control (heavy control action). The choice of $\mathbf{R}$ and $\mathbf{Q}$ should be such that the terms in the objective function contribute equally to the value of the performance index.

6.4 Controller specifications

The main control objective is to maintain uniform output gauge with a reduced thickness standard deviation as was discussed in section 6.2. The tension control has to be regulated in order to decrease the adverse effect tension deviations has on the thickness control loop.

From measured plant data of the Steckel Mill under investigation, the AGC system used on this mill is capable of regulating the centerline gauge with a standard deviation of $\sigma_{y_1} = 0.02mm$ ($3\sigma_{y_1} = 60\mu m$)[8] for the chosen operating point . From the logged data nothing can be concluded regarding constraints on the tension outputs of the process. The solution of the constrained optimization of a performance index yields an optimal solution satisfying the constraints [94] on the manipulated and controlled variables. The on-line optimization time is dictated by the speed of the process.

The output constraint imposed on the output gauge is[9],

$$9.7184mm - 60\mu m \leq y_1 \leq 9.7184mm + 60\mu m. \tag{6.5}$$

The output limit on the tensions is specified as,

$$0 \leq y_2 \leq 131kN + 3.5MN < k(\epsilon, \dot{\epsilon}, \theta)A_{cross_1}, \tag{6.6}$$

$$0 \leq y_3 \leq 119kN + 2.4MN < k(\epsilon, \dot{\epsilon}, \theta)A_{cross_2}. \tag{6.7}$$

From the limits imposed on the tension outputs it is evident that the tension setpoints ($T_{1_{sp}} = 131kN$ and $T_{2_{sp}} = 119kN$) can be increased. The following constraints are applicable on the dynamic hydraulic stroke,

$$|u_1| \leq 1mm. \tag{6.8}$$

This limitation is taken as the stroke domain for which the linear model was identified. The choice for the range of linearization is and defined in section 5.4.1.1. In [18] it is suggested that a dynamic hydraulic stroke of 5mm is excessive when a regulatory GPC controller tries to negate the effects of a 1mm hydraulic stroke disturbance.

A rate constraint can be imposed on the hydraulic stroke and it is suggested by T.S. Bilkhu [1] that the rate constraint of a 15Hz hydraulic system is,

$$|\dot{u}_1| \leq 4m.s^{-1}, \tag{6.9}$$

and a maximum acceleration of the hydraulic system is,

$$|\ddot{u}_1| \leq 500m.s^{-2}. \tag{6.10}$$

[8] The controlled variables y_i and the manipulated variables u_i (for $i \in [1, 2, 3]$) are defined in section 5.4.

[9] The average exit gauge value was obtained from the logged data for two similar strips rolled by the Steckel Mill under investigation.

As was reported in section 5.4.1.1 the hydraulic systems modelled on either side of the mill closely resemble a 15Hz hydraulic system and the constraints specified in equations 6.9 and 6.10 can be used.

The limits on the coiler speed inputs are imposed to reflect the valid linear range obtained from the step tests (see section 5.4.1.2) are defined as follows:

$$-0.2m.s^{-1} \leq u_2 \leq +0.2m.s^{-1}, \tag{6.11}$$

$$-0.2m.s^{-1} \leq u_3 \leq +0.2m.s^{-1}. \tag{6.12}$$

These 3 phase cyclodrive synchronous motors, for the Steckel Mill under consideration, are rated at 5MW. The rated torque of each motor is 60 $MN.m^{-1}$, with a startup torque capability of 250% for a maximum of 60 seconds. In [1, 108] similar magnitudes are specified for coiler motors. The speed control of synchronous AC motors is discussed in [109]. In this dissertation the emphasis falls on process modelling and it is thus assumed that cascaded speed controllers are in place.

The most important limit on the speed control inputs are the rates at which the motor speeds should change. Each motor has a limited amount of torque available to accelerate the mechanical load. The load can not be accelerated immediately ($\dot{u}_i(t) \neq \infty, \forall i \in [2,3]$) due to the large inertia associated with the strip on the coiler bobbin, the bobbin itself, and the rotor of the motor [109]. The strip on the bobbin and the coiler drum itself form the load of the motor, and an investigation into the changing inertia of this strip-bobbin combination needs to be done. Values of the dimension and mass of the bobbin ($R_{coil\&drum}$) are unknown and the radius of the strip on the bobbin combination increase according to the relationship $R_{coil\&drum} = \frac{\vartheta_{coiler\ tangential}}{\omega_{coiler\ drive}}$.

In this work it is suggested that the rate constraints on the acceleration of the coiler motors are more important than the actual speed limits of these two control inputs. The equation of dynamic stability for a synchronous machine is calculated [109] by equating the torques of the motor and load system, and is given as,

$$T_{max} sin\delta = K_j\ddot{\delta} + K_d\dot{\delta} + T_L, \tag{6.13}$$

where,

T_{max}: The maximum rated torque of the synchronous motor;

δ : The power angle[10];

$K_j\ddot{\delta}$: The acceleration torque of the motor;

$K_d\dot{\delta}$: The damping torque of the system;

T_L : The load torque.

[10] At steady state the load and motor torques are equal at the power angle.

The load torque incorporates the varying mass and radius of the coiled strip and bobbin combination. The limit on the angular acceleration of the coiler motor can be calculated using Eq. 6.13 and the fact that $\ddot{\delta}$ and the motor angular acceleration ($\ddot{\theta}_m$) are the same.

The tangential acceleration of the strip at the coiler motors, $\dot{u}_1, \forall i \in [2,3]$ are related to the angular acceleration of the coiler motor according to the relationship, $u_i = \ddot{\theta}_{coiler_{front/back}} R_{coil\&drum_{front/back}}, \forall i \in [2,3]$. The unavailability of some of the parameters in Eq. 6.13 make it difficult to fix the rate limits on u_2 and u_3, and it is proposed that this problem should be addressed before a MPC controller is designed for the process.

6.5 Conclusions

In this chapter an introduction of control problems associated with rolling mills is given. An initial control problem is formulated and the proposed control method is discussed. Limitations on the manipulated variables are given, taking into account that the proposed control method is MPC. These limitations are important in determining whether the constrained optimization problem is feasible or not.

Chapter 7

Conclusion and recommendations

7.1 Conclusion

In this dissertation a hot rolling mill process was modelled in order to yield a nonlinear plant simulator that was used in the identification of a linear plant model. The linear plant model can be used for control system design purposes. The hot rolling mill investigated in this dissertation was based on an industrial Steckel Mill. Literature on Steckel Mills are scarce and this work partially fill this void. Possible reasons for this lack of literature are that Steckel Mills are installed mainly in developing countries or where a large product mix are produced. South Africa has at least 3 hot rolling Steckel mills making this work applicable to the South African rolling industry.

Process behaviour was modelled in order to reflect centerline gauge behaviour, thickness crown behaviour and tensions in the strip on either side of the roll gap. The mill simulator was constructed by modelling the 4-high mill stand as an equivalent 2-roll pack rolling mill. This approximation has been made in [59] and is suggested in [40]. The rollers were modelled as continuous masses yielding distributed parameter systems, while the rest of the mill stand elements were lumped together. From this modelling approach a partial differential equation model was derived describing the dynamic behaviour of the mill stand. The spatial and time dependencies found in the PDE model was solved using the Assumed Modes Method, normally used in the analysis of vibration problems [54]. This spatial dynamic model gives the simulator the capability to simulate the bending of the rolls and to account for the crown behaviour of the strip associated with roller bending.

The nonlinear behaviour of the hydraulic actuators was modelled from first principles and this model was combined with the mill stand model, resulting in an 18th order nonlinear state-space model. Eight states of the mill simulator are associated with the rolling mill stand. The other 10 states are attributed to the two similar hydraulic systems.

The material behaviour in the roll gap was accounted for by using Orowan's roll gap model. The

calculation of the specific rolling force that the strip exerts on the working rollers was evaluated along the length of the rollers (perpendicular to the rolling direction), resulting in a distributed load that acts on the two roll packs. This distributed load serves as input to the 18th order state-space model used in the simulator.

The interaction between the roll gap model and the applied tensions to the strip, while rolling, was modelled and investigated. From this work it can be stated that the tension interactions do influence the centerline exit thickness, but the interaction is small, for the chosen operating point. A conjecture (based on the importance of tension control for cold rolling) can be made that the tension interactions will feature more during the later passes in the Steckel rolling mill schedule.

The mill simulator was used to identify a linear time invariant MIMO transfer function model, that can be used for control system design at the operating point at which the plant was linearized.

7.2 Contribution of this work

Current automation projects can be worth millions of dollars and there are many companies around the world that specialize in automation of rolling mill processes, for example Kvaerner, Cegelec, Siemens, Mannesman Demag, Tippins to name a few. These companies rely on the accuracy of their models and a lot of time and resources are invested in the development of proprietary models. With this dissertation a research program was launched that will ultimately help with the industrial research of rolling mills in South Africa.

This work has further contributed to the field of modelling of rolling mills by modelling a Steckel hot rolling mill process. Modelling work on rolling mills are normally documented for multistand hot rolling mills, and literature of investigations into the tension interactions on the thickness behaviour of the strip for a Steckel mill are scarce, if not non-existent.

One of the aims of this dissertation was to develop a nonlinear mill simulator that can be used in a continuing research program that will ultimately investigate the feasibility of applying Model Predictive Control to a Steckel Hot Rolling Mill process.

The main contributions of this work can be summarized as:

- A nonlinear plant simulator was developed, with which an investigation into the nonlinear behaviour and interactions between the;
  - hydraulic actuators,
  - mill dynamics,
  - and the material properties of the strip being rolled was completed successfully.

One of the leading rolling mill researchers, R-M Guo [8], stated that in order to evaluate a comprehensive total gauge control loop it might be necessary to model all of the above components as well as the dynamics of the drives and the motors. In [8] this involved modelling was not done, and only the hydraulic actuators were modelled in detail. The work in this dissertation addresses the modelling and the identification of the interactions between the key components itemized above. This investigation is considered a significant contribution to the field of dynamic hot rolling mill modelling.

- The nonlinear plant simulator uses practical plant data as inputs and is also tuned in order to reflect adequate practical process behaviour;
- The nonlinear simulator is able to simulate the thickness profile (and in particular the centerline exit thickness) and tension behaviour of a hot rolled strip while rolling.
- The modularity of the simulator is such that the simulator can be extended to investigate the shape forming process of the strip and this extension is one of the recommendations for further projects;
- The simulator can be used to derive linear models on any part of the process speed curve, e.g. on the speed up, speed down ramp or at threading speed, by specifying different input files.
- Similarly linear models can be identified for any rolling pass of the rolling schedule, by specifying the appropriate input files.

The creation of a simulator of a Steckel hot rolling mill, modelled according to an existing practical mill that agrees acceptably with the literature and practical data, is seen as a major contribution in the absence of extensive literature on Steckel hot rolling mills.

The work in this dissertation should be seen as the foundation of a new research program aimed at investigating model based control techniques applied to the Steckel hot rolling mill process.

7.3 Recommendations

The recommendations for future research projects are concerned with process modelling and control projects. Both sections of the recommendations are divided into graduate and undergraduate research projects.

7.3.1 Modelling and identification projects

Graduate projects

- The investigation into the mill stand behaviour for the four roller model can be conducted. In the work for this dissertation this model was only partially solved. It should be noted that the time variant and invariant case of the four roller model (discussed in section A.2) increase the complexity of the simulator and the simulation time increases substantially.

- The shape forming of the strip should be incorporated into the current mill simulator. In chapter 3 a possible modelling approach is discussed.

- An investigation and model extension should be conducted to identify the influence that thermal crown build-up on the rollers has on the strip thickness crown.

- The effect of roller wear over time on the strip crown might be an interesting avenue to pursue, but might only be of importance if an adaptive mill simulator needs to be created, due to the slow varying structural changes.

- Torsional vibration modelling of the connecting drive spindles between the mill motor and the work rolls, should be incorporated in the current simulator as is proposed by Dobrucki et al. [40] and investigated in [110]. The modelling of the drive and motor dynamics might form an integral part of this study, just as the dynamics of the hydraulic actuators formed an integral part of the modelling in this dissertation .

Undergraduate projects

- The nonlinear plant simulator can be used to identify different linear plant models at different points of the process speed curve as well as for different passes.

- The current capability of the simulator is not yet fully exploited, and an undergraduate project can focus on the identification of transfer functions between the thickness crown outputs and the hydraulic stroke inputs on either side of the mill centerline. The application of the hydraulic strokes need not be seen as one manipulated variable and transfer functions can also be identified for differential gauge operation.

7.3.2 Control projects

Graduate projects

- The application of MPC on a supervisory level to the Steckel rolling mill process should be conducted according to the initial control problem formulation of chapter 6. The results obtained should be compared to the current control schemes used on the investigated Steckel mill.

- The possible economic benefit of the proposed control method on the speed up ramp of the mill speed needs to finally be assessed, in order to verify intuition.

- An interesting project might be an investigation into the optimal mill setup.

Undergraduate projects

- An study could be conducted in order to identify traditional industrial and advanced (academia orientated) control methods used for Steckel hot rolling mills. Simulations of these methods can proof valuable to the first listed graduate control project.
- And lastly the optimal setup problem might also be addressed by an undergraduate student.

Final Word

The modelling and control of a rolling mill is a challenging but applicable field of research in the context of the large steel and aluminium industries found in South Africa. Competitive rolling mill companies rely on state of the art automation and instrumentation of their plants. This state of the art knowledge is confined to leading European countries, America and Australia. The result being that the South African rolling companies pay top dollar for this knowledge.

The South African rolling mill companies can benefit from local research conducted on modelling and control of rolling mills, generating in-house knowledge obtained from the local research projects. This dissertation lays the ground for a successful continuing research programme on modelling and control of hot rolling mills.

Bibliography

[1] M. J. Grimble, M. R. Katebi, G. Hearns, and M. A. Johnson, "International training course in hot rolling mill control and technology," 14-18 September 1998.

[2] G. E. Dieter, *Mechanical metallurgy*, ch. 7. McGraw-Hill, 1986.

[3] Unknown, "International rolling technology course," tech. rep., Broner and IAS, 1998.

[4] A. Lederer, "State of development of steckel mills," *Metallurgical Plant and Technology International*, vol. 16, no. 3, pp. 56–69, 1993.

[5] J. Andorfer, D. Auzinger, M. Hirsch, G. Hubmer, and R. Pichler, "Controlling the mechanical properties of hot rolled strip," *Metalurgical Plant and Technology*, no. 5, pp. 104–110, 1997.

[6] P. V. Lopresti and T. N. Patton, "An approach to minimum cost steel rolling," *Proceedings of the IEEE*, vol. 58, no. 1, pp. 23–30, 1970.

[7] L. M. Pederson and B. Wittenmark, "Multivriable controller design for a hot rolling mill," *IEEE Transactions on Control System Technology*, vol. 6, no. 2, pp. 304–312, 1998.

[8] R.-M. Guo, "Evaluation of dynamic characteristics of hagc system," *Iron and Steel Engineer*, pp. 52–61, July 1991.

[9] R.-M. Guo, "Optimal profile and shape control of flat sheet metal using multiple control devives," *IEEE Transactions on Industry Applications*, vol. 32, no. 2, pp. 449–457, 1996.

[10] V. Ginzburg, *Profile and flatness of flat rolled products, Part I*, vol. 5 of *Rolling mill technology series*, ch. 1 and 2, pp. 1–31. Pittsburgh, Pensylvania: International rolling mill consultants, United Engineering Inc., 1990.

[11] C. Devadas, I. V. Samarasekera, and E. H. Hawbolt, "The thermal and metallurgical state of steel strip during hot rolling: Part iii. microstructural evolution," *Metallurgical Transactions A-Physical Metallurgy & Materials Science*, vol. 22A, no. 2, pp. 335–349, 1991.

[12] J. V. Roey, H. Vergote, and R. Mielke, "Accurate profile and flatness control on a modernized hot strip mill," *Iron and Steel Engineer*, pp. 29–33, February 1996.

[13] G. Hearns and M. J. Grimble, "Robust hot mill thickness controller," in *Preprints of the Proceedings of the 9th IFAC MMM Conference*, pp. 215–220, 1998.

[14] G. McNielly, G. M. van der Mollen, M. A. Johnson, and T. Lee, "Control of thickness profile whilst maintaining flatness in hot strip tandem rolling," in *13th Triennial World Congress, San Francisco, USA*, pp. 451–456, 1996.

[15] M. Morari and J. H. Lee, "Model predictive control: past present and future," *Computers and Chemical Engineering*, vol. 23, pp. 667–682, 1999.

[16] Y. Anbe, K. Sekiguchi, and H. Imanari, "Tension control of a hot strip mill finisher," in *13th Triennial IFAC World Congress*, pp. 439–444, 1996.

[17] R.-M. Guo, "Development of a mathematical model for strip thickness profile," *Iron and Steel Engineer*, pp. 32–39, September 1990.

[18] M. J. Grimble and M. R. Katebi, "Predictive optimal control of hot strip finishing mills," in *IFAC Automation in the Steel Industry, Kyongju, Korea*, IFAC, Elsevier, 1997.

[19] F. R. Camisani-Calzolari, Z. M. Smit, I. K. Craig, and R. Torr, "Scrap reduction in the rolling of aluminium sheet," in *IEEE International Simposium on Industrial Electronics*, (Pretoria, South Africa), 1998.

[20] R. Soeterboek, *Predictive control, A unified approach.* Prentice Hall International Seiries in Systems and Control Engineering, 1992.

[21] E. Scholtz, M. Lewis, H. Pretorius, and J. Botha, "Control practice on a steckel hot rolling mill process." Subject EBB780 in Department Electrical and Electronic Engineering.

[22] J. G. Bekker, "Modelling and control of an electric arc furnace," Master's thesis, Department of Electrical and Electronic Engineering, University of Pretoria, 1998.

[23] F. R. Camisani-Calzolari, "Modelling and control of the secondary cooling zone in continuous casting," Master's thesis, Department of Electrical and Electronic Engineering, University of Pretoria, 1998.

[24] W. F. Hosford and R. M. Caddell, *Metal forming, Mechanics and metallurgy*, ch. 7. Prentice Hall Inc., 1983.

[25] R.-M. Guo, "Heat transfer of laminar flow cooling during strip acceleration on hot strip mill runout tables," *Iron and Steel Maker*, pp. 49–59, August 1993.

[26] G. F. Bryant, J. M. Halliday, and P. D. Spooner, "Tandem mill scheduling as a two point boundary value problem," *Automatica*, vol. 9, pp. 223–232, 1973.

[27] M. J. Grimble and M. A. Johnson, *Optimal Control and Stochastic Estimation*, vol. 2, ch. 13, pp. 975–997. St Edmundsbury Press Ltd, Bury St. Edmunds, 1988.

[28] E. Orowan, "The calculation of roll pressure in hot and cold flat rolling," *Proceedings of the Institution of Mechanical Engineers*, vol. 150, pp. 140–167, 1943.

[29] T. Sheppard, "Shape in metal strip: 'the state of the art'," in *Shape Control*, pp. 11–18, 1976.

[30] C. Devadas and I. V. Samarasekera, "Heat trasfer during hot rolling of steel strip," *Ironmaking and Steelmaking*, vol. 13, no. 6, pp. 311–321, 1986.

[31] A. F. Macalister, P. J. Reeve, and P. Smith, "Predictive control of temperature and width for hot strip mills," in *Preprints of the Proceedings of the 9th IFAC MMM Conference*, pp. 243–250, 1998.

[32] W. Y. D. Yuen, "On the heat transfer of a moving composite strip compressed by two rotating cylinders," *Transactions of the ASME, Journal of Heat Transfer*, vol. 107, pp. 541–548, 1985.

[33] A. Kumar, I. V. Samarasekera, and E. B. Hawbolt, "Roll-bite deformation during the hot rolling of steel strip," *Journal of Materials Processing Technology*, vol. 30, pp. 91–114, 1992.

[34] S. F. Wong, P. D. Hodgson, C. J. Chong, and P. F. Thomas, "Physical modelling with application to metal working, especially to hot rolling," *Journal of Materials Processing Technology*, 1996.

[35] C. Devadas, I. V. Samarasekera, and E. B. Hawbolt, "The thermal and metallurgical state of steel strip during hot rolling: Part i. characterization of heat transfer," *Metallurgical Transactions A-Physical Metallurgy & Materials Science*, vol. 22A, no. 2, pp. 307–319, 1991.

[36] C. Devadas, I. V. Samarasekera, and E. H. Hawbolt, "The thermal and metallurgical state of steel strip during hot rolling: Part ii. factors influencing rolling loads," *Metallurgical Transactions A-Physical Metallurgy & Materials Science*, vol. 22A, no. 2, pp. 311–321, 1991.

[37] V. Ginzburg, *Profile and flatness of flat rolled products, Part I*, vol. 5 of *Rolling mill technology series*, ch. 2, pp. 35–41. Pittsburgh, Pensylvania: International rolling mill consultants, United Engineering Inc., 1990.

[38] N. Troyani, "Nonlinear geometrically adaptive finite element model of the coilbox," *Numerical Heat Transfer, Part A*, vol. 30, pp. 849–858, 1996.

[39] A. Swiatoniowski, "Interdependence between rolling mill vibrations and the plastic deformation process," *Journal of Materials Processing Technology*, vol. 61, pp. 354–364, 1996.

[40] W. Dobrucki and A. Bar, "Changes in roll-gap shape in the case of vibrations in a four high rolling mill stand," *Journal of Materials Processing Technology*, vol. 61, pp. 328–337, 1996.

[41] U. S. Dixit and P. M. Dixit, "Finite-element analysis of flat rolling with inclusion of anisotropy," *International Journal of Mechanical Sciences*, vol. 39, no. 11, pp. 1237–1255, 1997.

[42] P. Montmitonnet, P. Gratacos, and R. Ducloux, "Application of anisotropic viscoplastic behaviour in 3d finite-element simulations of hot rolling," *Journal of Materials Processing Technology*, vol. 58, pp. 201–211, 1996.

[43] P. Hartley, C. E. N. Sturgess, and G. W. Rowe, "Experimental and theoretical studies of workpiece deformation, stress and strain during flat rolling," *International Materials Review*, vol. 34, no. 1, pp. 19–34, 1989.

[44] R. B. Sims, "The calculation of roll force and torque in hot rolling mills," *Proceedings of the Institution of Mechanical Engineers*, vol. 168, no. 6, pp. 191–200, 1954.

[45] N. A. Fleck and K. L. Johnson, "Towards a new theory of cold rolling thin foil," *International Journal of Mechanical Science*, vol. 29, no. 7, 1987.

[46] H. Ford and J. M. Alexander, "Simplified hot-rolling calculations," *Journal of the Institute of Metals*, vol. 92, pp. 397–404, 1963-64.

[47] R. Hill, *The mathematical theory of plasticity*. Oxford University Press, 1983.

[48] P. P. Benham and R. J. Crawford, *Mechanics of engineering materials*. Longman Scientific and Technical, 1987.

[49] W. Y. D. Yuen, A. Dixon, and D. N. Nguyen, "The modelling of the mechanics of deformation in flat rolling," *Journal of Materials Processing Technology*, vol. 60, pp. 87–94, 1996.

[50] W. L. Roberts, *Hot Rolling of Steel*. Marcell Dekker, 1983.

[51] S. S. Rao, *Mechanical vibrations*. Addison-Wesley Publishing Company, second ed., 1990.

[52] L. Meirovitch, *Elements of vibration analysis*, ch. 7. McGraw Hill, 1986.

[53] L. Meirovitch, *Computational methods in structural dynamics*, ch. 6, 7 and 8. Netherlands: Sijthoff and Noordhoff, 1980.

[54] L. Meirovitch, *Analytical methods in vibrations*, ch. 5 and 6. Macmillan Publishing, 1967.

[55] P. R. Evans, D. E. Hill, and N. D. Vaughan, "Dynamic characteristics of a rolling mill," *Proceedings of the Institution of Mechanical Engineers*, vol. 210, pp. 259–271, 1996.

[56] B. T. Boulter, "The effect of speed-loop bandwidths and line speed on system natural frequencies in multispan strip processing systems," *IEEE Transactions on Industry Applications*, vol. 35, no. 1, pp. 126–134, 1999.

[57] E. C. Larke, *The rolling of strip, sheet and plate*. Chapman and Hall, 1957.

[58] R.-M. Guo, "Prediction of strip profile in rolling process using influence coefficients and boussinesq's equations," *Transactions of the ASME, Journal of Manufacturing Science and Engineering*, vol. 119, pp. 220–226, May 1997.

[59] L. M. Pederson, "Multivariable thickness control of a hot rolling mill," Master's thesis, Department of Automatic Control, Lund Institute of Technology, 1995.

[60] S. Timoshenko, *Vibration problems in engineering*. D. van Nostrand Company, IInc., third ed., 1955.

[61] F. Hollander and A. G. Reinen, "Automatic shape control-hoogovens' 88-in. hot strip mill," *AISE Yealy Proceedings*, 1976.

[62] M. D. Stone and R. Gray, "Theory and practical aspects in crown control," *Iron and Steel Engineer*, pp. 75–87, August 1965.

[63] R.-M. Guo, "Development of an optimal/shape level-2 control model for rolling mills with multiple control devices," *IEEE Transactions on Control System Technology*, vol. 6, no. 2, pp. 172–179, 1998.

[64] P. Bhowal and S. K. Mukherjee, "Modeling and simulation of hydraulic gap control system in a hot strip mill," *ISIJ International*, vol. 36, no. 5, pp. 553–562, 1996.

[65] V. B. Ginzburg, "Dynamic characteristics of automatic gage control system with hydraulic actuators," *AISE Year Book*, pp. 75–83, 1984.

[66] T. J. Viersma, *Analysis, synthesis and design of hydraulic servo systems and pipelines*, ch. 4, pp. 85–89. Elsevier Scientific Publishing Company, 1980.

[67] C. R. Burrows, *Fluid power servomechanics*, ch. 3, pp. 61–71. Van Nostrand Reinhold Company, 1972.

[68] MOOG Controls Limited, *Servovalves with bushing and integrated electronics; D661- G, S and H series; ISO 4401 size 05*.

[69] J. G. Lee and O. H. Kim, "Development of a new hydraulic servo cylinder with mechanical feedback," *Control Engineering Practice*, vol. 7, pp. 327–334, 1999.

[70] W. C. Chen, I. V. Samarasekera, A. Kumar, and E. B. Hawbolt, "Mathematical modelling of heat flow and deformation during rough rolling," *Ironmaking and Steelmaking*, vol. 20, no. 2, pp. 113–126, 1993.

[71] J. H. Matthews, *Numerical methods for mathematics, science and engineering*. Prentice Hall Internatianl Editions, 2 ed., 1992.

[72] G. Stephanopoulos, *Chemical process control: An introduction to the theory and practice.* Prentice Hall International Editions, 1984.

[73] J. R. Davis and D. . Associates, *Stainless steels, ASM speciality handbook.* ASM International, 1996.

[74] W. L. Lyuben, *Process modelling, simulation and control for chemical engineers.* McGraw-Hill International Edintions, 1989.

[75] C. R. Bester, "Oorgangsgedrag van 'n voertuigbladveer," Master's thesis, Department of Mechanical Engineering, University of Pretoria, 1993.

[76] W. T. Thomson, *Theory of vibration with applicastions.* Chapman and Hall, 4 ed., 1993.

[77] ABB, *Stainless load cells for roll force measurement in hot and cold rolling mills; Millmate Roll Force Systemsloadcell*, November 1998.

[78] T. Tamiyam, K. Furui, and H. Iida, "Analysis of chattering phenomenon in cold rolling," in *International Conference on Steel Rolling*, vol. II, pp. 1191–1202, September 1980.

[79] P. Huzyak and T. L. Gerber, "Design and application of hydraulic gap control systems," *AISE Year Book*, pp. 331–338, 1984.

[80] M. Berenguel, M. R. Arahal, and E. F. Camacho, "Modelling the free response of a solar plant for predictive control," *Control Engineering Practice*, vol. 6, pp. 1257–1266, 1998.

[81] E. Scholtz, I. K. Craig, and P. C. Pistorius, "Sheet thickness and tension modelling for a steckel hot rolling mill process." Accepted for IEEE Africon Conference September 1999, Cape Town, South Africa.

[82] S. Haykin, *Communication systems*, ch. 9. John Wiley and Sons, 1994.

[83] L. Ljung, "System identification toolbox. for use with matlab," 1997.

[84] K. J. Astrom and B. Wittenmark, *Computer controlled systems, Theory and design.* Prentice Hall Information and System Sciences Series, 3 ed., 1997.

[85] M. Morari and N. L. Ricker, *Model Predictive Control toolbox, For use with MATLAB.* The Math Works Inc.

[86] E. Scholtz, "Predictive control: an introduction, literature survey and application." Advanced Literature Study, Department of Electical and Electronic Engineering, University of Pretoria, June 1999.

[87] C. E. Garcia, D. M. Prett, and M. Morari, "Model predictive control: Theory and practice-a survey," *Automatica*, vol. 25, no. 3, pp. 335–348, 1989.

[88] D. W. Clarke, C. Mohtadi, and P. S. Tuffs, "Generalized predictive control-part i. the basic algoritghm," *Automatica*, vol. 23, no. 2, pp. 137–148, 1987.

[89] D. W. Clarke, C. Mohtadi, and P. S. Tuffs, "Generalized predictive control-part ii. extensions and interpretations," *Automatica*, vol. 23, no. 2, pp. 149–160, 1987.

[90] D. G. Fisher, "Process control: an overview and personal perspective," *The Canadian Journal of Chemical Engineering*, vol. 69, pp. 5–26, 1991.

[91] M. Morari and E. Zafiriou, *Robust Process Control*. Prentice Hall, 1989.

[92] D. E. Seborg, T. F. Edgar, and D. A. Mellichamp, *Process dynamics and control*, ch. 27. Wiley Series in Chemical Engineering, 1989.

[93] A. E. Bryson and Y.-C. Ho, *Applied optimal control*. Hemisphere Publishing Corparation, 1975.

[94] Y. Yavin and C. Frangos, "Open-loop motion planning strategies for a vehicle towing three trailers," *Mathematical Computation and Modelling*, vol. 20, no. 7, pp. 47–58, 1994.

[95] D. W. Clarke, ed., *Advances in Model-Based Predictive Control*. Oxford Science Publications, 1994.

[96] D. W. Clarke and C. Mohtadi, "Properties of generalized predictive control," *Automatica*, vol. 25, no. 6, pp. 859–875, 1989.

[97] C. Bordons and E. F. Camacho, "A generalized predictive controller for a wide class of industrial processes," *IEEE Transactions on Control System Technology*, vol. 6, no. 3, pp. 372–387, 1998.

[98] T. J. J. van den Boom, "Model based predictive control." LernModul Nr.6, Swiss Society for Automatic Control, January 1997.

[99] J. C. G. Boot, *Quadratic programming*, ch. 9. North Holland Publishing Company, 1964.

[100] J. A. Rossiter, J. R. Gossner, and B. Kouvaritakis, "Infinite horizon stable predictive control," *IEEE Transactions on Automatic Control*, vol. 41, no. 10, pp. 1522–1527, 1996.

[101] P. Scokaert and D. Clarke, "Stabilising properties of constrained predictive control," *IEE Proc.-Control Theory Appl.*, vol. 141, pp. 295–304, September 1994.

[102] P. Scokaert, "Infinite horizon generalized predictive control," *International Journal of Control*, vol. 66, no. 1, pp. 161–175, 1997.

[103] A. Zheng and M. Morari, "Stabilbty of model predictive control with mixed constraints," *IEEE Transactions on Automatic Control*, vol. 40, no. 10, pp. 1818–1823, 1995.

[104] J. B. Rawlings and K. R. Muske, "The stability of constrained receding horizon control," *IEEE Transactions on Automatic Control*, 1993.

[105] A. Zheng, R. Balakrishnan, and M. Morari, "Constrained stabilization of discrete-time systems," *International Journal of Robust and Nonlinear Control*, vol. 5, pp. 461–485, 1995.

[106] H. Demircioglu and D. Clarke, "Generalised predictive control with end-point state weighting," *IEE Proceedings-D*, vol. 140, pp. 275–282, July 1993.

[107] D. W. Clarke and R. Scattolini, "Constrained receding-horizon predictive control," *IEE Proceedings Part D*, vol. 138, no. 4, pp. 347–354, 1991.

[108] E. A. Lewis, "A-c driven sendzimer mill," *Iron and Steel Engineer*, January 1997.

[109] P. C. Sen, *Principles of electric machines and power electronics*. John Wiley and Sons, 1989.

[110] A. Swiatoniowski, "Interdependence between rolling mill vibrations and the plastic deformation process," *Journal of Materials Processing Technology*, vol. 61, pp. 354–364, 1996.

[111] D. H. E. Butler, M. A. Churches, Y. Anbe, and H. Naitoh, "Compensation of a digitally controlled static power converter for the damping of rolling mill torsional vibration," *IEEE Transactions on Industry Applications*, vol. 28, March/April 1992.

[112] A. Randall, P. J. Reeve, and A. F. MacAlister, "Disturbance attenuation in a hot strip rolling mill via feedforward adaptive control," in *13th IFAC Triennial World Congress, San Francisco, USA*, pp. 463–468, 1996.

Appendix A

Appendix A

A.1 Rolling Mill Definitions

As with any industrial process a lot of process terminology is used that are not common industrial terms. In this section a brief description of the most common terms used in the process description and problem formulation of this dissertation is given.

- **Reversing mill:** A reversing mill is a single stand mill that uses multiple passes to achieve the desired reduction. The rolling mill drive can rotate both ways and the strip can be rolled against the direction of the general process flow.
- **x-High Rolling Stand:** The rolling stand has x number of rolls.
- **Steckel Rolling Mill:** A Steckel rolling mill is a four high reversing single or tandem stand mill [4]. In this work only a single stand mill will be investigated.
- **Finishing Mill:** The term finishing mill is a global name and can consist of 5 to 7 non reversing tandem mill stands or a single/double tandem reversing mill stand/s as is the case with a Steckel rolling mill. The main differences between the different types of finishing mills are the annual throughput of the mills. The tandem non reversing mills are capabale of higher processing speed and has higher throughputs.
- **Work- and Backup Rolls:** A typical four high mill has two work rolls and two backup rolls. The work rolls are in contact with the strip being rolled and the backup rolls are fitted to support the thinner work rolls [57]. The work rolls are driven by the main mill drive motor [111].
- **Roll gap:** The roll gap is defined as the contact zone between the strip being rolled and the working rolls of the mill stand [2, 24, 28].
- **Pass:** A pass is defined as the action of passing the whole length of strip through the roll gap of the mill. The terminology of a pass is only used for a reversing type mill.

- **Threading:** The rolling of strip is normally a batch process, although there are examples of continuous processing lines. For a Steckel rolling mill the rolling of strip proceeds as a batch process and the mill speed is ramped up to a constant speed, called the threading speed, and decelarated before the strip is delivered after the completion of the pass.

- **Gauge:** The gauge of the strip is defined as the centerline thickness of the strip.

- **Profile** ($\sum$): Profile is defined as the distribution of thickness over the width of the strip [61]. The profile is determined by the shape of the unloaded work rolls, the required reduction and thus the rolling forces, rolling speeds, strip width, material properties of the strip and the rolls.

- **Crown** (C_r): Crown of the strip is defined as the thickness difference in the width of the sheet between the middle of the strip and a point near the edge. If the profile of the strip is convex the it is said that the strip has positive crown and similarly a concave profile is labelled negative crown [61]. Crown and profile are expressed as,

$$Cr = h_m - h_r, \sum = \frac{C_r}{h_m}, \tag{A.1}$$

  where h_m is the centerline thickness of the sheet and h_r is the thickness of the strip near the edge. The terminology **Camber** and **Crown** are used interchangeably by the rolling mill community.

- **Shape:** Is defined as a transverse distribution in strain across the width of the strip. When the percentage reduction in the strip thickness reduction varies across the width a transverse variation in elongation will result. The application of tension to the strip whilst rolling will convert some or all of the variation in elongation into a transverse stress distribution across the strip width. The strip shape is latent if the mean applied tension is great enough to pull the strip flat. If all the length change is not converted into a stress distribution the strip will exhibit flatness defects, such as buckles, and the shape is said to be "manifest". If the percentage reduction in the strip is constant across the strip width there will be no transverse variation in stress and the strip will have zero or perfect shape.

- **Flatness**: Flatness refers to the ability of the strip to lie flat when placed on a flat surface with no applied tension to the strip. Flatness is a function of how the the thicknes crown evolves during the rolling process. Flatness is related to to shape in that a transverse variation in stress may result in a buckled strip when the appied tension is removed. When the reduction in the thickness profile is not uniform pass to pass, poor flatness arises due to uneven longitudinal extensions across the strip width. This uneven longitudinal extensions are seen as buckling or warping effects [112]. The shape can be defined as,

$$S = \frac{L - \lambda}{\lambda} = \left(\frac{A\pi}{2\lambda}\right)^2 = \frac{\Delta L}{L}, \tag{A.2}$$

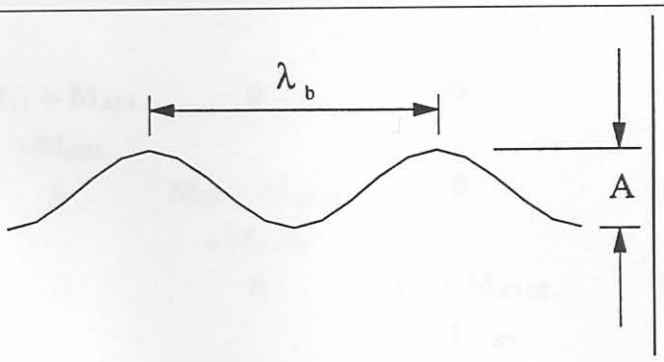

Figure A.1: Shape Definition

where L is the length of the strip, λ is the wavelength of the shape defect (center buckle or edge buckle assuming a sinusiodal waveform) and ΔL is the non uniform elongation of the strip over the width. In Fig. A.1 the variables featured in Eq. A.2 are shown.

- **Units of shape:** There are a few units used to express strip shape namely,

$$i.\ Mon = \frac{\Delta L}{L} 10^4, \tag{A.3}$$

$$ii.\ Mon.cm^{-1} = \frac{\Delta L}{L} \frac{10^4}{w}, \tag{A.4}$$

$$iii.\ I\ unit = \frac{\Delta L}{L} 10^5, \tag{A.5}$$

where w is the strip width.

Although many other terminologies are used they are however self explanatory and will not hamper the understanding of this dissertation.

A.2 Four Roller Model

The solution methodology is similar to the two roller model. The mass and stiffness matrices differ and are given as,

$$\widehat{\mathbf{M}} = \begin{bmatrix} \mathbf{M}_{11} + \mathbf{M}_{dL1} + \mathbf{M}_{dR1} & \mathbf{0} & \mathbf{0} & \mathbf{0} \\ \mathbf{0} & \mathbf{M}_{22} + \mathbf{M}_{dJL1} + \mathbf{M}_{dJR1} & \mathbf{0} & \mathbf{0} \\ \mathbf{0} & \mathbf{0} & \mathbf{M}_{33} + \mathbf{M}_{dJL2} + \mathbf{M}_{dJR2} & \mathbf{0} \\ \mathbf{0} & \mathbf{0} & \mathbf{0} & \mathbf{M}_{44} + \mathbf{M}_{dL2} + \mathbf{M}_{dR2} \end{bmatrix} \tag{A.6}$$

$$\widehat{\mathbf{K}}(t) = \begin{bmatrix} \mathbf{K}_{11} + \mathbf{K}_{c11}(t) & -\mathbf{K}_{c12}(t) & \mathbf{0} & \mathbf{0} \\ -\mathbf{K}_{c21}(t) & \mathbf{K}_{22} + \mathbf{K}_{c22}(t) + \mathbf{K}_{strip_{22}} + \mathbf{K}_{Jd22L} + \mathbf{K}_{Jd22R} & -\mathbf{K}_{strip_{23}} - \mathbf{K}_{Jd23L} - \mathbf{K}_{Jd23R} & \mathbf{0} \\ \mathbf{0} & -\mathbf{K}_{strip_{32}} - \mathbf{K}_{Jd32L} - \mathbf{K}_{Jd32R} & \mathbf{K}_{33} + \mathbf{K}_{c33}(t) + \mathbf{K}_{strip_{33}} + \mathbf{K}_{Jd33L} + \mathbf{K}_{Jd33R} & -\mathbf{K}_{c34} \\ \mathbf{0} & \mathbf{0} & -\mathbf{K}_{c43}(t) & \mathbf{K}_{44} + \mathbf{K}_{c44}(t) + \mathbf{K}_{strip_{44}} + \mathbf{K}_{Jd44L} + \mathbf{K}_{Jd44R} \end{bmatrix} \tag{A.7}$$

The solution of the time variant four roller model requires that at each time step the assumed stiffness matrix be recalculated. After this recalculation an eigenvalue problem is solved and the modal matrix is obtained. The vertical displacements at the same time step are recalculated and from this the nonlinear spring for the interface loading can be recalculated. This iterative process is terminated as soon as the draft of the strip stabilizes. Once this is achieved the simulator advances to the next time step. The four roller model falls outside the scope of this dissertation.